NASA SP-180

SECOND CONFERENCE ON SONIC BOOM RESEARCH

Held at the

NATIONAL AERONAUTICS AND SPACE ADMINISTRATION

Washington, D. C.

May 9-10, 1968

NASA SP-180

SECOND CONFERENCE ON
SONIC BOOM RESEARCH

EDITED BY
IRA R. SCHWARTZ

Proceedings of a conference held at the National Aeronautics and Space Administration, Washington, D. C., May 9-10, 1968, on research on the generation and propagation of sonic booms and cochaired by W. D. Hayes of Princeton University and A. R. Seebass of Cornell University.

Scientific and Technical Information Division
OFFICE OF TECHNOLOGY UTILIZATION 1968
NATIONAL AERONAUTICS AND SPACE ADMINISTRATION
Washington, D.C.

For sale by the Superintendent of Documents,
U.S. Government Printing Office, Washington, D.C. 20402
Price $1.00
Library of Congress Catalog Card Number 68–62087

Preface

The proceedings of the Second Conference on Sonic Boom Research held at NASA headquarters, Washington, D.C., on May 9–10, 1968, are reported in this NASA Special Publication. This conference was organized by the Research Division of the Office of Advanced Research and Technology. It was, in essence, a follow-on meeting to the first Sonic Boom Conference, the proceedings of which are reported in NASA SP–147.

The purpose of this conference was to review the current status of the NASA University Program on Sonic Boom Research, to survey the current research program at the NASA centers, to determine those areas of sonic boom research that are the most pressing from the standpoint of commercial supersonic transport (SST) operation, and to determine which, if any, of the various avenues of research appear to be the most promising with regard to sonic boom overpressure reduction.

The entire first day and the morning of the second day of the meeting were devoted to the presentation of the invited papers covering the status of the various NASA projects. A. Richard Seebass served as chairman of these sessions. The afternoon session of the second day was devoted to an informal open discussion of the state of the art of sonic boom theory. The subjects discussed in this session could be categorized into two principal topics which serve to answer the following two questions: How far have we proceeded in developing methods of analysis and understanding of sonic boom phenomena? How far have we proceeded in devising methods of reducing sonic boom for feasible aircraft designs? Wallace D. Hayes served as chairman of this discussion session.

As was the situation last year, and to reiterate a statement made in last year's report (NASA SP–147), "it is difficult to overemphasize the importance of the phenomenon we call the sonic boom." In July 1968 the President of the United States signed into law a bill requiring the Federal Aviation Administration (FAA) Administrator to ". . . prescribe and amend such rules and regulations as he may find necessary to provide for the control and abatement of aircraft noise and sonic boom. . . ." Sponsors of the legislation said it was broad enough to

allow the FAA to ban supersonic flights entirely unless the boom problem is brought under control. Several other countries are considering regulations restricting proposed SST's to subsonic flight over populated areas. It is the consensus of opinion that the SST's must be capable of supersonic operation over land to be a true economic success. Such aircraft should be able to fly supersonically anywhere, over land as well as water, without causing human discomfort or structural damage.

It is not certain yet how much sonic boom overpressure will be acceptable for humans. Present thinking is that the overpressures may have to be reduced to values as low as 1 pound per square foot to be acceptable. Thus, it is apparent that every aerodynamic technique of reducing the overpressure must be investigated. A large number of investigations and significant progress have already been made by NASA in cooperation with the Federal Aviation Administration. Much more scientific understanding of the problem is needed before a large reduction in sonic boom is accomplished.

As a result of last year's conference and after discussing the sonic boom problem with the FAA and the U.S. Air Force, the following 10 areas were defined for further research on the generation and propagation of sonic booms: (1) validity of the basic theory, (2) midfield signature modification, (3) atmospheric effects, (4) effects of accelerations and maneuvers, (5) multipole effects and lateral spreading, (6) pressure distributions on various geometrical configurations, (7) lift contribution to the far-field downward momentum flux, (8) sonic boom of exotic configurations, (9) engine stream-tube area effects, and (10) techniques for predicting the sonic boom of hypersonic aircraft.

Also, it was concluded at last year's meeting, April 12, 1967, that there was a clear need for the active participation of knowledgeable aerodynamicists and engineers in sonic boom research in order to elevate our level of understanding. Accordingly, the Research Division of the Office of Advanced Research and Technology, NASA Headquarters, established the following seven research programs in six universities to complement the in-house program at the NASA Ames and Langley Research Centers and to investigate the 10 basic research areas:

New York University	A. Ferri and L. Ting	Low boom configurations, N-wave reflections
Cornell University	E. L. Resler, Jr., and F. K. Moore	No boom-lifting configurations, far-field theory
The Aeronautical Research Institute of Sweden.	M. T. Landahl	Nonlinear effects

Colorado University	A. Busemann	Boom reduction
Princeton University	W. D. Hayes	Second-order wave theory, geometric acoustics, propagation through a caustic (ray envelope)
Cornell University	A. R. Seebass and A. R. George	Azimuthal redistribution
Columbia University	M. B. Friedman	Theory of the superboom

The progress made during the past year by the NASA centers and contractors represents substantial advances in developing methods of analysis and understanding of sonic boom phenomena and in devising methods, particularly aerodynamic techniques, of reducing sonic boom for practical aircraft designs. For example, in regard to the analysis and understanding of sonic boom phenomena, the straightforward technique for predicting the propagation of a sonic boom from a slender aircraft can now be conveniently employed with the assumption that nonlinearity does not affect the rays. Use of such an assumption permits one to calculate directly the nonlinear modifications of the signature. Great advances have been made in the understanding of geometric acoustics with winds and variable sound speed. Also a linearized theory for flow fields around aircraft has been well known for many years. However, life is not all that simple in view of the fact that the linearized theory referred to above does not provide a dependable and consistent first-order description of the flow field far from the aircraft. In addition, nonlinear effects exist near the aircraft.

For practical considerations and importance the following theoretical problems have been identified, and though better understood, remain unsolved:

(1) Prediction of sonic boom signatures near a caustic
(2) Nonlinear effects on ray tubes
(3) Diffraction into shadow zones
(4) Nonlinear effects near the aircraft
(5) Effects of turbulence

Our researchers believe that they can find practical solutions to these basic problems because the methods of solution are presently within focus.

During the past year, the Aeronautical Research Associates of Princeton under contract to NASA developed a computer program that will compute the full overpressure signature anywhere within the field for an aircraft in unsteady supersonic flight in a horizontally stratified atmosphere with steady winds. Although the program cannot account for the vertical winds, these effects are usually small compared with those of the horizontal winds.

A major portion of the meeting was devoted to reporting the progress that was made during the past year regarding the development of aerodynamic techniques to reduce the sonic boom. Foremost in the minds of the researchers is the well-recognized fact that technological advancements that produce improved overall efficiency for SST aircraft, such as improvements in engine thrust to weight ratio, lift-to-drag ratio, structural weight, and fuel consumption, will reduce sonic boom intensities. Above all, the reduction of the sonic boom is not to be realized at the expense of aircraft efficiency.

Several papers presented at this meeting discussed promising aerodynamic techniques for reducing the sonic boom. Antonio Ferri showed that redistribution of lift along the length of present SST configurations results in near-field effects that provide maximum sonic boom overpressure of the order of 1 pound per square foot at no expense to the lift-to-drag ratio of the airplane at cruise. This is a significant reduction compared with the maximum boom overpressure of 2 pounds per square foot for present configurations selected for the supersonic transport. For a given lift and volume of an aircraft there is a lower bound to the far-field overpressure. This results from the fact that, while the lift contribution to sonic boom can be reduced by the addition of suitable volume elements, there is no way of avoiding the boom attributed to lift alone without modifying the Bernoulli constant of the flow. Thus, Ferri has attempted to approach these lower bounds with aircraft configurations that have realistic skin friction and wave drag contributions and not unusual structural requirements.

A. R. George's paper has shown how quadrupole effects can also be used to approach this theoretical lower bound. Other interesting boom reduction techniques currently being studied are discussed by Resler, Seebass, Hayes, Carlson, and McLean in this volume.

In an assessment of the status of our sonic boom research program at this meeting, it was concluded that there are no carefully documented experimental results for the overpressure signature in the vicinity of a caustic that results from an aircraft acceleration maneuver or an ambient sound speed gradient. Because no theory presently exists for the overpressure signature at a caustic and because the pressures are greatly intensified there, it appears that much more experimental work is needed. It should be possible to simulate the maneuver effects in ballistic ranges. The ambient sound speed gradient effects can also be duplicated in shock tubes, supersonic wind tunnels, and certain simulators. The NASA Langley Research Center has recently obtained some qualitative information on the effect of sound speed gradient in a ballistic range. Further experi-

mental work on this problem is being planned by several groups in the NASA contract program to complement the in-house program.

Finally an assessment of the proceedings of this meeting has indicated to me and to those researchers who participated in the meeting that significant progress has been made during the past year in our understanding and analysis of the generation and propagation of sonic boom. Further, it has been analytically demonstrated in the NASA program during the past year that the utilization of a particular aerodynamic technique can result in large reductions in sonic boom overpressures. This is especially significant in that it allows us to expect vast improvements in future SST conceptual designs from both improvements in aircraft operating efficiency as well as through novel aircraft designs. It is yet too early to predict whether any of these design techniques will lead the way to the development of a domestic SST that will be allowed to fly supersonically over land as well as over water. It is to be expected that more definitive answers will be forthcoming as the various promising avenues of approach are explored in much greater detail.

I. R. SCHWARTZ
Research Division
Office of Advanced Research and Technology

Contents

INVITED PAPERS

CONTRIBUTED REMARKS

INVITED PAPERS

Atmospheric Effects on the Sonic Boom

I. Edward Garrick
Langley Research Center, NASA

INTRODUCTION

The material presented at the conference was based to a large extent on a paper presented at the International Association of Meteorology and Atmospheric Physics, XIV General Assembly of the International Union of Geodesy and Geophysics, Lucerne, Switzerland, and published recently as NASA Technical Note D–4588 (ref. 1). For this reason, only a condensed discussion of this material is given here, and some newer information will be stressed.

Acceptance by the general public of supersonic transports will depend in great measure on the characteristics of their sonic booms (ref. 2). These characteristics are affected by several factors which depend on design, operations, and environment or atmospheric conditions. Design factors such as weight, size, lift, and volume distributions and operation factors such as altitude, Mach number, and flight path may be accounted for, or even predicted, by existing theoretical methods which have been closely verified under controlled conditions, such as in a supersonic wind tunnel. However, the effects of environment or atmospheric conditions, such as wind, temperature, and pressure gradients and turbulence, like the prediction of weather itself, remain probabilistic or statistical in nature.

The report aims to summarize and discuss some of these atmospheric effects, including the findings of several flight studies. Much of the flight information has already been published; however, in the paper by D. J. Maglieri in this volume entitled "Sonic Boom Ground Pressure Measurements for Flights at Altitudes in Excess of 70 000 Feet and at Mach Numbers up to 3.0," some of the most recent data are included. It is hoped herein to account for or explain, at least qualitatively, the kinds of statistical information on peak pressures that are found by field measurement.

ANALYTICAL CONSIDERATIONS

Only a broad overview of the theoretical background is mentioned here. Prediction of sonic boom characteristics has been based on methods in which idealized atmospheres are assumed. For example, in his basic work on the flow fields of bodies of revolution, Whitham assumed a uniform atmosphere. Randall employed a correction factor to account for an isothermal hydrostatic (exponential) atmosphere.

Effects of a layered or stratified atmosphere with arbitrary steady or slowly varying winds and temperatures were studied by Palmer, Friedman, Kane, and Sigalla. This work makes direct use of classical concepts of geometrical (ray) acoustics and permits comparison of results for a nonstandard atmosphere with those for the standard atmosphere. It also leads to means for predicting effects of maneuvers and explains in large measure the focusing and channeling of energy of acoustical signals. Many references are given in reference 3 by Kane and Palmer, a report which contains the most detailed study of meteorological effects on the sonic boom, based on an analysis of NASA data obtained prior to the summer of 1964. (See also ref. 4.)

It is pertinent to mention briefly some recent work on propagation in a stratified atmosphere sponsored by the Langley Research Center under contract and conducted by Aeronautical Research Associates of Princeton, Inc. This work, to be published, is authored by Wallace D. Hayes, Rudolph C. Haefeli, and Helene Kulsrud. It presents a theory, based on geometric acoustics, and a calculation program for tracing the pressure signature from the vicinity of the airplane to the ground, as influenced by passage through a steady layered atmosphere. The program will give the location, intensity, and time history for both level flight and for maneuvers. See also a paper entitled "Similarity Rules for Nonlinear Acoustic Propagation Through a Caustic" by Professor Hayes in this volume.

Turbulence and temperature fluctuations are known to have important modulating effects on the distortion of the sonic boom pressure signatures. Theoretical considerations are needed to explain anomalous spiky signatures and to rationalize the statistical data. It may be noted that a large literature exists relevent to sinusoidal sound (or light) with substantial contributions by authors from the U.S.S.R. For an account of this work which starts with contributions of A. M. Obukov, see the books by Tatarski and Chernov (refs. 5 and 6). In particular, the method of Rytov, combined with the random variable properties of patches of turbulence, has led to log normal characteristics for the statistics of the scattered pressure amplitudes. Experimental measurements of Kallistratova for sound scattering and of Tatarski for light scattering tend to confirm trends indicated by theory.

Many others have contributed to the theoretical background of the interaction of turbulence with sound or shock waves, and only a few names are mentioned here: Lighthill, Ribner, Palmer, Muller, and Matschat. Despite the encouraging analytical efforts, relevant statistical predictions for sonic booms at present seem to depend mainly on measurements from airplane flights. In presenting the measured data subsequently, it is convenient in general to normalize the measured data in relation to a nominal overpressure calculated from the simple theory of Whitham or Randall, or from that of a layered standard atmosphere. One such scheme programed for computing machines is given in reference 7.

A recent significant contribution to the theory of effects of atmospheric turbulence on sonic booms by S. C. Crow was made known to the author through a preprint (ref. 8). It is believed appropriate to include herein the following complete summary from this report.

Recorded pressure signatures of supersonic airplanes often show intense, spiky perturbations superimposed on a basic N-shaped pattern. A scattering theory, incorporating both inertial and thermal interactions, is developed to explain the spikes. Scattering from a weak shock is studied first. An exact solution of the scattering equation, finite at the shock and everywhere behind it, is derived in the form of a surface integral over a paraboloid of dependence, whose focus is the observation point and whose directrix is the shock. The solution is found to degenerate at the shock into the result given by ray acoustics. Eddies in the Kolmogorov inertial subrange are found to be the main source of sonic-bang spikes, and Kolmogorov's similarity theory is used to show that, for almost all separations h between the shock and the observation point, the mean-square pressure perturbation equals $(\triangle p)^2\ (h_c/h)^{7/6}$, where $\triangle p$ is the pressure jump across the shock and h_c is a critical distance predicted in terms of meteorological conditions. The mathematically predicted mean-square pressure perturbation at the shock itself is found to be finite but enormous. The exact solution of the scattering equation is generalized for arbitrary waveforms, and the approximate relation $G(f)=G^N(f)\ (1+(f/f_c)^{7/6})$ is established between the energy spectrum $G^N(f)$ of undeformed sonic bang and its mean perturbed spectrum $G(f)$. The critical frequency f_c, inversely proportional to h_c, is found to be as low as 63 cps for an idealized model of atmospheric turbulence. The conclusion is reached that scattering can augment considerably the psychological impact of a sonic bang.

ATMOSPHERIC TURBULENCE

In recent years, much information on the local structure of the atmosphere has been assembled (for example, ref. 9). It is known that characteristic lengths of turbulence in the lower atmosphere below 1000 to 2000 feet (or about 305 to 610 meters) depend on height above terrain. It is also believed that much of the distortion of sonic boom pressure signatures attributed to turbulence may occur at the lower altitudes. An interesting detailed view of the vortex structure near the ground is afforded by figure 1 which is from ref. 10. This figure

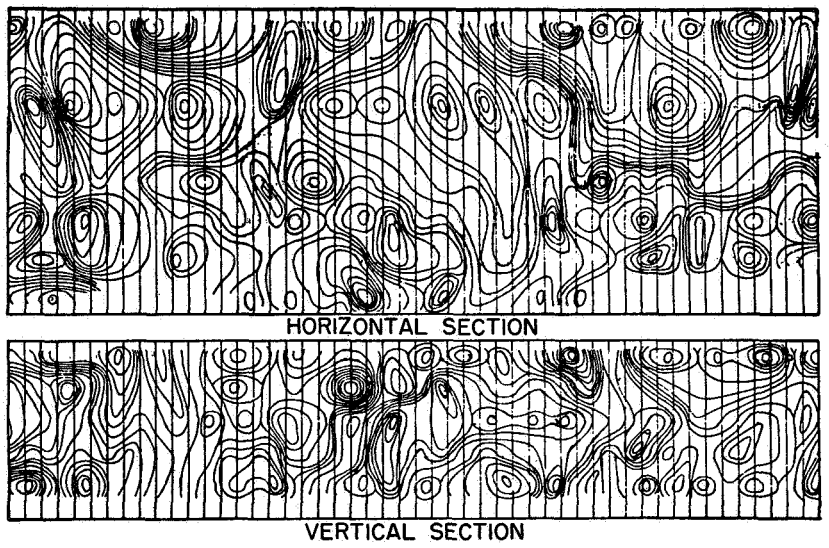

FIGURE 1.—Gust structure near the ground as indicated by isotachs (ref. 9).

shows equal velocity contours, or isotachs, obtained from measurements taken during 25 seconds of gusty weather. The horizontal section shows the isotachs obtained from measurements taken at eight stations along an array of 50-foot (15.2-meter) poles equally spaced over a linear distance of 420 feet (128 meters). The vertical section shows the isotachs obtained from measurements taken at five equally spaced stations up a 250-foot-high (76.2-meter) tower. In each section, the ordinate represents distance along the array or up the tower, and the abscissa is time. During the sampling period the average wind traversed a distance of over 1000 feet (304.8 meters).

Turbulence in the upper atmosphere has been probed by instrumented airplanes (ref. 11). Typical results of measurement for moderate turbulence are shown in figure 2 as the variation of power spectral density of vertical velocity with wave number (1/wavelength). The dashed extension to the measurements follows the theoretically indicated 5/3 power of the wave number. The shape of this curve tends to be relatively invariant while the amplitude is a function of the severity of the turbulence. The curve represents the Kolmogorov inertial subrange; for lower wave numbers than those shown, the dynamical processes originating the turbulence dominate and influence the spectral shape. For higher wave numbers than those shown, dissipative processes converting turbulence to heat begin to dominate. The curve shows the distribution of power in the various wavelengths and the area under the curve yields the

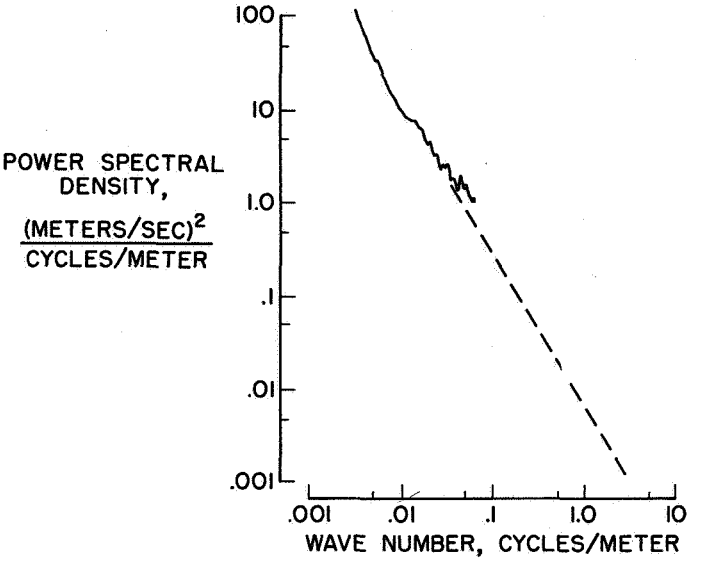

FIGURE 2.—A spectrum of atmospheric turbulence (ref. 10).

total power. This same type of figure can also apply approximately near the ground with relatively less power in the longer wavelengths. From its spectral distribution, it may be determined that a normal sonic boom pressure signature of 0.3- to 0.4-second duration covers acoustic wavelengths that range from about 1000 meters to fractions of a meter. Thus, the interaction of the pressure signature and the turbulence occurs over the entire spectrum shown and includes acoustic wavelengths less than and greater than the characteristic vortex sizes. The turbulence of smaller scale than the sound wavelengths tends to produce isotropic scattering, whereas the scattering of larger scale turbulence is directional.

FILTERING THE N-WAVE

Insight into subjective effects of sonic booms and into frequency response requirements of measuring instruments is obtained by study of the amplitude and frequency content of the N-wave of various durations and rise times, as has been done. Further insight has been obtained by applying various filtering techniques to the analog signal of the N-wave. Two typical results are shown in figure 3: (*a*) filtering so that frequencies below 10 hertz are not measured, and (*b*) filtering out all frequencies above 30 hertz. The amplitude is not changed very much, but, whereas filtering out the high frequencies yields a rounded N-wave, filtering out the low frequencies gives a sharp rise and a distorted wave. Thus, the high frequencies

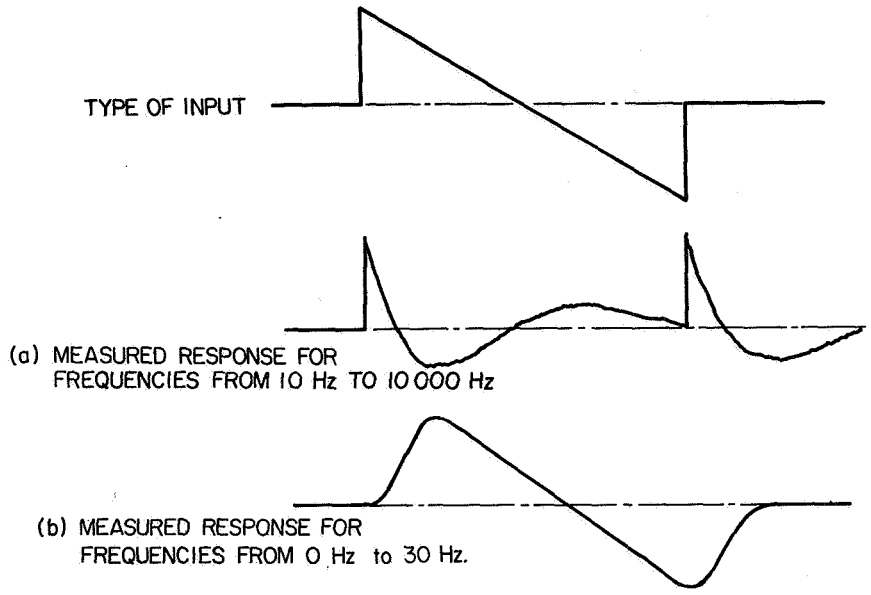

FIGURE 3.—Effects of filtering low or high frequencies from an N-wave.

seem dominant in defining the rapid compressions of the N-wave, and the lower frequencies appear dominant in defining the expansion. However, while filtering out high frequencies suffices to obtain rounded signatures, it is not a necessary requirement, because these signatures may also be obtained by a shifting of the phases of the high-frequency components, as will be further discussed.

MEASURED DATA

Wave Shapes

An indication of the measured variations in wave shapes at ground level is given in figure 4 for airplanes of three different sizes. The associated durations are approximately 0.1, 0.2, and 0.3 second. These signatures generally fall in several classes:

Normal	representing signatures closely resembling theoretically calculated N-waves
Peaked	representing signatures wherein the pressure peak is amplified relative to the basic N-wave
Rounded	representing signatures with longer rise times and lower peaks than the N-wave

Combinations and variations of these signatures also occur.

It is known that near the airplane the pressure signature is quite complex, regardless of atmospheric effects, and that with increased distance the nonlinear characteristics of the propagation process in

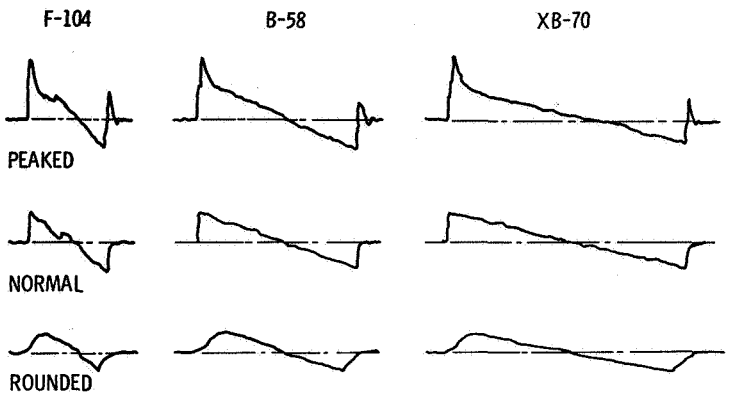

FIGURE 4.—Variation in measured sonic boom pressure signatures at ground level for small, medium, and large airplanes in steady level flight (ref. 2).

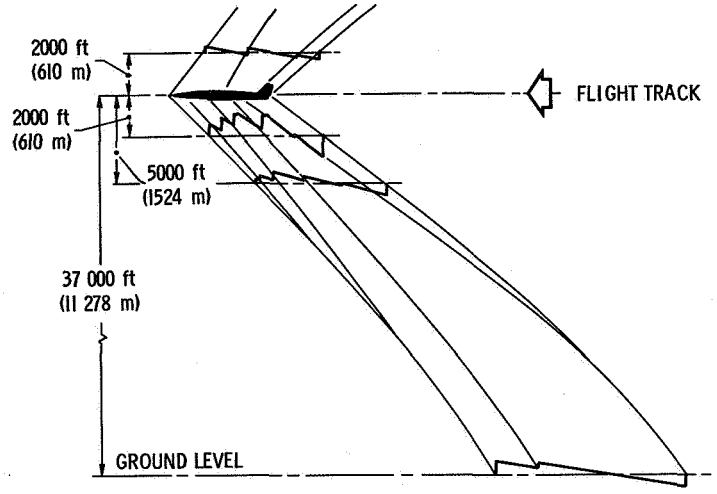

FIGURE 5.—Indication of signatures measured only a few thousand feet from the XB–70 airplane in flight and that at the ground (ref. 2).

quiescent atmosphere tend to simplify the signature and to produce the N-wave signature. Figure 5 shows results of probe flights of the flow field of the XB–70 airplane flying at $M=1.5$ and at an altitude of 37 000 feet (11.28 kilometers) made by an F–104 airplane at various separation distances. The detailed geometry of the airplane is reflected in the near-field signatures both above and below the airplane. Of particular interest is the signature at ground level which indicates that for an altitude of 37 000 feet the far-field N-wave is not fully achieved for this large airplane, rather a hybrid-type, near-field signature exists.

Sonic Boom Pressures

Measured sonic boom pressure signatures for two flights of the same airplane type are shown in figure 6. The pressure signatures on the right were obtained when surface winds were about 28 knots (14.4 m/sec) and rather gusty, and those on the left were obtained for much lower wind velocities. These signatures were obtained at one station by microphones separated by only 100 feet (30.48 meters) in a cross-arrangement. However, as indicated in reference 11, similar variations, indicating wave-shape distortion on the one hand, and lack of distortion on the other hand, were measured over a 150-square-mile (388.5-km^2) area during the same two flights.

Statistics of Pressure Peaks

A number of flight programs during which routine measurement of sonic boom signatures was made with carefully calibrated pressure instrumentation have been conducted and reported. The most extensive of these was a 6-month flight program at Oklahoma City (ref. 13). However, only fragmentary observations were made of associated weather conditions. The investigation demonstrated that wide variations in the signature types were associated with dynamics of the atmosphere; moreover, the distributions of pressure peaks appeared to follow approximately a log normal probability curve—

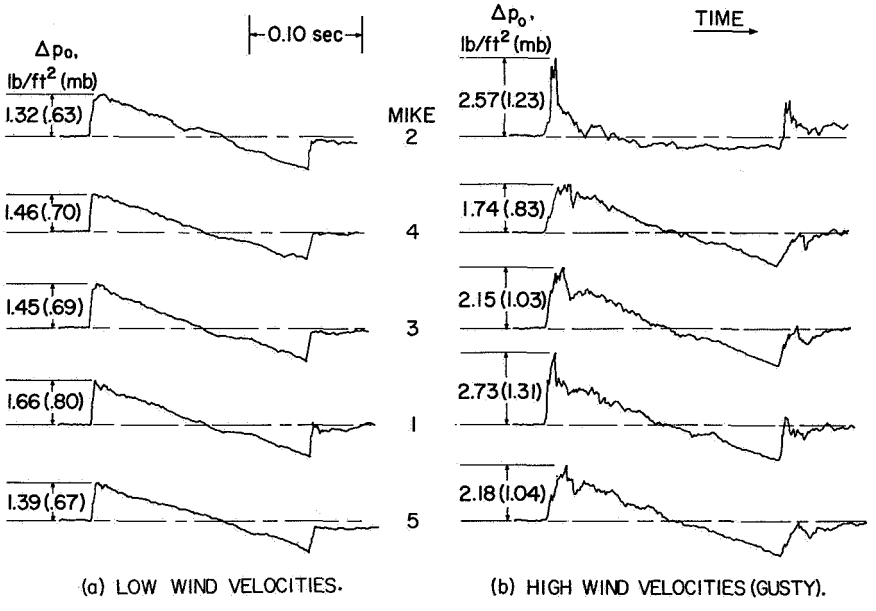

FIGURE 6.—Time histories of sonic boom overpressures showing wave-shape variations measured for two flights of a B–58 airplane on different days (ref. 11).

that is, if the pressure peaks are plotted as log pressure or in decibels, an approximately Gaussian or normal distribution occurs. Also shown by this study was the result that the impulse also followed such a distribution law, although it has smaller variance or standard deviation. The approximate theory for scattering of sound (monochromatic waves) by turbulence also yields a normal distribution for the logarithm of the amplitude (ref. 5). The theory indicates that given certain sufficient information about the structure of turbulence, a calculation of the variance of the distribution of peaks for sonic booms may be feasible. Palmer has already made some preliminary estimates in this regard.

In conjunction with the XB–70 flights a number of accompanying flights of B–58 and F–104 airplanes were made. The Mach number and altitude ranges covered were from $M=1.5$ to 2.5 and $h=11.3$ to about 18 kilometers for the XB–70 airplane, $M=1.5$ to 1.65 and $h=9.7$ to 12.2 kilometers for the B–58 airplane, and $M=1.3$ to 1.4 and $h=5.2$ to 6.3 kilometers for the F–104 airplane. The nominal calculated overpressure for all these airplanes was about 1 millibar. The data in figure 7 for the three airplanes were obtained in late morning flights from November 1966 to January 1967, when generally small turbulence and convectivity occurred. Despite the large differences in airplane operating conditions and signature durations, a strikingly similar probability distribution pattern for the three airplanes appears (the log normal distribution is linear on this type of plot).

Tabular Summary

Table I provides a convenient summary of some of the results of several flight programs (refs. 12 to 14). Presented are the ratios of the mean values measured to the nominal values calculated. The ratios of the ranges of $\pm 1\sigma$ and $\pm 2\sigma$ relative to the mean of the pressure ratio are also given. (These ratios may be regarded as corresponding to a chosen mean pressure ratio of unity.) The $\pm 3\sigma$ values as extrapolated are also presented and represent 99.7 percent of the data. This latter result is only suggestive and, as mentioned in reference 3, these extreme values may be conservative. The pressure measurements were made under the flight track, except where the lateral distance is noted. The largest variability in the ratio factors occurs at the farthest lateral distances and for the lowest supersonic Mach numbers where ray paths in the atmosphere are longest. However, the nominal calculated values are generally lower at the lateral positions because of the greater distances. The numerical factor of the mean overpressure for the $\pm 2\sigma$ range of ground-track data varies from a maximum of 1.78 (Oklahoma City data) to a minimum of 1.22

TABLE I.—*Statistical Variations of Sonic Boom Overpressures*

Test site	Time period	Range		Mean of $\frac{\Delta p_{o_{meas}}}{\Delta p_{o_{calc}}}$	Ratios relative to mean for range			Number data samples
		Mach no.	Altitude, km		$\pm 1\sigma$	$\pm 2\sigma$	$\pm 3\sigma$	
Oklahoma City 1	Feb. to Apr. 1964	1.3 to 2.0	6.4 to 12.5	[a] 0.825	0.76 to 1.30	0.58 to 1.70	0.45 to 2.21	652
Oklahoma City 3 [b]				[a] 1.04	.73 to 1.37	.53 to 1.86	.39 to 2.55	654
Oklahoma City 4 [c]				[a] .96	.67 to 1.51	.45 to 2.23	.30 to 3.31	637
Oklahoma City 1	May to July 1964	1.2 to 1.6	8.5 to 14.0	[a] .925	.75 to 1.34	.56 to 1.78	.42 to 2.37	549
Oklahoma City 3 [b]				[a] 1.20	.74 to 1.35	.56 to 1.92	.42 to 2.37	554
Oklahoma City 4 [c]				[a] 1.38	.68 to 1.49	.46 to 2.39	.31 to 3.23	548
Edwards Air Force Base.	Nov. 1966 to Jan. 1967.	1.3	9.4	[d] .855	.78 to 1.28	.61 to 1.64	.47 to 2.11	1378
Chicago	Jan. to Mar. 1965	1.2 to 1.66	11.6 to 14.6	[d] .92	.77 to 1.29	.60 to 1.67	.46 to 2.15	191
Edwards Air Force Base.	Sept. to Oct. 1961	1.5 to 2.0	9.4 to 21.3	[d] 1.035	.90 to 1.11	.81 to 1.23	.73 to 1.36	135
Combined (fig. 14).		1.2 to 2.0	9.4 to 21.3	[d] .942	.82 to 1.24	.67 to 1.53	.54 to 1.87	358
Edwards Air Force Base.	Nov. 1966 to Jan. 1967.	1.5 to 2.5	11.3 to 18.3	[d] 1.00	.91 to 1.10	.82 to 1.22	.74 to 1.36	447
Edwards Air Force Base.	Nov. 1966 to Jan. 1967.	3.0	21.3+	[d] .98	.86 to 1.16	.74 to 1.34	.64 to 1.56	578

[a] Nominal overpressure calculated for isothermal atmosphere.
[b] 5-mile offset from flight track.
[c] 10-mile offset from flight track.
[d] Nominal overpressure calculated for standard atmosphere.

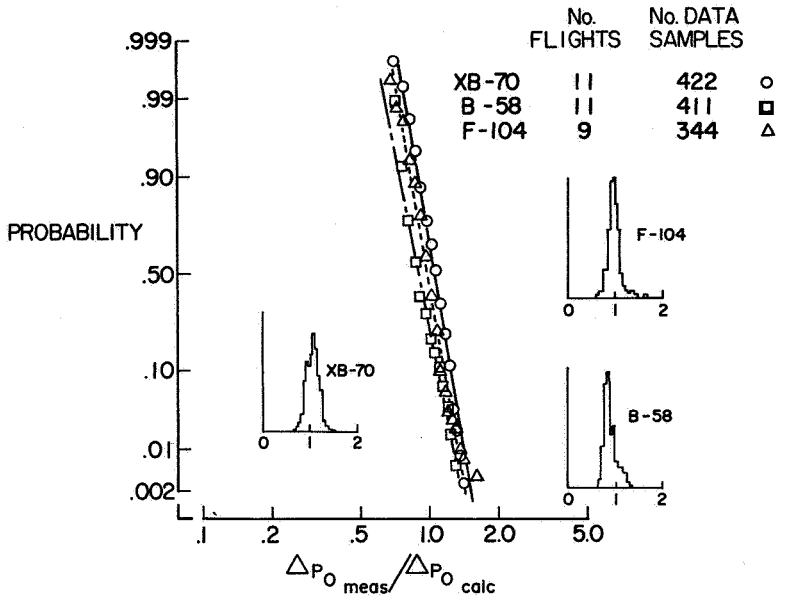

FIGURE 7.—Probability of exceeding a given value of the ratio of measured to calculated ground overpressures along the flight track for the XB–70, B–58, and F–104 airplanes. (Time intervals of flights of the three airplanes varied from about 2 to 5 minutes.)

(Edwards winter data). The data in the table cover a wide range of Mach numbers; in particular, data at $M=3$ obtained at Edwards Air Force Base are included.

A histogram of combined data is shown in figure 8, representing over 4000 data samples taken on ground track for various aircraft. Because the calculation schemes for $\Delta p_{0_{calc}}$ differed slightly, this figure is basically only of qualitative interest.

Measured Overpressure Signatures Along Range

In one of the recent studies with the F–104 airplane, an 8000-foot horizontal (2.44-kilometer) range instrumented with many microphones was employed. The pressures were measured at about 40 stations along the range. Figure 9 shows some results for the overpressures, which indicate a remarkable wavelike pattern. Apparently long waves in the atmosphere of the order of 10^3 meters are influencing the pattern of the results. Experimental results suggest that this is a moving pattern and that the approximate Gaussian distribution pattern for the overpressures would exist at each station. A gradual change along the range from peaked to rounded signature is apparent.

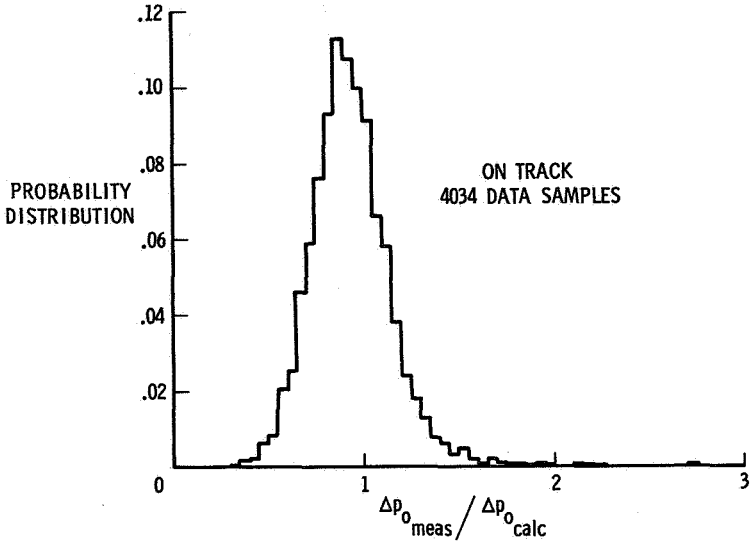

FIGURE 8.—Histogram of combined data taken along ground track for various aircraft.

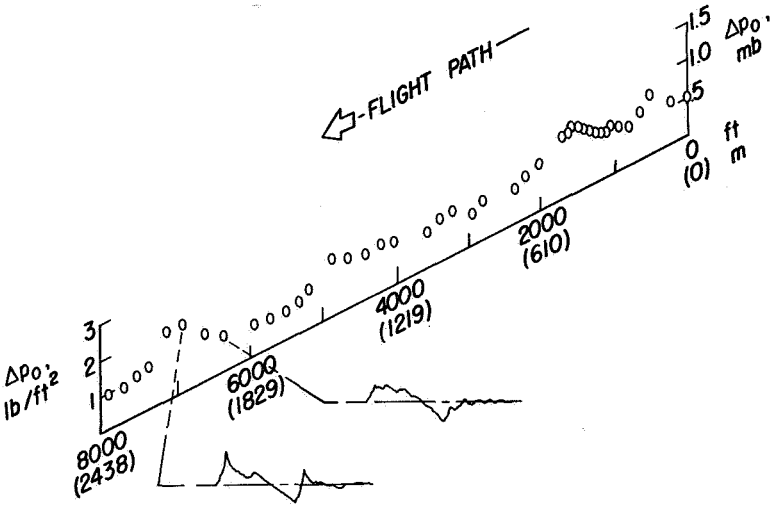

FIGURE 9.—Overpressures as a function of distance on the ground track for F-104 airplane in steady flight at a Mach number of 1.3 and an altitude of 30 500 feet, with two sample signatures.

The measured positive impulse also shows a wavelike pattern, but considerably reduced in variance.

The mechanism of the apparent embedding of the local pattern of turbulence within a systematic larger pattern is not understood. It

is of interest to examine the spectra of two signatures, one having a peaked and the other a rounded wave shape as indicated in figures 9 and 10. The stations for these measured signatures were 600 feet (183 meters) apart. The calculated amplitude squared, or energy, spectra of the signatures are shown in figure 10. Phase plots were also obtained but are not reproduced herein. Only relatively small changes occur in the envelopes of the amplitudes, despite the large change in signatures. As indicated previously in the discussion of figure 3, differences between peaked and rounded signatures may be reflected in the presence or absence of high frequencies in the associated spectra. For the wave shapes and spectra of figure 10, the higher frequencies are apparent for both signatures; but calculations of the relative phases showed that the lower frequencies of the spectra appear well correlated and coherent, whereas for the higher frequencies the relative phases of the two waves tend to become random. The general theory of sound scattering also indicates reduced coherence of sound waves and increased fluctuations in phase with increase in frequency. After passage through uncorrelated patches of turbulence, the higher frequency components of the N-type wave tend to become random both in phase and amplitude. This behavior is also in accord with the central limit theorem in probability. Synthesis of waves with N-wave amplitude distribution and random phase distribution analytically should yield interesting statistics for the peak amplitudes. It is thus suggested that the turbulence scattering leads to a phase scrambling process taking place for the higher frequencies.

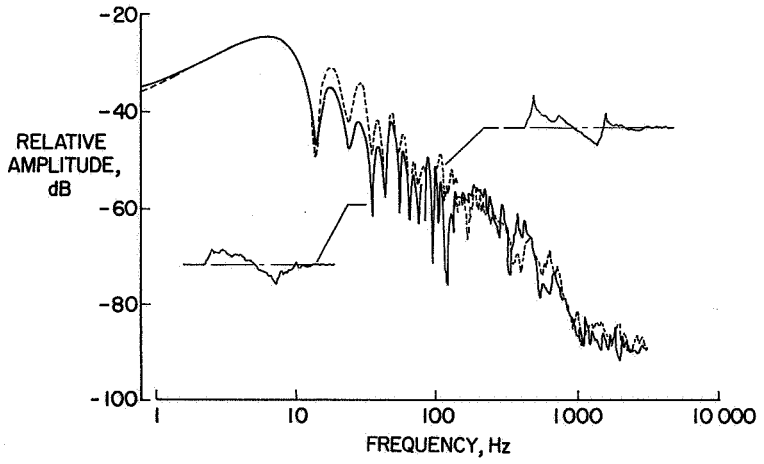

FIGURE 10.—Energy spectra for the two different sonic boom pressure signatures in figure 9. (The relative amplitude is given by 10 $\log_{10}|f(\omega)|^2$.)

CONCLUDING REMARKS

The paper reviews pertinent information obtained in recent years relating to atmospheric effects on the sonic boom and, in particular, includes some results of various flight programs. These atmospheric effects are complex, and a statistical approach appears necessary. The statistics of peak pressures follow approximately a log normal distribution, a result that is indicated by existing theory for pure (sinusoidal) sound. A tabular summary of the flight data gives the standard deviations of pressure peaks relative to nominal calculated values of the mean. Information is included on observed variations of sonic boom signatures for different types and sizes of airplanes. The spectral content of some ideal and some measured pressure signatures is exhibited and discussed with reference to peakedness or roundedness of the wave.

REFERENCES

1. GARRICK, I. E.; and MAGLIERI, D. J.: A Summary of Results on Sonic-Boom Pressure-Signature Variations Associated With Atmospheric Conditions. NASA TN D–4588, 1968.
2. Stanford Research Institute: Sonic Boom Experiments at Edwards Air Force Base. NASBEO–1–67 (Contract AF 49(638)–1758), CFSTI, U.S. Dept. Com., July 28, 1967.
3. KANE, EDWARD J.; and PALMER, THOMAS Y.: Meteorological Aspects of the Sonic Boom. SRDS Rept. No. RD64–160 (AD 610 463), FAA, Sept. 1964.
4. KANE, EDWARD J.: Some Effects of the Atmosphere on Sonic Boom, NASA SP–147, 1967, pp. 49–63.
5. TATARSKI, V. I. (R. A. SILVERMAN, trans.): Wave Propagation in a Turbulent Medium. McGraw-Hill Book Co., Inc., 1961.
6. CHERNOV, LEV A. (R. A. SILVERMAN, trans.): Wave Propagation in a Random Medium. McGraw-Hill Book Co., Inc., 1960.
7. CARLSON, HARRY W.: Correlation of Sonic-Boom Theory With Wind-Tunnel and Flight Measurements. NASA TR R–213, 1964.
8. CROW, S.: Distortion of Sonic Bangs by Atmospheric Turbulence, NPL Aero Rept. 1260, British National Physical Laboratory, Aerodynamics Division, March 11, 1968.
9. LUMLEY, JOHN L.; and PANOFSKY, HANS A.: The Structure of Atmospheric Turbulence. Interscience, c. 1964.
10. SHERLOCK, R. H.; STOUT, M. B.; DOW, W. G.; GAULT, J. S.; and SWINTON, R. S.: Storm Loading and Strength of Wood Pole Lines and a Study of Wind Gusts. Edison Elec. Inst., c. 1936.
11. HOUBOLT, JOHN C.; STEINER, ROY; and PRATT, KERMIT G.: Dynamic Response of Airplanes to Atmospheric Turbulence Including Flight Data on Input and Response. NASA TR R–199, 1964.
12. HILTON, DAVID A.; HUCKEL, VERA; and MAGLIERI, DOMENIC J.: Sonic-Boom Measurements During Bomber Training Operations in the Chicago Area. NASA TN D–3655, 1966.
13. HILTON, DAVID A.; HUCKEL, VERA; STEINER, ROY; and MAGLIERI, DOMENIC J.: Sonic-Boom Exposures During FAA Community-Response Studies Over a 6-Month Period in the Oklahoma City Area. NASA TN D–2539, 1964.

14. HUBBARD, HARVEY H.; MAGLIERI, DOMENIC J.; HUCKEL, VERA; and HILTON, DAVID A. (With appendix by HARRY W. CARLSON): Ground Measurements of Sonic-Boom Pressures for the Altitude Range of 10,000 to 75,000 Feet. NASA TR R–198, 1964. (Supersedes NASA TM X–633.)

Sonic Boom Ground Pressure Measurements for Flights at Altitudes in Excess of 70 000 Feet and at Mach Numbers Up to 3.0

DOMENIC J. MAGLIERI
Langley Research Center, NASA

INTRODUCTION

During the past several years a substantial amount of sonic boom flight research data have been obtained for a wide range of operating conditions. (See Garrick's paper "Atmospheric Effects on the Sonic Boom" in this volume and ref. 1.) The material of this paper relates particularly to the effects of extreme altitude and represents the results of some recent sonic boom signature measurements associated with operation of the SR–71 airplane. The data were obtained during the Edwards Air Force Base Sonic Boom Evaluation Program conducted in 1966–1967 time period (ref. 2). About 2000 data points were recorded from 35 flights at altitudes in excess of 70 000 feet and at Mach numbers to 3.0.

Variations of the measured ground pressure signatures for ontrack and for lateral measuring station locations are illustrated and the statistical variations of the overpressure, positive impulse, wave duration, and shock wave rise time are presented. The above data are useful directly for evaluating the effects of altitude and Mach number on the sonic boom ground exposure patterns. The results of these studies will also permit validation of available theories regarding aircraft source generation and the propagation of shock waves from high altitudes.

WAVEFORM VARIATIONS

Three sample tracings of SR–71 sonic boom pressure time histories measured along the ground track are presented in figure 1. These signatures represent the range of wave shapes observed during these studies, and they are noted to vary from a normal N-wave, to a peaked wave, and to a rounded wave. This type variation is similar to those observed previously for the F–104, B–58, and XB–70 aircraft (ref. 1). The signatures of figure 1 are also used to define the quantities: overpressure, Δp_0, positive impulse, I_0, rise time, τ, positive time duration, Δt_0, and total time duration, ΔT.

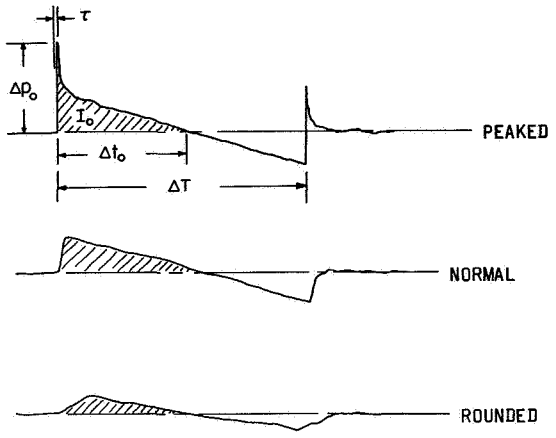

FIGURE 1.—Tracings of measured SR–71 sonic boom pressure-time histories along ground track showing some waveform categories and signature definitions.

GROUND TRACK MEASUREMENTS

Figure 2 includes tracings of sonic boom pressure signatures measured along the ground track of the airplane at various altitudes from below 50 000 feet to in excess of 70 000 feet and Mach numbers to about 3.0. It can be seen that all the waveforms presented are of the N-wave type and are similar in nature to those obtained for the B–58 aircraft of reference 3. In general, the peak-pressure values decrease and the time durations of the waves increase as the altitude of the aircraft is increased. Based on other related analytical work, it is estimated that the sonic boom signature, overpressure, and time period variations are attributable mainly to altitude rather than Mach number effect.

The bow wave peak overpressures obtained from signatures of the type shown in figure 2 are presented in figure 3 as a function of airplane altitude for steady level flight. The data of figure 3 were measured at distances within 3 nautical miles of the aircraft ground track. Each symbol represents an individual mission, the blocked-in symbols being the average of the measurements obtained on 20 to 64 microphones. The circle symbols represent data from flights made during the November 1966 to January 1967 time period for which atmospheric conditions were observed to be somewhat more quiescent than those during the six flights of the June 1966 time period as represented by the diamond symbols. The plot of figure 3 represents results of 28 flights for a total of 928 data samples.

At the present time the calculated sonic boom characteristics of the SR–71 aircraft are not available. However, predicted and measured overpressures (ref. 4, fig. 16, and ref. 3, fig. 30) are available

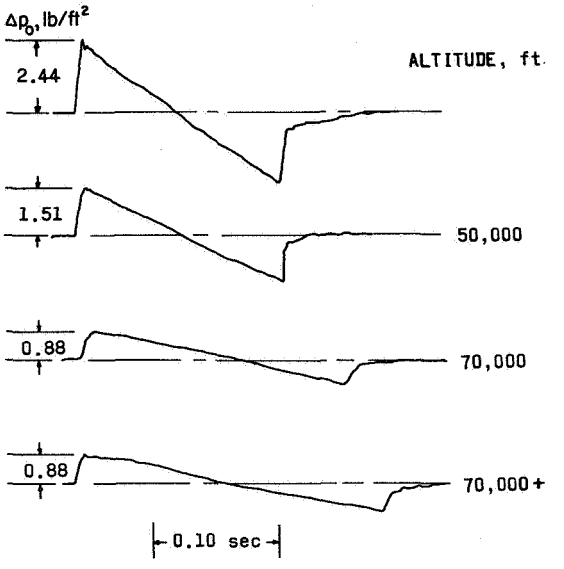

FIGURE 2.—Tracings of SR–71 sonic boom signatures measured along ground track for aircraft at various altitudes and Mach numbers.

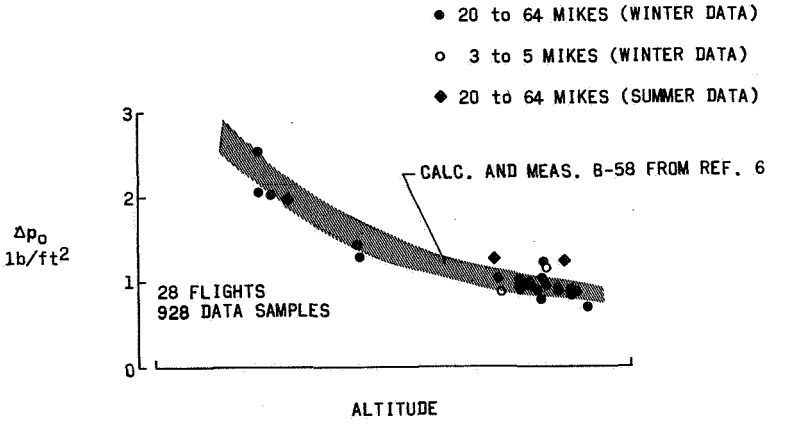

FIGURE 3.—Measured peak overpressures along ground track as a function of altitude for airplanes in steady level flight. Data are for a range of Mach numbers to 3.0.

for the B–58 aircraft, which is about the same size and weight as the SR–71, and the above B–58 data are shown as the stippled band in figure 3 for comparison.

It can be seen from figure 3 that the SR–71 measurements are in general agreement with the measurements and calculations for the B–58 operating in the same altitude range. This result would suggest

that no unusual phenomena are observed because of the extreme altitude flight conditions of these tests.

Since average values are plotted in figure 3, the data points do not represent the extreme variations of the measurements. Variations of the individual measurements will be illustrated in subsequent figures.

LATERAL SPREAD MEASUREMENTS

Figure 4 contains tracings of sonic boom signatures at various lateral distances out to about 27 miles from the ground track for flights at an altitude of about 70 000+ feet and a Mach number of about 3.0. As seen in figure 2, the pressure signatures have the gross features of N-waves except for extreme lateral distances. The rise times of the signatures of figure 4 become longer and the overpressures decrease as the lateral distance from the flight track increases. The wave period, however, does not seem to vary in a systematic manner with increasing distance as was the case for increasing altitude in figure 2. These findings are similar to those obtained for other aircraft (refs. 3 and 5).

Overpressure data from signatures of the type shown in figure 4 are plotted in figure 5 as a function of lateral distance from the flight track for two altitude ranges. The solid curves shown in figure 5 are the predicted overpressure variations for the B–58 aircraft (ref. 4). The dashed vertical lines are estimates of the lateral extent of the pressure patterns based on atmospheric refraction (ref. 6). The

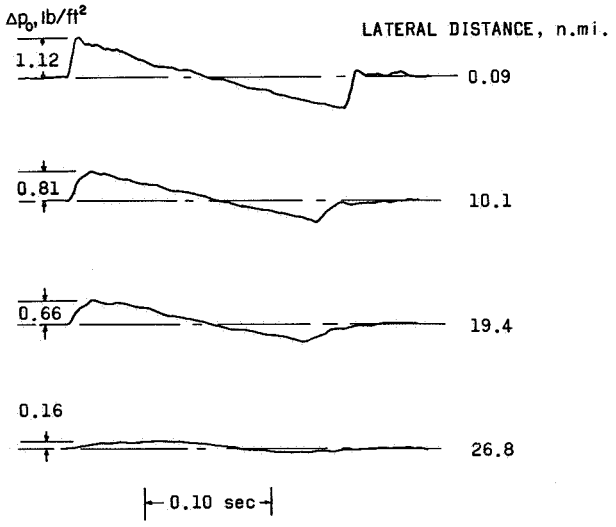

FIGURE 4.—Tracings of SR–71 sonic boom ground pressure signatures as measured at various lateral distances from the ground track for the aircraft at an altitude of 70 000+ feet and a Mach number of about 3.0.

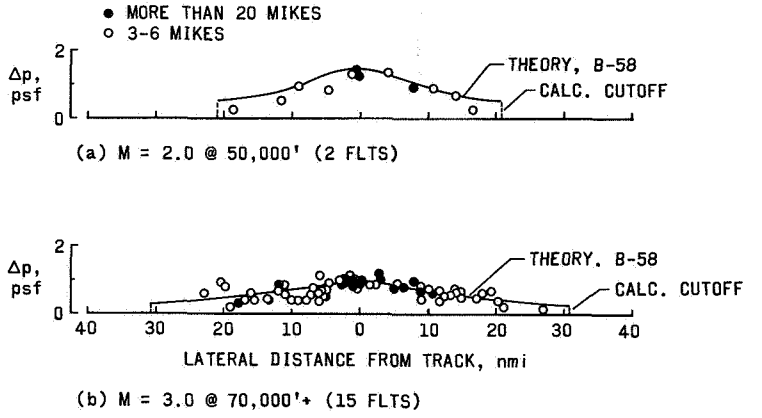

FIGURE 5.—Sonic boom overpressures for the SR–71 aircraft as a function of lateral distance for two different flight conditions.

overpressures are seen generally to be a maximum along the ground track and to decrease with increasing lateral distance. The prediction of the lateral cutoff point appears to correlate well with the data for the Mach number and altitude ranges of these tests.

STATISTICAL VARIATIONS

Analyses of the SR–71 data have been made to determine the statistical variations of peak overpressures, Δp_0, positive impulse values, I_0, time durations, Δt_0 and ΔT, and rise times. These data are presented in the form of histograms in figures 6 through 9 for all flights in the altitude range 70 000+ feet and for measurements made within ± 3 miles of the aircraft ground track.

Figure 6 contains a histogram showing the variation of the measured ground pressures. The results shown are for 22 flights giving 704 data samples. The overpressure interval for plotting was taken as 0.05 psf. It can be seen that the largest number of events is associated with overpressure values of the order of 0.9 psf. Values ranged from about 0.55 psf to about 2.0 psf, and one extreme value of about 2.6 psf was encountered.

A presentation similar to that of figure 6 is shown in figure 7 for the positive impulse values. An examination of the histogram of figure 7 indicates that the variability in the impulse is generally less than for the associated overpressures of figure 6, and this result is consistent with the findings of other similar studies.

Figure 8 includes histograms showing the variability of the total time durations, ΔT, and the positive time durations, Δt_0, of the SR–71 sonic boom signatures. It can be noted that variations of the order of ± 25 percent exist, and these results are consistent with

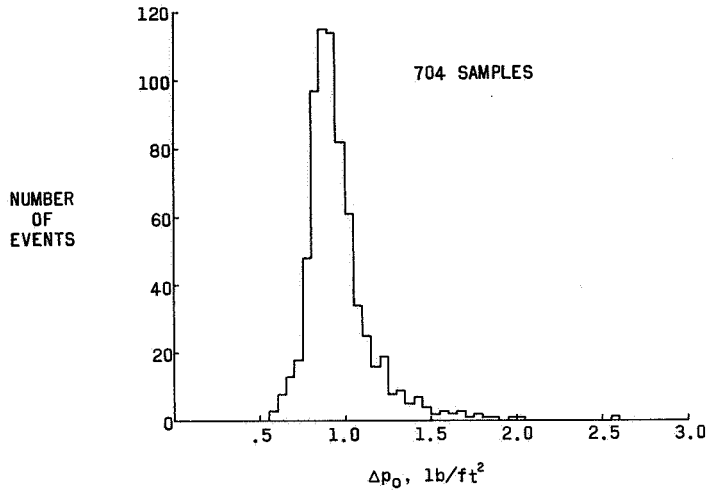

FIGURE 6.—Histogram showing variability of peak bow wave overpressure of SR–71 sonic boom signatures for aircraft operating at 70 000+ feet and Mach number about 3.0. Data are for measurements within ±3 nautical miles of ground track.

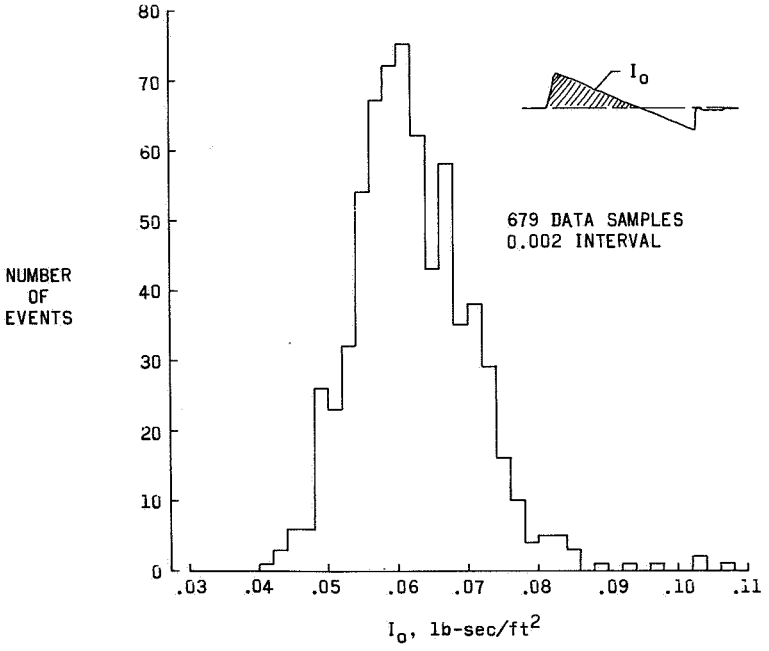

FIGURE 7.—Histogram showing variability of positive impulse or SR–71 sonic boom signatures for aircraft operating at 70 000+ feet and Mach number about 3.0. Data are for measurements within ±3 nautical miles of ground track.

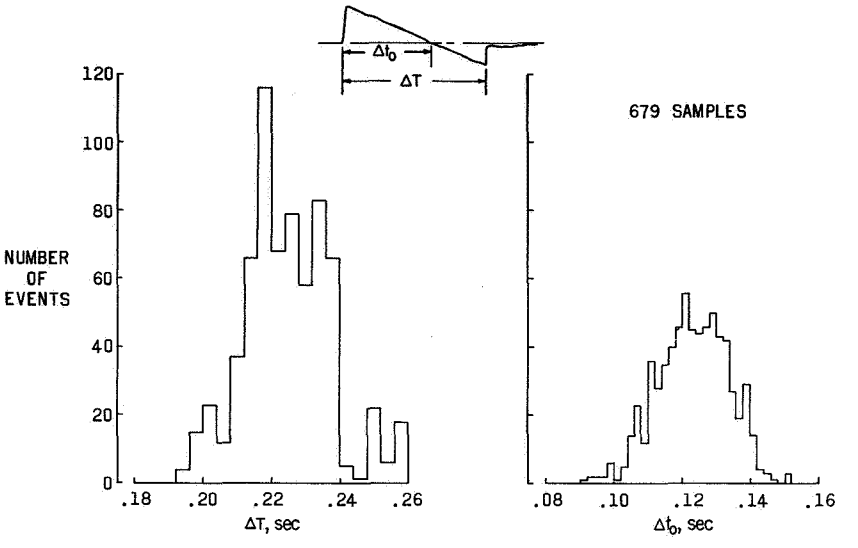

FIGURE 8.—Histograms showing variability of the time durations of SR–71 sonic boom signatures for aircraft operating at 70 000+ feet and Mach number about 3.0. Data are for measurements within ±3 nautical miles of ground track.

similar data shown for the B–58 in reference 2. Variations of the positive time durations and the overpressures can both cause variations in the impulse; however, inspection of figures 6, 7, and 8 suggests that the overpressure variation is the dominant factor.

The data of figure 9 relate to the rise times of the waves. Rise time data per unit overpressure are plotted in histogram form using a plotting interval of 0.001. For the types of waves illustrated schematically in figure 1, the rise time is defined as the time from the onset of bow shock overpressure to the time of the maximum overpressure value. It can be seen that rise time ratios (and therefore absolute rise times since the overpressures are of the order unity) of from near zero to as large as about 0.065 are observed and the most frequently encountered value is about 0.01. Generally longer rise times are associated with rounded waveforms and much shorter rise times are associated with peaked waveforms.

Since the rise time of the wave is a significant factor in the subjective response to sonic booms, an evaluation of this parameter was made for the range of flight conditions encountered. These data are presented in figure 10 as the variation of the bow wave rise times per unit overpressure as a function of altitude for measurements made within ±3 miles of the ground track. The data symbols represent the average values of the measurements and the vertical lines indicate

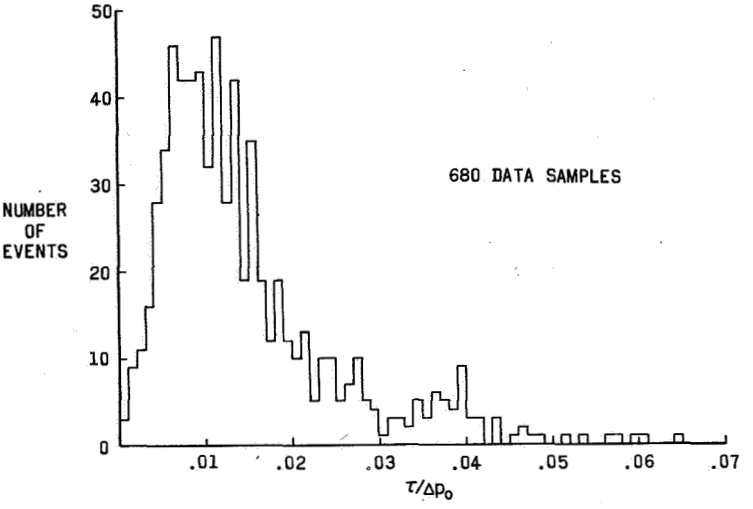

FIGURE 9.—Histogram showing variations of bow wave rise time to peak value of overpressure as measured from flights within ±3 nautical miles of ground track for the altitude range 70 000+ feet.

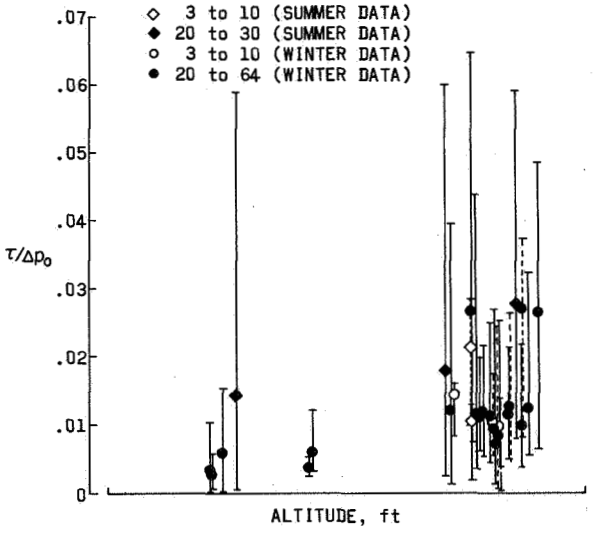

FIGURE 10.—Variation of boom wave rise time to peak value of overpressure as measured from SR–71 flights within ±3 nautical miles of ground track as a function of altitude. Data symbols represent average values for each flight along with maximum and minimum values observed.

the extreme spread of the data observed for each particular flight. It can be seen from the figure that there is considerable scatter, but, in general, the rise time per unit overpressure increases as the altitude of the aircraft increases. These results are similar to those obtained for the B–58 aircraft of reference 7. There is, therefore, the suggestion that the increased altitude results generally in longer rise times.

CONCLUDING REMARKS

Sonic boom measurements have been obtained from 35 flights of the SR–71 vehicle at altitudes in excess of 70 000 feet and Mach numbers to 3.0. No unusual phenomena were encountered for the extreme altitude and Mach number ranges of these tests, and the results fit generally into the established patterns of other available sonic boom flight data from F–104, B–58, and XB–70 aircraft.

REFERENCES

1. SEEBASS, A. R., ED.: Sonic Boom Research. NASA SP–147, 1967.
2. Stanford Research Institute: Sonic Boom Experiments at Edwards Air Force Base. NSBEO–1–67 (Contract AF 49(638)–1758), CFSTI, U.S. Dept. Com., July 28, 1967.
3. HUBBARD, HARVEY H.; MAGLIERI, DOMENIC J.; HUCKEL, VERA; and HILTON, DAVID A. (with appendix by HARRY W. CARLSON): Ground Measurements of Sonic-Boom Pressures for the Altitude Range of 10,000 to 75,000 Feet. NASA TR R–198, 1964. (Supersedes NASA TM X–633)
4. CARLSON, HARRY W.: Correlation of Sonic-Boom Theory With Wind-Tunnel and Flight Measurements. NASA TR R–213, 1964.
5. MAGLIERI, DOMENIC J.; HILTON, DAVID A.; and MCLEOD, NORMAN J.: Experiments on the Effects of Atmospheric Refraction and Airplane Accelerations on Sonic-Boom Ground-Pressure Patterns. NASA TN D–3520, 1966.
6. RANDALL, D. G.: Methods for Estimating Distributions and Intensities of Sonic Bangs. R. & M. No. 3113, British A.R.C., 1959.
7. MAGLIERI, DOMENIC J.; PARROTT, TONY L.; HILTON, DAVID A.; and COPELAND, WILLIAM L.: Lateral-Spread Sonic-Boom Ground-Pressure Measurements From Airplanes at Altitudes to 75,000 Feet and at Mach Numbers to 2.0. NASA TN D–2021, November 1963.

Laboratory Sonic Boom Research and Prediction Techniques

HARRY W. CARLSON
Langley Research Center, NASA

INTRODUCTION

The present discussion is intended to serve as an addendum to the report "Experimental and Analytic Research on Sonic Boom Generation at NASA" given at the NASA Conference on Sonic Boom Research, April 12, 1967, and published in NASA SP–147. Among the topics to be considered are refinement of the prediction methods which were discussed at some length in the previous report and the extension of wind-tunnel tests into the low hypersonic speed range. In addition, attention is directed to experimental data applicable to the multipole concepts for boom reduction under current consideration. Finally, some preliminary laboratory experiments dealing with shock propagation are described.

SYMBOLS

A	effective cross-sectional area
h	airplane altitude or lateral distance from model
l	airplane or model length
M	Mach number
Δp	incremental pressure attributed to flow field of airplane or model
Δt	time increment measured with respect to the arrival of the airplane bow shock
Δx	distance measured parallel to airplane or model longitudinal axis from bow-shock position to point on pressure signature
α	angle of attack
δ_E	elevon deflection
Δh	vertical separation distance between generating airplane and probe airplane

DISCUSSION

Data from recently completed wind-tunnel tests of a 6-inch-long model of the XB–70 airplane are now being utilized in an effort to assess the applicability of present theoretical prediction methods to a complex configuration in the sensitive extreme near-field region of the flow. For the sample data shown in figure 1, it is seen that the basic theory which considers the area distribution for $M=1.5$ area rule cutting planes and the lift distribution for a flat wing surface

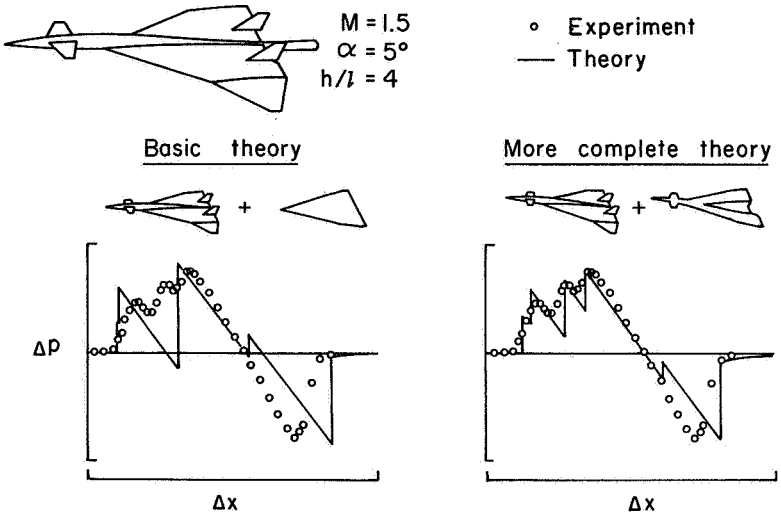

FIGURE 1.—XB–70 wind-tunnel data use in refinement of prediction techniques.

does not completely predict the shape of the measured signature. A more complete theoretical treatment which considers the angle of attack attitude in derivation of the area and lift developments, and which accounts for interference effects by employment of a newly developed computing program for a warped lifting surface in conjunction with a canard or horizontal tail, is seen to result in an improved correlation. It should be pointed out, however, that for the large distances encountered in flight, where the signature is more fully developed, the more complete theory would result in an almost negligible change in the prediction. The impulse calculated for the more complete theory is only 2 percent greater than for the basic theory. The measured impulse is about 10 percent greater than the predicted value, which indicates a 5 percent difference in the extrapolated value of the bow shock at large distances. In view of uncertainties concerning the nature of the model boundary layer, it is not known whether extrapolated experimental data or the theory

would offer the best estimate for the airplane. A completely laminar boundary was assumed for the model calculations.

Analysis of signatures obtained in probe flights for the B–58 airplane have brought to light an unexpectedly large effect of control surface deflection. As shown in figure 2, an improved correlation of experiment and theory results where the theory accounts for the estimated 7.5° deflection of the elevon (trailing edge up). Because of the increase in the impulse, this effect is expected to account for

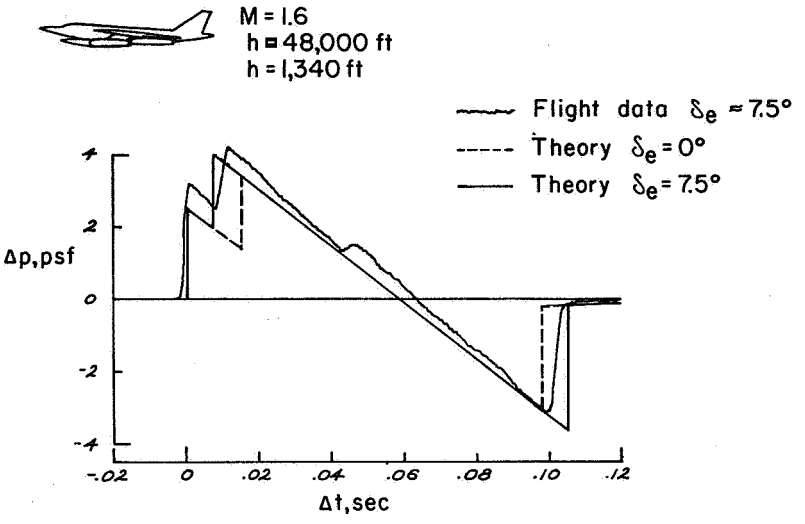

FIGURE 2.—B–58 probe flight data use in refinement of prediction techniques.

about a 5-percent increase in ground overpressures. Elevon deflection can have this degree of influence on the positive part of the signature because more lift must be generated on the forward part of the airplane to compensate for the negative lifting force on the control surface. Thus it is suggested that control deflections be taken into account whenever high precision is required in theoretical predictions. However, it is believed that this particular case of airplane and flight condition represent a rather extreme situation.

As a first step in the extension of the Langley wind-tunnel program to hypersonic speeds, tests were performed on a systematic series of body shapes at Mach numbers up to 4.63. An example of data from these tests is shown in figure 3. For the lower Mach number, the correlation of theory and experiment is quite good, at least for the positive part of the signature, and is representative of results obtained at Mach numbers below 3 for slender bodies. As might have been expected, discrepancies between theory and experiment increase

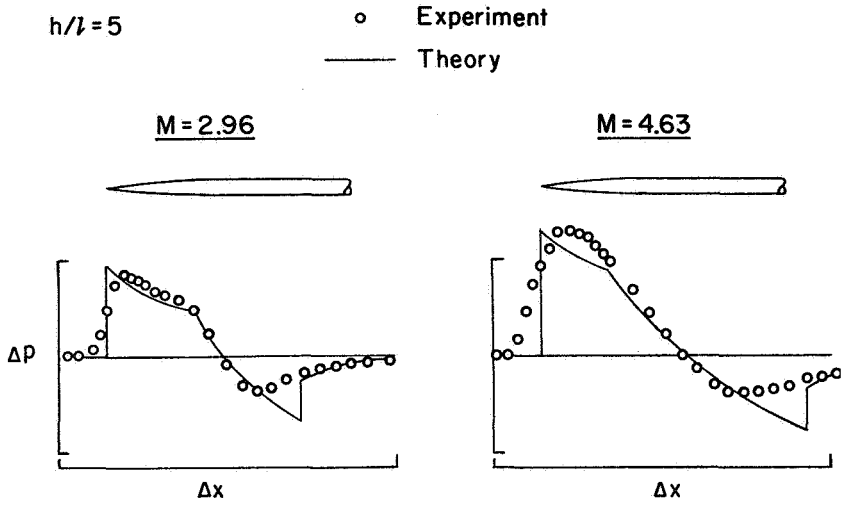

FIGURE 3.—Preliminary wind-tunnel tests at high supersonic speeds.

with increasing Mach number and with increasing diameter-to-length ratio. Part of the discrepancy may be attributed to the increased model boundary-layer effect at the higher Mach numbers. The theory shown in the figure does not include the effect of boundary-layer thickness. However, it seems clear also that there is some failure of the Whitham method and that further theoretical studies are required. The body of revolution tests will be supplemented by an experimental investigation of simple lifting wings at speeds up to $M=4.63$ planned for the near future.

With the current interest in the use of multipoles as a means of achieving sonic boom reductions, it is thought appropriate to reexamine the results of wind-tunnel tests dealing with this subject. The purpose of the experiments, which were conducted about 10 years ago at the request of Dr. Busemann, was to examine the persistence of the directional properties of shocks created by quadrupoles. Measured signatures for a quadrupole device having a hatchet shape are shown in figure 4. As shown by the data, although there are quite large differences in pressure signature characteristics at one body length, the flow has become nearly axially symmetric at only eight body lengths.

In another of the tests, a ducted quadrupole was studied. The shape was formed by distortion of a cylinder 2 inches in length and 0.625 inch in diameter to form a 2:1 ellipse inlet section and a 2:1 ellipse exit section with major axes 90° apart. Data for this configuration, shown in figure 5, indicate a significant difference at

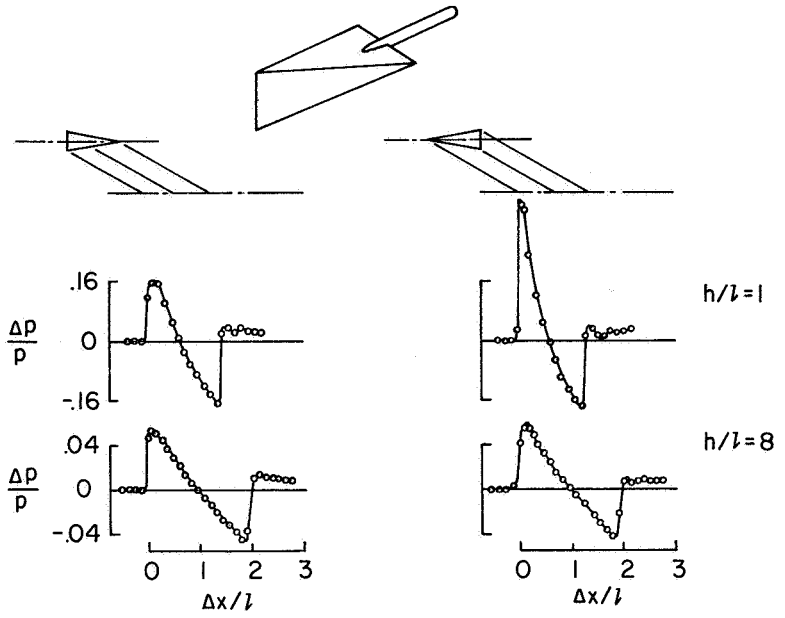

FIGURE 4.—Wind-tunnel tests of a multipole device. Quadrupole, $M=2.0$.

eight body lengths between the signatures measured below and to the side of the configuration. Differences in impulse suggest that a 10-percent difference in far-field overpressures should be expected. These results, then, indicate that significant directional properties are produced by quadrupoles only when the pressure-producing surfaces are displaced a significant distance from the body axis.

Because these directional properties are achieved at the expense of large departures from conventional aircraft geometry and because the benefits may stem in part from the increase in effective body length defined by supersonic area rule concepts, the results are compared in figure 6 with an estimated signature for a parabolic body having the same effective length and the same maximum cross-sectional area. The area distribution for the quadrupole body (determined by $M=2.0$ cutting planes) includes the effect of an estimated laminar boundary layer and has the stream-tube capture area removed. This analysis indicates that benefits of the quadrupole are slight when compared with the simpler expedient of lengthening the body.

This survey of miscellaneous research items will conclude with a description of some recent laboratory studies of shock-wave propagation conducted by Dr. Raymond Barger of the Langley Research Center. The peculiar behavior of a shock wave in the region near a focus was studied by means of the experimental setup shown in

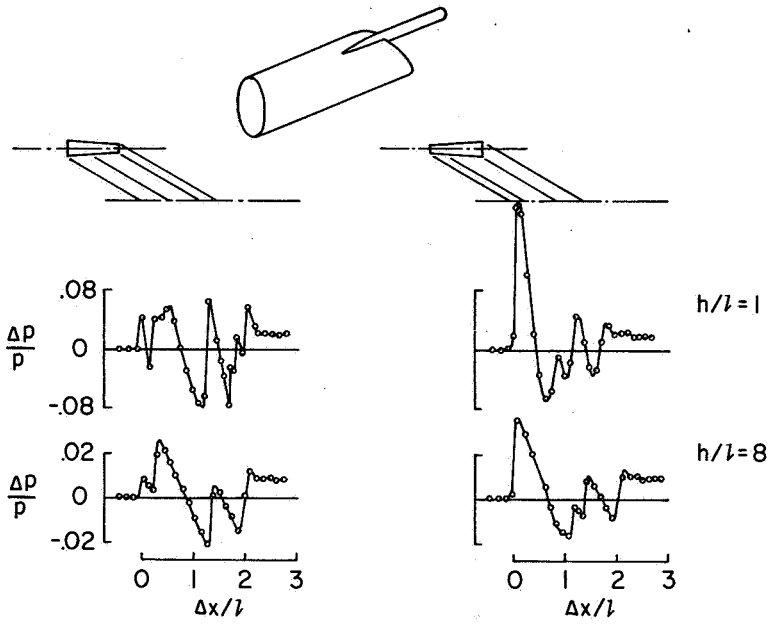

FIGURE 5.—Wind-tunnel tests of a multipole device. Ducted quadrupole, $M=2.0$.

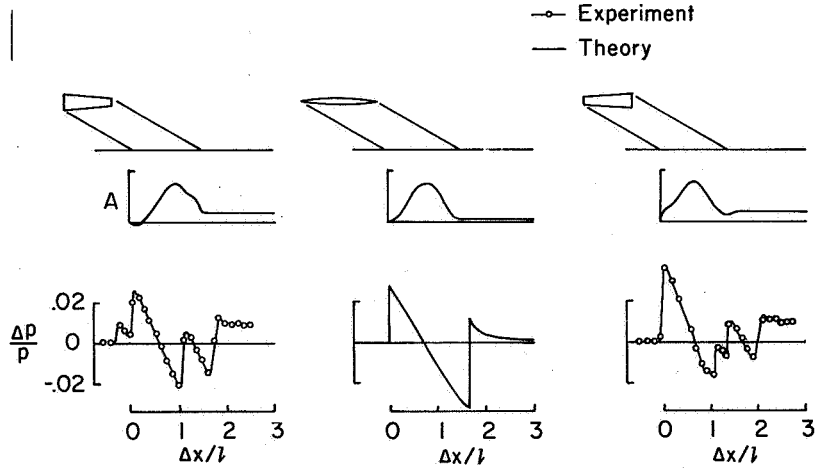

FIGURE 6.—Ducted quadrupole compared with a parabolic body. $M=2.0$, $h/l=8$.

the sketch of figure 7. An N-wave signature triggered by a spark was reflected from parabolic mirrors so as to converge the shock front at a sharply defined focus. Before the focus, as shown in the signature at the left, there is a normal N-wave with a leading positive pressure jump. At the focus the measurements show not only a large amplification of the shock intensity, but also a change in signa-

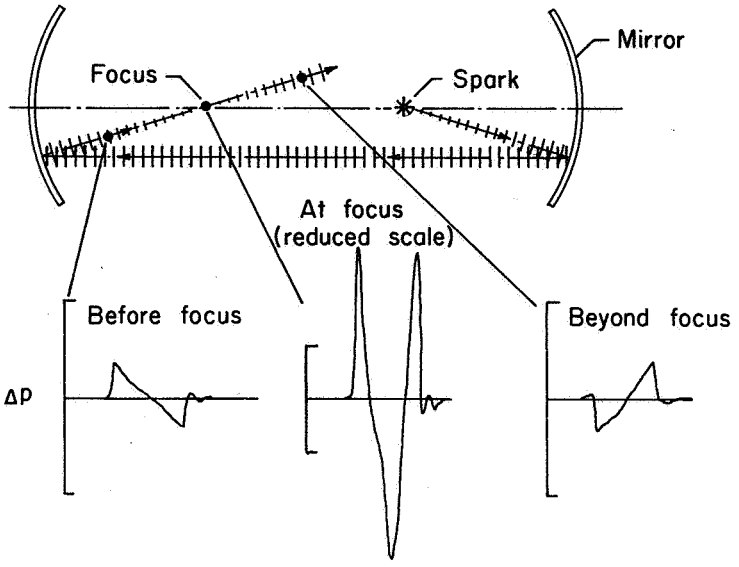

FIGURE 7.—Laboratory study of shock field behavior at and near a focus.

ture shape identified as a phase shift of 90°. Beyond the focus there is the interesting condition of a leading expansion portion of the signature and a signature which corresponds to an 180° phase shift. These results are in agreement, at least qualitatively, with the predictions given by the laws of geometric acoustics.

A second laboratory experiment deals with focusing a shock front in the presence of a temperature gradient. In this experiment a small projectile was fired down an instrumented range in which was placed a chamber with a heated wall to produce a temperature gradient normal to the path of the projectile. The primary instrumentation consisted of pressure transducers and apparatus for schlieren photography. Some of the photographic results are shown in figure 8. The path of the projectile traveling at a Mach number of about 1.1 is indicated at the top of each photograph. For the photograph at the left, there was no temperature gradient. At the center where a moderate temperature gradient was introduced, a noticeable curvature of the shock front is evident. The temperature is higher near the bottom of the picture, corresponding to the real atmosphere situation. At the right, the gradient is large enough so that the speed of sound near the center of the field is equal to the speed of the body. There, as would be expected, the shock front becomes normal to the flight path and loses its identity.

With further development, these laboratory techniques could serve

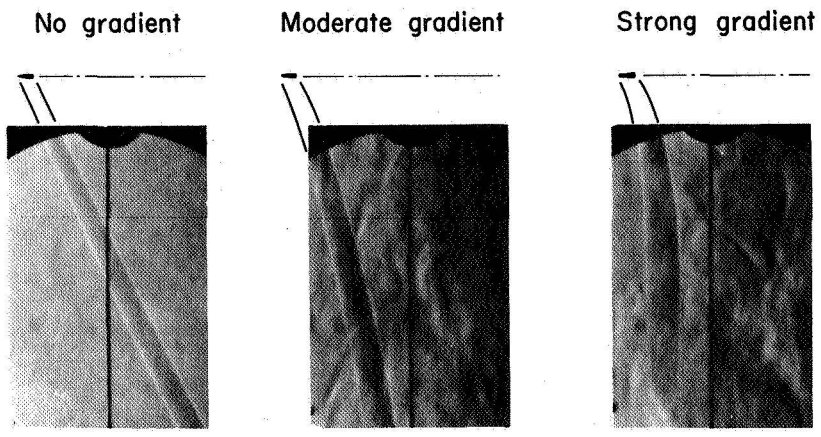

FIGURE 8.—Laboratory study of shock field behavior in a temperature gradient

a valuable purpose in the study of various aspects of propagation theories which have been developed and others which are now being developed.

Configuration Design for Specified Pressure Signature Characteristics

F. EDWARD MCLEAN
Langley Research Center, NASA

INTRODUCTION

Near-field design concepts, which have evolved from NASA studies (refs. 1–3), appear to offer a promising means for alleviating the sonic boom problem associated with the supersonic transport (SST). These studies have shown that, for certain flight conditions, the effective shape of a large airplane can be tailored to provide ground pressure signatures which may be more desirable than the typical far-field N-wave. This paper presents design requirements for the plateau pressure signature and the signature with finite rise time, two signature shapes which exhibit interesting possibilities for sonic boom reduction. Consideration will be given to problems associated with the practical attainment of these pressure signatures within the normal operating regime of a supersonic transport.

SYMBOLS

A_e	effective area distribution of airplane or model equivalent body, including effect of lift as well as volume
x	distance measured along longitudinal axis from airplane or model nose
$\triangle p$	incremental pressure attributed to flow field of airplane or model
p	reference pressure
M	Mach number
h	altitude
W	weight
$\triangle t$	incremental time from onset of pressure disturbance
W_g	gross weight
t_r	time required for maximum pressure rise within pressure disturbance (see fig. 5)
$\triangle x$	distance measured parallel to longitudinal axis of airplane from point on linear theory characteristics from nose of airplane to point on pressure signature

NEAR-FIELD SIGNATURES UNDER CONSIDERATION

During the course of research on the sonic boom problem, NASA has investigated the pressure rise characteristics of a number of airplane configurations and equivalent body shapes (refs. 1–5). Considerations of near-field design concepts have been focused on the generating shapes and signature types illustrated in figure 1. In the left side of the figure is the plateau pressure disturbance. This signature shape, which is generated by an effective area development that varies as the three-halves power of distance along the axis, is characterized by a constant pressure region behind the bow shock. For airplane operating conditions where it is possible to generate this type of signature on the ground, the total pressure rise in the disturbance would be somewhat less than that of the corresponding far-field N-wave (ref. 1). The plateau pressure signature has found particular application in the reduction of sonic boom overpressures during the critical transonic climb portion of a supersonic transport mission.

A pressure signature with finite rise time is illustrated in the right side of figure 1. This signature is generated by an effective area distribution, which varies as the five-halves power of distance along the axis, to about the midpoint of the body length. Aft of the body midpoint, the area development is a much more complicated variation with distance along the axis. The interesting feature of the pressure signature with finite rise time is that there is no instantaneous

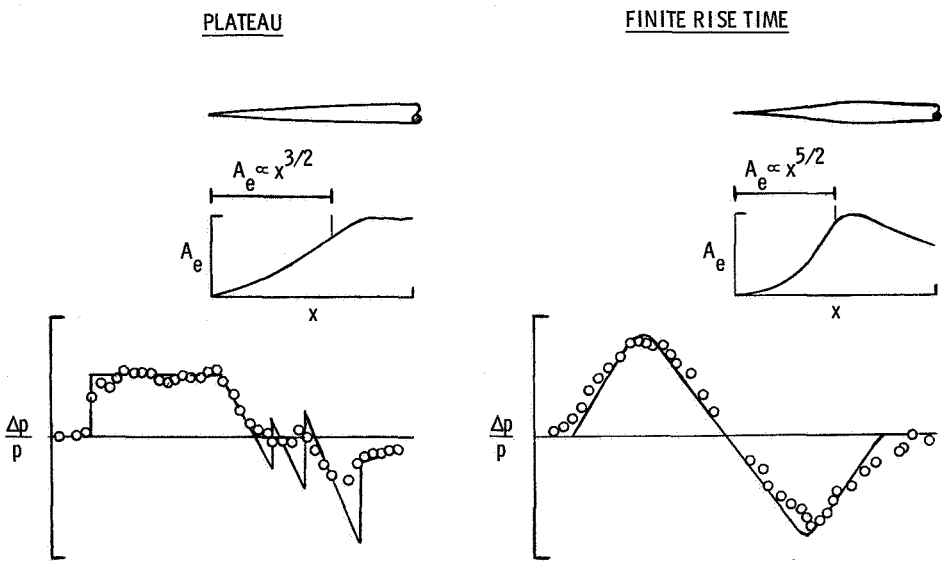

FIGURE 1.—Near-field pressure signatures under construction.

shock pressure jump, but rather a gradual pressure rise at both the bow and tail portions of the signature. If the buildup in pressure can be extended over an appreciable rise time, on the order of 10 to 15 milliseconds, there are indications that the noise associated with the sonic boom disturbance can be virtually eliminated (refs. 3 and 4). However, because of the extreme design requirements for this type of signature, the practicality of its application is still under investigation.

Note that the experimental pressure signatures of figure 1 were measured in the flow fields of bodies of revolution with the required area developments. The work of Hayes (ref. 6) permits relationships to be drawn between the pressure rise characteristics of equivalent bodies of revolution and lifting airplane configurations. These relationships have been widely used in sonic boom investigations.

USE OF PLATEAU SIGNATURE IN DOMESTIC SST STUDY

The sonic boom problem raises some serious questions as to the acceptability of domestic or overland flight of the supersonic transport. Because of the economic importance of such a domestic operation, however, the Langley Research Center of NASA has recently conducted a study of the feasibility of a relatively low-boom, domestic supersonic transport. In the development of the domestic SST study configuration, the most advanced aerodynamic technology and concepts were utilized. Near-field design procedures were used to take advantage of the sonic boom overpressure reductions which have been indicated for the plateau pressure signature.

The manner in which near-field design concepts were applied to

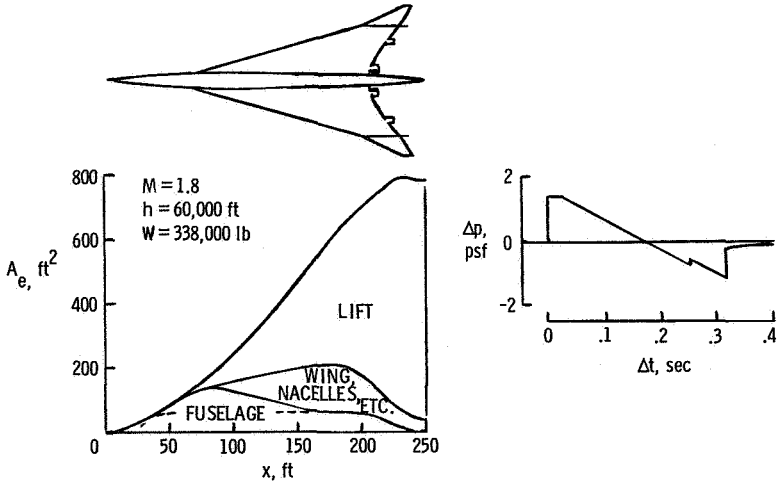

FIGURE 2.—Use of plateau signature in domestic SST study.

the domestic SST study configuration is illustrated in figure 2. Because airplane shaping for a specified signature can be accomplished only at one flight condition, a near-field design Mach number (M= 1.8) was chosen, intermediate between the critical transonic (M=1.2) and cruise (M=2.7) Mach numbers. At the design Mach number (M=1.8), the volume and lift elements of the airplane were carefully tailored to provide a three-halves power effective area distribution for the assumed altitude of 60 000 feet and airplane weight of 338 000 pounds. The plateau pressure signature which would be expected for these flight conditions is shown in the right side of figure 2.

Near-field sonic boom overpressures which would be generated by the domestic SST study configuration are compared with corresponding far-field or N-wave overpressures in figure 3. For most of the flight Mach number regime, the previously mentioned application of near-field design concepts leads to overpressure levels considerably below far-field values. The sonic boom characteristics of the study configuration vary little with Mach number and are at a level of about 1.4 psf. Note that the benefits from the plateau pressure design are felt on either side of the near-field design point and persist up to the cruise Mach number of 2.7. At cruise conditions, however, the sonic boom approaches far-field levels.

Although only minimum overland flights of proposed international supersonic transports are currently anticipated, some consideration is being given to off loading fuel from these airplanes for the shorter domestic ranges of about 2500 nautical miles. It would be interesting, therefore, to compare the sonic boom characteristics of these off-loaded

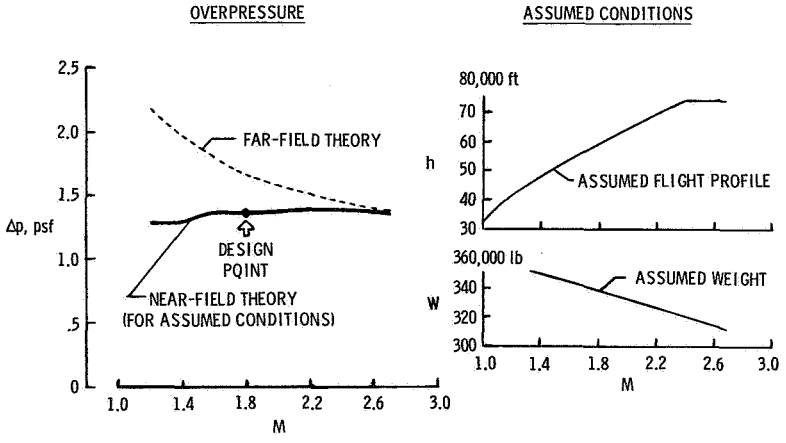

FIGURE 3.—Sonic boom characteristic of domestic SST study configuration compared with far-field theory.

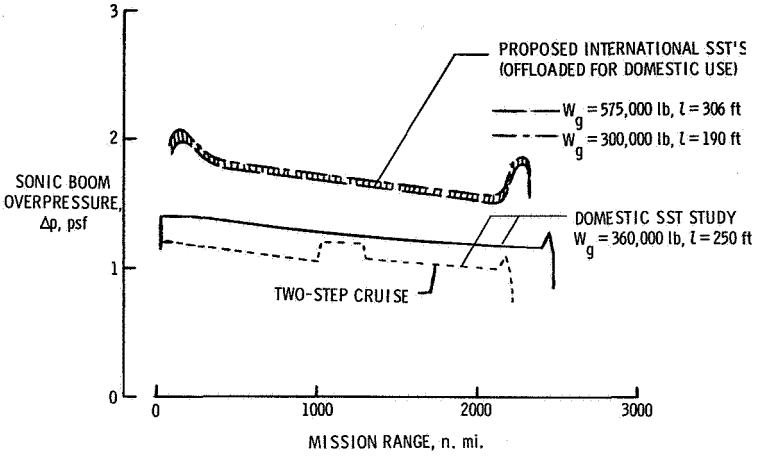

FIGURE 4.—Sonic boom of domestic SST study configurations compared with sonic boom of proposed SST's.

international SST's with the sonic boom characteristics of the NASA domestic SST study configuration. This comparison is made in figure 4. The band of values at the top of the figure represents the sonic boom characteristics of off-loaded versions of proposed international SST's as a function of mission range. For these airplanes, the overpressures approach 2.0 psf at the beginning and end of the mission and reach a minimum value of about 1.7 psf at the end of cruise. Note that the relatively small ($W_g = 300\,000$ pounds, $l =$ 190 feet), European-proposed international SST has slightly higher overpressure levels than the large ($W_g = 576\,000$ pounds, $l = 306$ feet), American-proposed SST.

The curves at the bottom of figure 4 indicate the sonic boom overpressure levels for the NASA domestic SST study configuration for two operating procedures. The solid curve corresponds to a one-step cruise operation at a Mach number of 2.7, and the dashed curve represents a two-step cruise procedure with cruise legs at $M = 1.6$ and $M = 2.7$. For one-step cruise operation, the maximum overpressure of the domestic study configuration is 1.4 psf, and the minimum overpressure is approximately 1.2 psf. The two-step cruise procedure leads to approximately a 0.2-psf reduction in sonic boom overpressure at some loss in range capability. Note that the overpressure levels for the NASA domestic SST study configuration are some 0.6 to 0.8 psf less than the values shown for proposed international SST's which have been adapted to domestic operation. This suggests the possible desirability of developing a supersonic transport configuration specifically for overland use.

CONSIDERATIONS OF PRESSURE SIGNATURES WITH FINITE RISE TIME

One of the most undesirable characteristics of the sonic boom disturbance is the instantaneous pressure jump which is normally associated with the bow and tail wave of the disturbance. The elimination or modification of these sharp pressure jumps would appear to be desirable. In reference 3, consideration was given to the design criteria necessary to spread the bow pressure rise over a finite time, and thus eliminate the instantaneous bow pressure jump. For normal operating conditions of the supersonic transport, this finite rise time consideration led to rather extreme design requirements of airplane length and slenderness. If the tail pressure jump is similarly modified to provide a finite rise time, more extreme design requirements would obviously result.

Figure 5 indicates the rather extreme design requirements necessary to produce a ground pressure disturbance with finite rise times at both the bow and tail of the disturbance. The figure is drawn for typical cruise conditions of a supersonic transport, $M=2.7$ and $n=$ 61 000 feet. To provide desirable rise times of 10 to 15 milliseconds at the ground, extreme airplane effective lengths are required. For anticipated supersonic transport weights, of the order of 600 000 pounds, an effective length of approximately 1000 feet would be required for the assumed operating conditions. In addition, the airplane effective area distribution would have to follow the development shown in figure 1 for a signature with finite rise time.

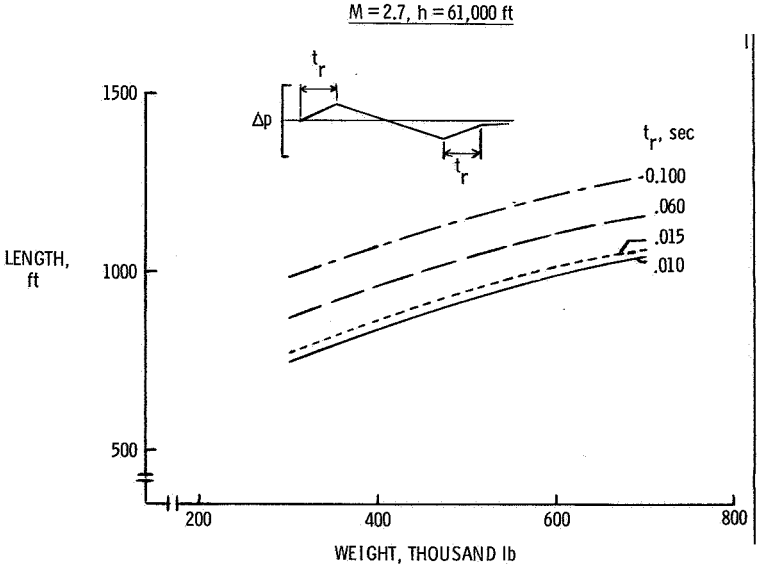

FIGURE 5.—Design requirements for signature with finite rise time.

The geometric problem associated with application of the extreme design requirements of figure 5 to a typical supersonic transport configuration is illustrated in figure 6. To produce a pressure signature at the ground with a desired 10- to 15-millisecond rise time, the effective area development of the basic configuration would be modified to the area distribution indicated by the dashed curve. This modification would require a substantial increase in effective area and length extensions of 400 feet ahead of and 300 feet behind the basic configuration. Such a geometric modification appears to be impractical.

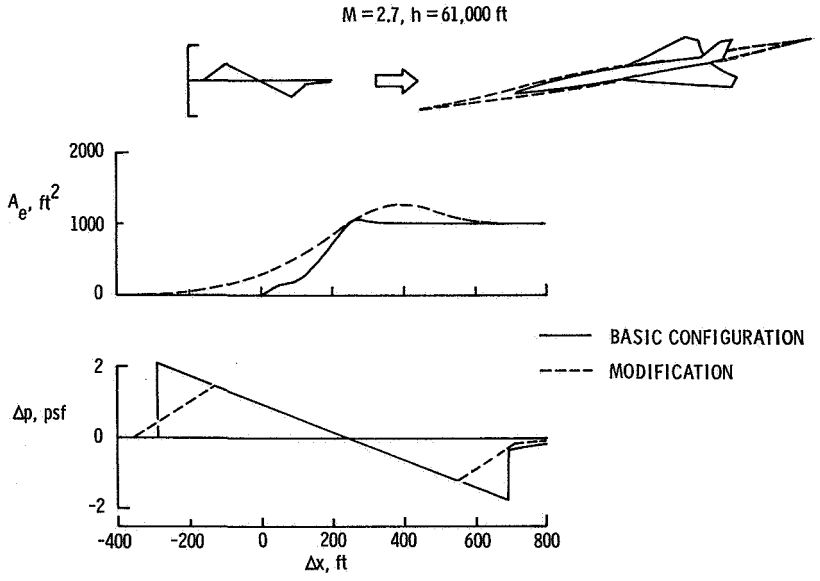

FIGURE 6.—SST modification for finite rise time.

Several schemes, such as the use of electrostatic effects or laser beams, have been proposed as possible ways of increasing the effective area and length of an airplane without resorting to geometrical modifications. Questions have risen as to how these schemes will provide the required control over area development or what the power costs would be. Recently, Carlson of NASA instituted a research program to provide answers to the latter question. Assuming that some unidentified force field or heat source is available, Carlson will determine the power required to create around the existing geometrical configuration a "phantom" body which will produce a pressure signature with finite rise time.

The model for Carlson's investigation is illustrated in figure 7. An entering stream tube of air, A_0, will be acted on by force or heat to produce the phantom boundary illustrated at the top of the figure.

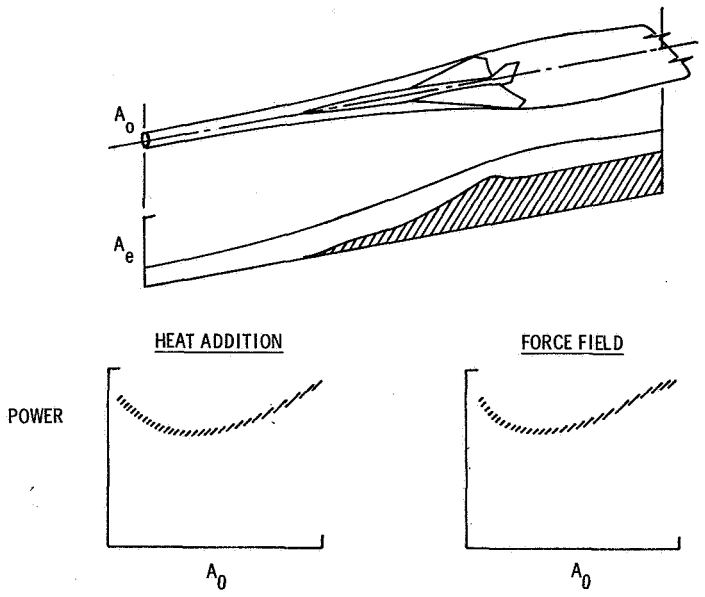

FIGURE 7.—Power requirements for creation of phantom body.

This boundary will alter the effective area distribution as indicated in the middle of the figure, with the cross-hatched region corresponding to the airplane and the solid curve representing the phantom body. Power required will vary with A_0 as indicated at the bottom of the figure. Preliminary results indicate that twice the maximum engine power available would be required to produce the modified signature illustrated in figure 6.

The extreme geometric modifications or power required to produce pressure signatures with finite rise times would perhaps prohibit their attainment under the normal flight conditions of a supersonic transport. Note, however, that these extreme design requirements are based on theoretical considerations alone. Random atmospheric distortions, which are not considered in the theory, have produced unexpected rise times in measured signatures. With the assistance of these atmospheric effects, the design requirements for this desirable type of signature might be brought within practical limits. Further investigation appears to be warranted.

CONCLUDING REMARKS

Near-field design concepts have been discussed in relation to the sonic boom problem of the supersonic transport. The practical application of the design requirements for a plateau pressure signature

to reduce the sonic boom overpressures of a domestic SST configuration has been demonstrated. Theoretical design requirements for pressure signatures with finite rise time have been presented for typical operating conditions of a supersonic transport. The problems associated with the practical attainment of these latter signatures have been considered.

REFERENCES

1. McLean, F. Edward: Some Nonasymptotic Effects on the Sonic Boom of Large Airplanes. NASA TN D–2877, 1965.
2. McLean, F. Edward; and Shrout, Barrett L.: Design Methods for Minimization of Sonic-Boom Pressure-Field Disturbances. Proceedings of the Acoustical Society of America, St. Louis, Mo., Nov. 3, 1965, pp. 519–525.
3. McLean, F. Edward; Carlson, Harry W.; and Hunton, Lynn W.: Sonic-Boom Characteristics of Proposed Supersonic and Hypersonic Airplanes. NASA TN D–3587, 1966.
4. Carlson, Harry W.: Experimental and Analytic Research on Sonic Boom Generation at NASA. NASA SP–147, 1967.
5. Carlson, Harry W.; Mack, Robert J.; and Morris, Odell A.: A Wind-Tunnel Investigation of the Effect of Body Shape on Sonic-Boom Pressure Distributions. NASA TN D–3106, 1965.
6. Hayes, W. D.: Linearized Supersonic Flow. North American Aviation Rept. AL–222, 1947.

Evaluation of Certain Minimum Boom Concepts

HARRY L. RUNYAN AND HERBERT R. HENDERSON
Langley Research Center, NASA

INTRODUCTION

This paper is concerned with two study programs relating to sonic boom alleviation. In the first, an experimental program was conducted to study the growth of the pressure from a basic two-dimensional configuration to its three-dimensional flow field. In the second program, several planforms were examined theoretically, and an attempt was made to formulate a sonic boom efficiency factor, the use of which would provide for a consistent comparison of candidate configurations.

EXPERIMENTAL PROGRAM

Concept and Model

The fundamental idea behind the theoretical work of Hayes (ref. 1) and Whitham (ref. 2) in the calculation of the sonic boom is the replacement of a three-dimensional aircraft with an equivalent body of revolution. This concept then presumes the accurate establishment of three-dimensional flow in the far field of the aircraft, and has been shown to be a very good approximation for normal airplane shapes through comparison with both wind-tunnel studies and actual flight experience.

The adequacy of the method, however, has not been thoroughly tested for shapes that do not appear essentially as bodies of revolution. As a matter of fact, many concepts for shockless or low-boom airplanes are being put forward on the basis of two-dimensional reasoning. One such configuration, developed on the basis of two-dimensional flow, is shown in cross section on figure 1. The idea here was to create a lifting pressure on the lower surface for a small distance involving a shock wave, then expand the flow to the original free stream direction, creating a shock canceling expansion segment which would be very close to the shock wave and to the airplane. This shock cancellation procedure would be repeated downstream for several steps, thus leading to a number of lifting segments, followed

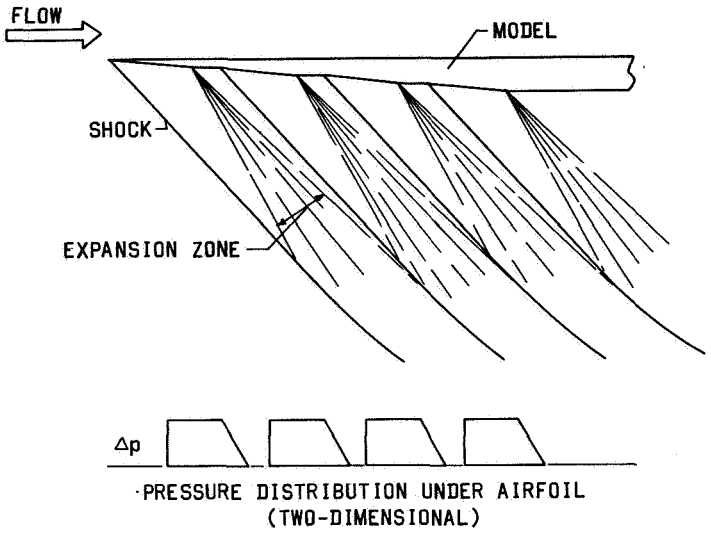

FIGURE 1.—Conceptual model for shock cancellation technique based on two-dimensional flow.

by shock canceling regions. The top of the aircraft would be flat and alined to the original stream flow direction in an effort to reduce any unwanted drag-producing shocks on the upper surface. Also, it was presumed that the engines could be designed so that they would exhaust at the same static pressure as the free-stream static pressure, thus eliminating closure shocks.

For the model concept illustrated in figure 1, the pressure (on a two-dimensional basis) was calculated just below the model. These stepped pressures as shown on figure 1 were used as input in an unpublished procedure using the method of characteristics for calculating the pressure on the ground through a standard stratified atmosphere. The calculated result for a 200 000-pound airplane at $M=3$ yielded an overpressure of one-fourth psf on the ground. This looked encouraging, so that a test model was subsequently constructed and tested in the Langley Unitary Plan Wind Tunnel at $M=2.7$. The model of span 4 inches had four steps, each step having an angle of approximately 5° and being ¾ inch long followed by a ¼-inch streamwise portion. The rear of the model was extended with a constant rectangular cross section which simulated the engine exhaust requirement of exhaust at free stream static pressure, and this constant cross section provided for the sting support.

Results

Pressure distributions below the model were obtained for several positions, and the flow field visualization was obtained by schlieren

photography. In figure 2 are shown the profile and plan view of the schlieren photograph for $M=2.7$. On the top of the figure the plan view is shown, and it is interesting to note that no discernible shock waves are seen to originate from the corners of the leading edge.

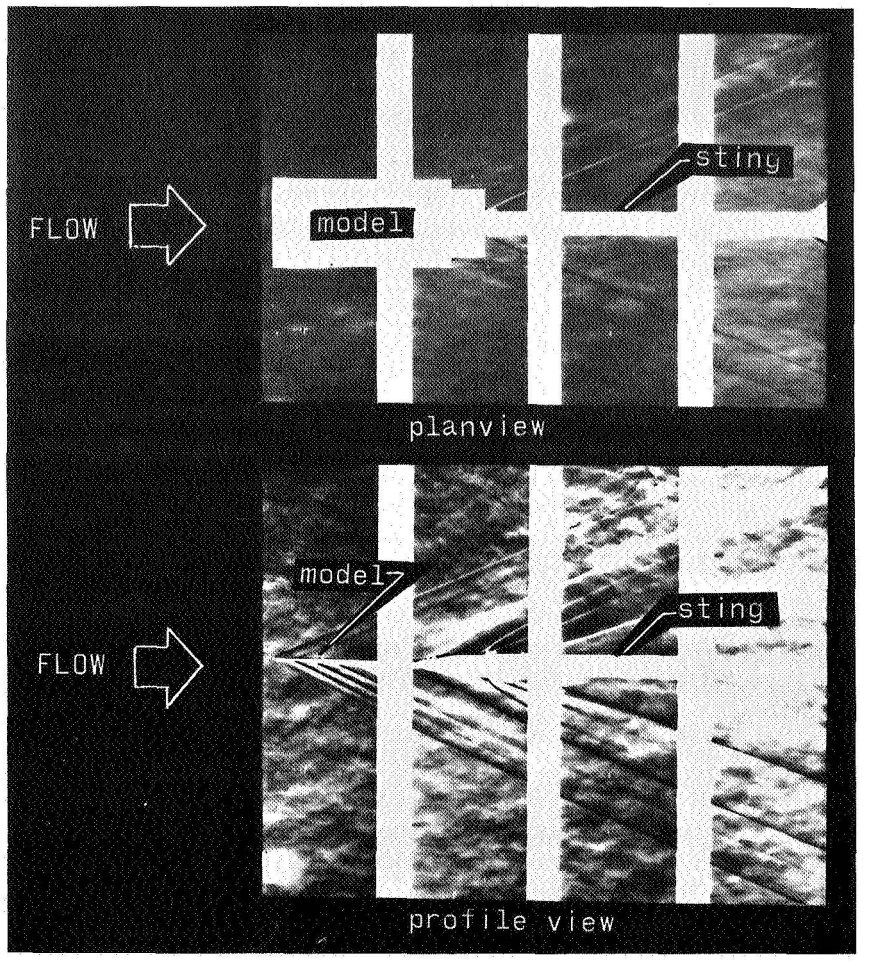

FIGURE 2.—Schlieren photograph of shock cancellation model test, $M=2.7$.

The lower photograph shows rather clearly the shock and expansion pattern. The dark lines indicate shock waves, and the light areas indicate the expansion zones. The vertical white lines are caused by the schlieren window supports which are external to the flow. By following the shock waves from the model, one can see the coalescence of the shock waves, and at the lower right the four shock waves generated at the model have been replaced by a rather strong leading edge

shock and two apparent weaker shocks. The remaining shocks in the photograph are attributed to the sting support.

Two pressure distributions were measured below the model at distances of 5 and 20 inches, and the results are shown in figure 3.

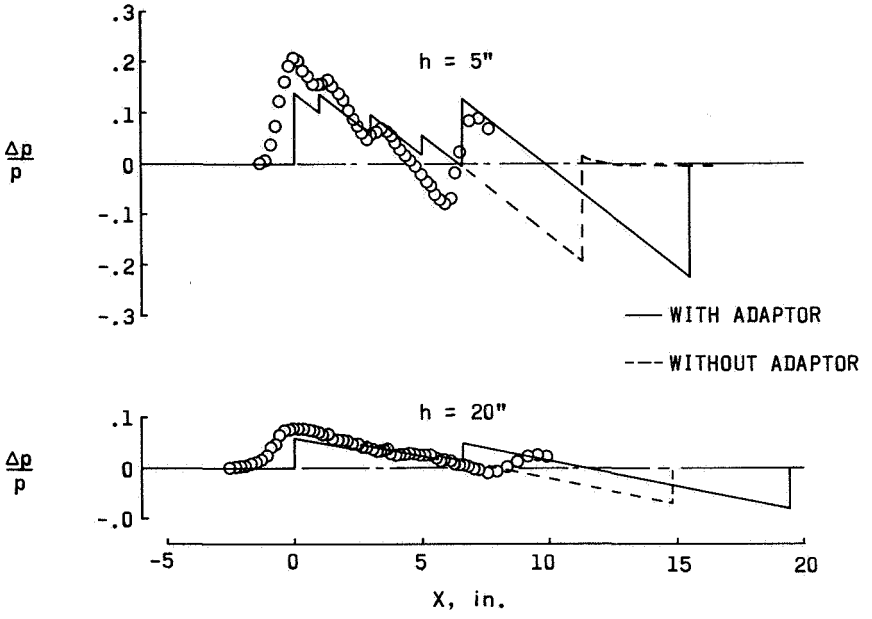

FIGURE 3.—Theoretical and experimental pressure distribution for shock cancellation model at 5- and 20-inch distance below model.

(Because the model was 4 inches in length, these measurement stations correspond to 1.25 and 5 body lengths.) The upper curve gives the results for the 5-inch distance. At least for the near position, it was thought that a pressure distribution similar to that shown below the model on figure 1 (two-dimensional type) would have been obtained at 1.25 body length position. Instead, the formation of a typical N-wave is already apparent, with the shocks from the steps showing only slight perturbations on the flow. The theory of Carlson (ref. 3) was used as a basis for the calculations shown. Considering that the theory was never intended to be used so close to the body and the body was not axisymmetric, the agreement is thought to be rather good. For the 5-body length position, the influence of the steps has been almost canceled, and relatively good agreement is found between theory and experiment, and a typical N-wave has been formed. For both cases, the influence of an adapter located between the model and the sting support was found to be rather strong, and calculated results with the effect of the adapter

included were made, and these should be compared to the experimental results.

It was mentioned previously that the two-dimensional pressure distribution just below the model was used as an input to a computer program to calculate the pressure on the ground through a standard but stratified atmosphere, and the resulting ground Δp was one-fourth psf. After the tests, the experimental pressure distribution at a distance of 20 inches below the model was used as input to the same computer program, and a ground pressure of 2.5 psf was calculated. This again illustrates the danger of deriving shockless or minimum boom configurations based on two-dimensional flow fields.

Discussion

A concept developed on two-dimensional reasoning has been studied, both experimentally and theoretically, and the major conclusion reached was the rapidity with which the three-dimensional flow was established and the relatively good agreement with a theory which has been developed for the so-called midfield or far-field cases. The results should serve as a reminder that minimum or zero boom concepts based on two-dimensional reasoning can be very misleading and that the development of three-dimensional flow is predominant and must be taken into account.

SONIC BOOM EFFICIENCY FACTOR

There are a large number of possible configurations for supersonic aircraft, some of which may provide low sonic booms. Factors, other than low boom, must be considered in evaluating a supersonic transport concept, and one of the more important is the lift-drag ratio (L/D), because the range and efficiency of the aircraft are highly dependent on this ratio. Other factors such as structural weight, engine-airframe integration, stability and control, and low-speed landing characteristics are of course important, but these will not be included in an efficiency factor. In studying a number of configurations, it seems worthwhile to form a ratio so that the various configurations could be systematically compared. Because it is desired to maximize L/D and minimize the sonic boom overpressure Δp, the ratio

$$\frac{L}{D\left(\frac{\Delta p}{p}\right)_g}$$

would form a suitable ratio for a comparative analysis, where $\left(\frac{\Delta p}{p}\right)_g$ refers to the maximum overpressure on the ground.

Utilizing this concept, three configurations were studied by use of the theory of reference 3. The calculated Δp was corrected for altitude and standard atmosphere effects to the Δp on the ground by use of the factor given in reference 3. The three configurations studied had rectangular, delta, and arrow planforms.

Calculations were performed for a constant-weight airplane of 400 000 pounds which might be suitable for transcontinental travel. Only the lift and drag attributed to a flat plate wing were calculated, and no skin friction drag was included in the drag estimate. For simplicity, it was also presumed that a fuselage could be designed which created no wave drag; e.g., by a Busemann biplane rotated 90° about its longitudinal axis. This would conceivably provide zero wave drag and thus the fuselage contribution would be small. Results for the three planforms are shown in table I. The dimension l is the streamwise length of the wing in feet, and b is the span in feet. The overpressure on the ground is Δp in pounds per square foot. The final column is the efficiency factor

$$\frac{L}{D\left(\frac{\Delta p}{p}\right)_g}$$

It is desired to obtain a configuration that has the highest efficiency factor, while at the same time having a low Δp. Results are given for three angles of attack. The planform having the highest efficiency factor of those studied is the 70° arrow wing of aspect ratio 20, at an angle of attack of 1°, which has a factor of 186 000 as well as having the lowest Δp of 0.67 psf. This configuration is shown in figure 4, and it is obvious that structural considerations would compromise this configuration. A surprising result of this study is the low efficiency of the delta wing, when compared to the arrow or even the rectangular wing. The efficiency factor for the delta wing is the lowest for all cases, and the ground Δp is the highest for all cases studied, when comparing the delta wing to the other two configurations. The rectangular wing of aspect ratio 1 rates next to the 70° arrow wing ($AR=20$) in the cases studied. Structurally, a flat rectangular wing may be an efficient structure, and if the weight factor were brought into the picture, it could conceivably be a practical configuration. It is felt that the efficiency factor concept should be broadened to include at least some structural weight parameter to form a more general efficiency factor.

TABLE I.—*Sonic Boom Efficiency Factors for Several Configurations (M=3, Airplane Weight = 400 000 Pounds, and Altitude = 70 000 Feet)*

Wing configuration	Aspect ratio	C_L	Area	Dimensions		Δp	$\frac{L}{D}\frac{1}{\left(\frac{\Delta p}{p}\right)_a}$
				l	b		
			$\alpha=1°$				
Rectangular	1.0	0.021	32 400	180	180	1.27	95 400
Rectangular	2.5	.023	30 200	110	275	1.58	76 800
Rectangular	5.0	.024	28 100	75	375	1.78	68 100
70° arrow	20.0	.044	15 700	770	560	.67	186 000
70° arrow	2.7	.210	3 300	130	94	1.78	69 800
70° delta	1.5	.331	2 050	75	54	2.18	56 900
			$\alpha=3°$				
Rectangular	1.0	.063	11 000	105	105	1.57	25 800
Rectangular	2.5	.070	9 000	60	150	1.85	21 800
Rectangular	5.0	.072	10 100	45	225	2.03	19 900
70° arrow	20.0	.131	5 250	445	332	1.05	39 600
70° arrow	2.7	.630	1 100	75	54	2.05	20 200
70° delta	1.5	.994	741	45	32	2.48	16 700
			$\alpha=6°$				
Rectangular	1.0	.126	5 600	75	75	1.71	11 800
Rectangular	2.5	.140	4 900	45	110	1.99	10 100
Rectangular	5.0	.145	4 500	30	150	2.24	8 990
70° arrow	20.0	.262	26 200	315	230	1.22	17 000
70° arrow	2.7	1.263	486	50	36	2.27	9 100
70° delta	1.5	1.993	326	30	22	2.74	7 530

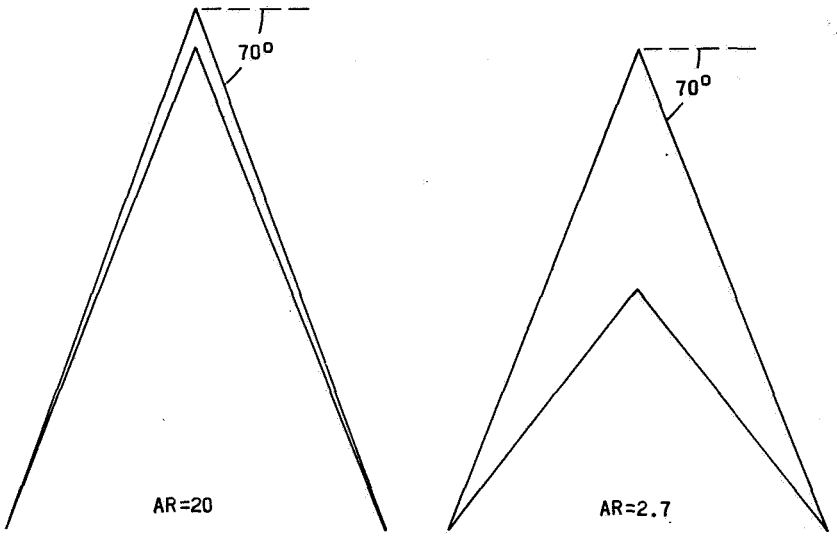

FIGURE 4.—Illustration of arrow wing configuration used in sonic boom efficiency factor study.

CONCLUDING REMARKS

The first part of this paper was concerned with an experimental and theoretical study of a rectangular configuration, and a study was made of the development of three-dimensional flow. In spite of the fact that the configuration physically did not resemble a body of revolution, as the theory assumes, relatively good correlation was obtained between theory and experiment at a distance of approximately only 1 body length. It emphasized the point that low-boom configurations based on two-dimensional reasoning may not perform according to expectancy, and that any configurations based on two-dimensional concepts must be studied in their real three-dimensional regime.

The second part of the paper suggests the use of a sonic boom efficiency factor $L/D(\Delta p/p)_o$. Three planforms were examined by the use of this factor, and it was found that the arrow wing of very high aspect ratio was the best configuration, having low boom and high L/D, with the rectangular wing second and, surprisingly, the delta wing having the least efficiency from the sonic boom standpoint.

It is felt that the structural aspects of these configurations should be studied, and a more complete efficiency factor formulated that would include structural weight.

REFERENCES

1. HAYES, WALLACE D.: Long-Range Acoustic Propagation in the Atmosphere. IDA Research Paper P–50, July 31, 1963.
2. WHITHAM, G. B.: The Flow Pattern of a Supersonic Projectile. Commun. Pure Appl. Math., vol. 5, 1952, pp. 301–348.
3. CARLSON, HARRY W.: Correlation of Sonic-Boom Theory With Wind-Tunnel and Flight Measurements. NASA TR R–213, December 1964.

315–766 O—68——5

Current Research in Sonic Boom

LYNN W. HUNTON
Ames Research Center, NASA

INTRODUCTION

The research program in sonic boom for this past year at the NASA Ames Research Center consists of three general study areas. The program covered the development and verification of new prediction methods (new computer methods and near-field experimental data method), a study of the effects of Mach number to 5.5, and a boom minimization study. The purpose of this paper is to review briefly the status of this research effort.

PREDICTION METHODS

There is a need for analytical methods that are capable of accurately predicting the near flow field pressures about arbitrary aircraft configurations for design optimization in connection with the sonic boom as well as the performance of the vehicle. Available theories are either too cumbersome mathematically for ease of handling on the computer (e.g., method of characteristics) or are limited in range of application (e.g., Whitham, ref. 1) because of some mathematical simplification such as the linear theory concept. As a result, problems of analysis can occur in flow regions very near the aircraft in connection with the design and arrangement of configuration components. To help remedy this situation, two new flow field prediction methods are currently under development. One of these, utilizing the latest in computer display technology, is described by Harvard Lomax in the paper entitled "Preliminary Investigation of Flow Field Analysis on Digital Computers With Graphic Display" in this volume. The second method, which will be developed under contract, consists of a modified version of an existing supersonic wing-body load calculation program wherein the configuration is represented with a spatial distribution of singularities over the entire wing and body surfaces. Because the classical method of Whitham, in contrast, uses an equivalent linear distribution of singularities located only

along the body axis, it is expected that somewhat improved solutions in the near field will be obtainable from this new calculation procedure.

The final prediction technique relates to a method that was developed at Ames for extrapolating experimental near-field pressure signature data obtained from wind-tunnel models to predict the sonic boom characteristics of airplanes flying at any altitude (ref. 2). This new procedure overcomes some of the limitations in previous experimental and theoretical techniques by permitting studies of relatively large models in the wind tunnel. Some verification of the procedure has been made with the XB–70 and the X–15 airplanes for Mach numbers of 1.8 and 5.5, respectively, as shown in figure 1. Using scale models of these airplanes, near-field pressures were measured in the wind tunnel in a plane one body length below each model. This near-field pressure signature was then used to predict the dashed curve for the XB–70 at a distance ratio of 4.5 to compare with available wind-tunnel data measured at that same distance. It can be seen that the comparison is good despite the definite near-field character of the curve. On the basis of the correlation shown for two distance ratios it is apparent for this case of a lifting airplane configuration that a reliable F-function can be partially defined from pressure measurements made as close as one body length from the configuration. As described in reference 2, this incomplete F-function is then believed valid for the calculation of the pressure signature at any distance ratio larger than that used in defining the F-function.

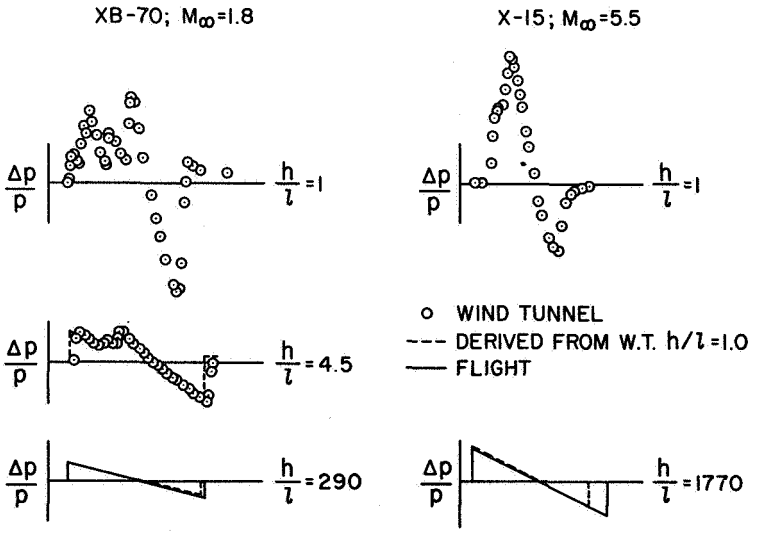

FIGURE 1.—Evaluation of experimental procedure.

Consequently, extrapolations of the overpressures are shown carried out to flight distance ratios for the actual airplanes flying at altitudes of 50 000 and 90 000 feet, respectively, to compare with available flight data obtained from NASA Flight Research Center. Again, the comparison shows very good correlation except behind the tail shock where there usually is a problem of simulating the actual airplane with a sting mounted model. It should also be mentioned that the experimental flight data as presented represent an average of the pressure readings from several pressure cells.

EFFECTS OF MACH NUMBER

The current interest in exploring the potential of the hypersonic air-breathing vehicle for purposes of global transportation raises several questions regarding the sonic boom problem. First, will the good correlation between experiment and the Whitham theory found at moderate supersonic Mach numbers persist at hypersonic Mach numbers? Second, how do the levels of overpressure compare between a supersonic and a hypersonic cruise mission? Third, at the higher Mach numbers, is the overpressure any less sensitive to changes in configuration geometry? These are some of the areas that have been investigated, as described in reference 3, and for this review examples of each will be considered briefly.

In figure 2 is shown a comparison of overpressure signatures from experiment and from the Whitham theory for a 7.5° half-angle cone cylinder for Mach numbers from 2 to 5.5. Experimental

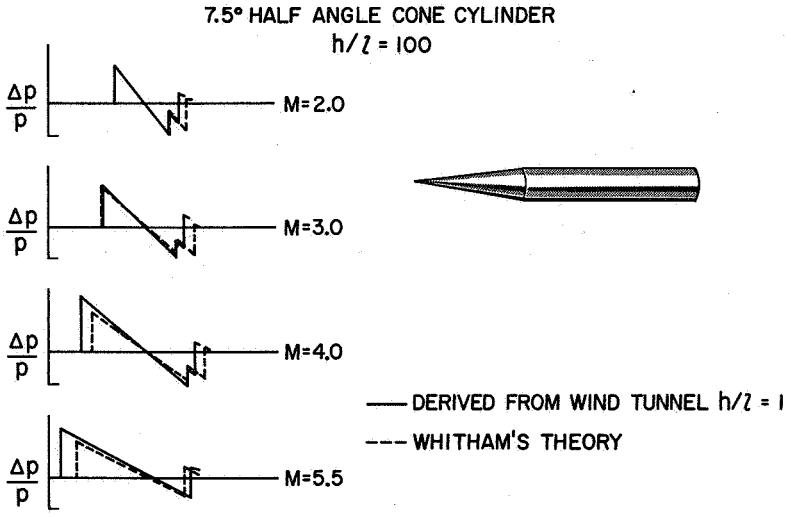

FIGURE 2.—Comparison of experiment with theory.

results were obtained at a distance of one body length and these data have been extrapolated to a distance ratio of 100 for the comparison. This distance ratio was chosen to ensure that the near-field restrictions on the application of the Whitham theory would not be a factor in the comparison. For this simple case of a body of revolution, for which the theory should be particularly suited, it can be seen that the correlation of experiment and theory for the bow shock is fairly good only to a Mach number of 3. Beyond Mach 3 the theory leads to a definite underprediction of the strength of the bow shock. This result is not too surprising in view of the assumptions used in the development of the Whitham theory which place a definite Mach number limitation on the theory (see ref. 1). Also to be noted is a significant increase in the signature length and an unbalancing of the positive and negative impulse areas. While these trends were predicted by the linear theory, the magnitude of these effects fell somewhat short of the measured characteristics.

In figure 3 consideration is given to a comparison of the overpressure levels for a supersonic and a hypersonic transport (HST) mission using geometrically similar blended wing-body configurations for the two cases. The SST is a smaller and lighter airplane with a gross weight of 500 000 pounds compared to 600 000 pounds for the HST. On the left of the figure is shown the assumed flight path schedule of altitude versus Mach number for a supersonic cruise at

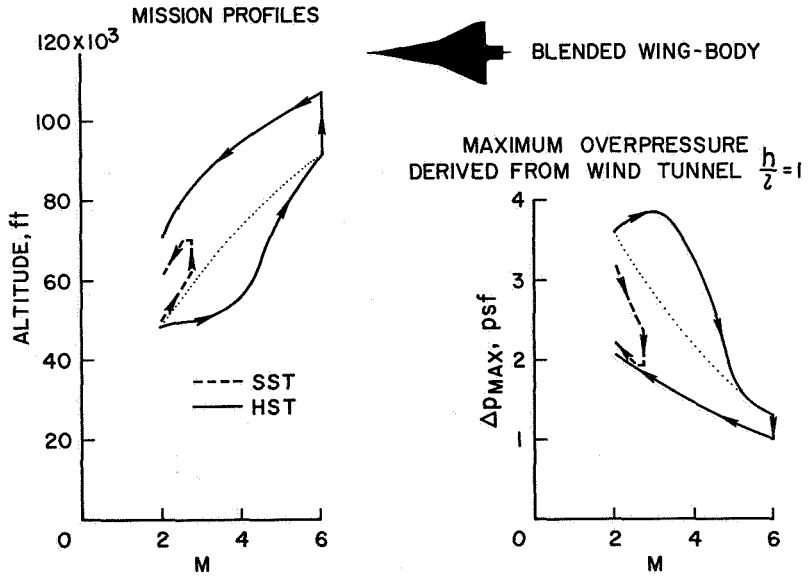

FIGURE 3.—Maximum overpressure for mission profiles.

Mach 2.7 and a hypersonic cruise at Mach 6. Starting at the same Mach number and altitude, each mission includes a climb and acceleration leg, a Breguet cruise, and a descent leg. On the right is shown the maximum overpressure as a function of Mach number that has been derived by extrapolation of wind-tunnel data obtained for the model at a distance ratio of one body length. At the start of the mission with both airplanes at the same Mach number and altitude, the overpressures are separated initially by differences attributed to size and gross weight of the airplanes. As can be seen, the hypersonic mission imposes rather severe overpressures during the climb, whereas in cruise it reduces the overpressure to about half that for the supersonic mission. If, with further technological developments in propulsion, the climb schedule for the hypersonic mission can be altered as shown by the dotted line, then the overpressure could be improved considerably.

Effects of configuration geometry on the maximum peak overpressures have been investigated at Mach numbers of 2, 3, 4, and 5.5 for three configurations representative of different concepts for airbreathing hydrogen-fueled hypersonic transport aircraft. The test models, illustrated in figure 4, were complete with empennage and simulated engine inlets and were 4 inches in length. Based on near-field measurements obtained at a distance of one body length, comparisons of the overpressure characteristics as shown in figure 5 were

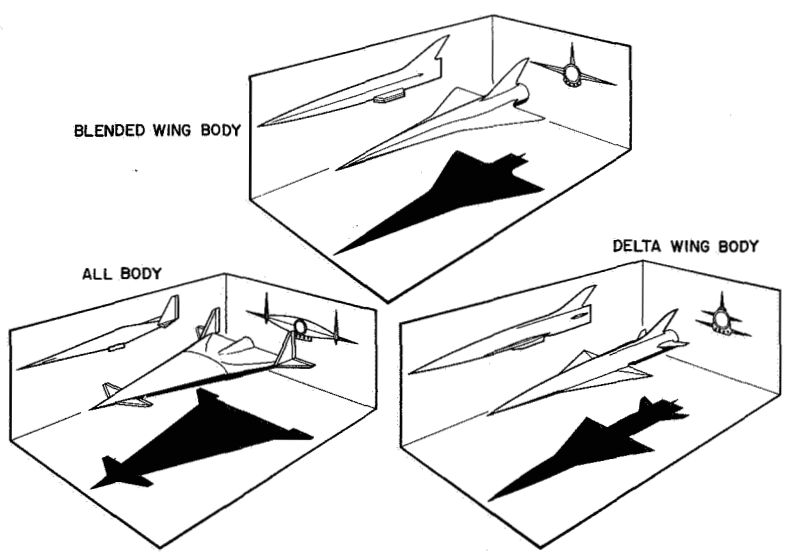

FIGURE 4.—Test models.

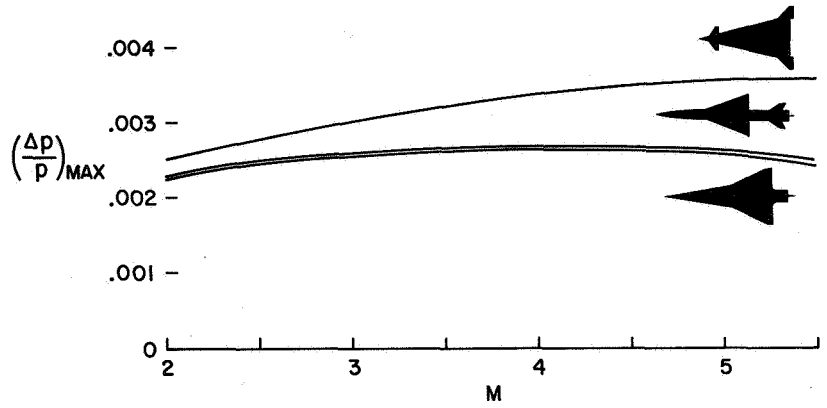

FIGURE 5.—Configuration effect: altitude, 50 000 feet; weight, 600 000 pounds; constant volume derived from wind tunnel $h/l=1$.

derived for the airplanes having constant volume and flying at a constant altitude of 50 000 feet and a weight of 600 000 pounds. Because of the volume constraint, the lengths of the assumed airplanes were not constant as shown by the silhouettes in the figure. It may be seen that the all-body configuration gave the highest overpressured level which worsened with increase in Mach number. While no attempt was made to optimize any of the configurations for boom purposes, it is believed that the canard on the all-body configuration in combination with the shorter length of this configuration may have been largely responsible for the measured differences in overpressure that are shown. From these limited results it is clear that the overpressure characteristics at the higher Mach numbers are sensitive to configuration differences at the moderate altitude considered.

BOOM MINIMIZATION

Based on current knowledge of the problem, the boom minimization program divides logically into two principal phases as shown below:

- Wing configuration study
  - Planform
  - Dihedral
  - Camber
    - Two-dimensional
    - Three-dimensional
- Wing-body integration
  - Conventional bodies
  - Shock canceling bodies

Because it is generally conceded that the thickness effects on sonic boom, in principle, can be handled by shock interference methods, the initial effort here is being directed at the lifting aspects of the

problem for which there are no known solutions. The approach taken, as the first step, is to examine wing configurations that are to some extent unconventional in order to search out possible new design concepts to boom minimization that may have been overlooked in earlier studies. Currently being explored are wing planform, dihedral, and camber. The investigation of camber includes studies of airfoil thickness distribution which is being examined in two-dimensional as well as three-dimensional tests.

The second phase of this program will involve an integration of the more promising lifting arrangements with bodies having optimum thickness. Included here will be conventional bodies with area ruling as required to yield favorable midfield signatures as well as shock canceling bodies that utilize perhaps a three-dimensional application of the shock interference concept of Busemann.

Shown in figure 6 is a display of the initial set of wing configurations

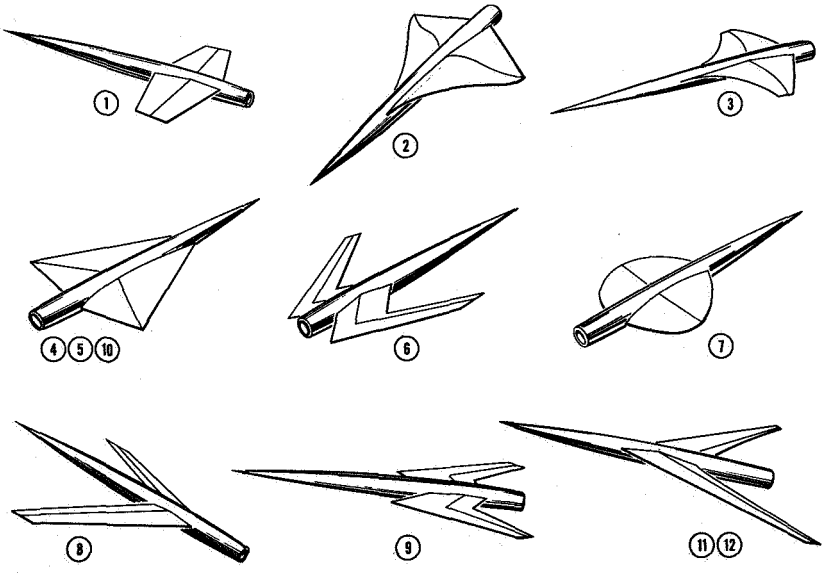

FIGURE 6.—Study configurations.

being examined. Each has been selected to feature some particular arrangement of the wing shock system, such as intersecting, curved, or vertically displaced shocks, to explore our understanding of shock system combinations. Consequently, this selection of wings is intended only to serve as a baseline for future work. In addition to these symmetrical configurations, the arrow wing is also being tested with a cambered airfoil section and the delta wing is being studied with wing dihedral of $\pm 10°$. The geometric parameters

held constant in this series included: the body with a parabolic arc nose and a length of 7 inches, the total wetted area, the wing span, the exposed aspect ratio, and the wing thickness consisting of a double-wedge section with a maximum thickness ratio of 5 percent. The one exception to these stated conditions was the circular wing which, to satisfy the wetted area requirement, had a smaller span and hence a lower aspect ratio.

A preliminary summary of the overpressure characteristics measured for these various wings in the presence of the fixed body is given in figure 7. Maximum peak overpressures resulting from the wing as a function of lift coefficient are presented for 12 wings for a Mach number of 1.4 and a distance of four body lengths. The assigned numbers, in addition to identifying the curves, can be seen to indicate the general progression of overpressure from the highest to the lowest level at the approximate lift coefficient for transition flight of 0.15. Also shown is a table on the right which is intended to summarize in somewhat gross terms the measure of success with which the characteristics of these several wings could be predicted by theory.

The principal conclusions to be drawn from this data summary are as follows:

(1) A relatively large spread in overpressures was obtained for this series of wings ranging from the unswept trapezoidal down to the highly sweptback arrow and the limits of this spread were predicted by theory.

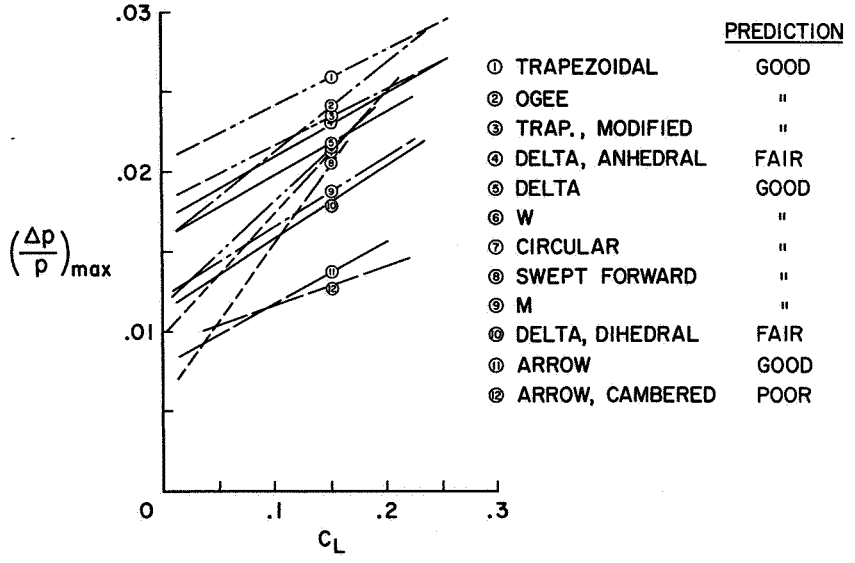

FIGURE 7.—Summary of wing peak overpressures: $M_\infty = 1.4$; $h/l = 4$.

(2) Camber for the arrow wing was advantageous at the higher lift coefficients and warrants further detailed study. This effect was not predicted by theory.

(3) The variation in lift effectiveness on the overpressure as evidenced by the differences in the slopes of the curves is quite large and preliminary estimates of these effects were generally successful. As already mentioned, some problems arose in the case of the cambered arrow wing.

(4) Wing dihedral on the delta configuration showed a surprisingly large effect on the overpressure which has been predicted with only fair success.

It is of interest to examine the dihedral effect in a little more detail. Using curve 5 for the plane delta as a reference, it can be seen that curve 4, for 10° anhedral, indicates a higher overpressure, whereas curve 10, for 10° dihedral, shows a significant reduction in overpressure. Also note, however, that these separated curves are nearly parallel which means that the effect of dihedral measured here is attributed primarily to a volume effect, presumably from the vertical displacement of the wing volume, and not to any favorable lift effect as had been questioned.

To help put these dihedral wing results into a little better perspective, figure 8 has been prepared which shows some additional characteristics measured at a Mach number of 1.7 and a lift coefficient of 0.2. First note on the left of the figure the small silhouette of the test configuration which is scaled to show the relative size and distance of the model from the probe station located at the ground level as tested in the wind tunnel that is equivalent to a distance of 4.5 body lengths. Also shown on the left are the peak overpressures measured

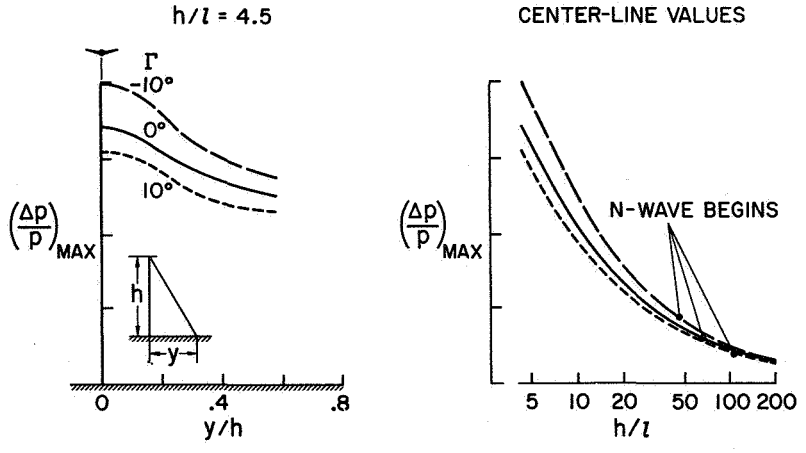

FIGURE 8.—Dihedral wing characteristics: $M=1.7$; $C_L=0.2$.

as a function of lateral to vertical distance ratio for the three values of wing dihedral. For this limited amount of data obtained to date the overpressures are orderly and only partial agreement with theory (ref. 4) has been found.

The curves on the right of figure 8 are intended to show the attenuation of the centerline maximum overpressures for the three dihedral wings out to large distance ratios that are commensurate with flight. These results have been derived from the measured centerline signatures on the assumption that these near-field characteristics would remain orderly out to any distance. This assumption needs further experimental investigation. Although it might appear from these curves that the effect of dihedral virtually disappears at the higher distance ratios, a close scrutiny of the results will show that the relative effectiveness of dihedral at this distance ratio of 200 is still some 60 percent of the relative effectiveness measured in the wind tunnel at the near-field distance ratio of 4.5. These results, however, are preliminary and a realistic assessment of the significance of wing dihedral cannot be made until a more thorough study is completed.

REFERENCES

1. WHITHAM, G. B.: The Flow Pattern of a Supersonic Projectile. Commun. Pure Appl. Math., vol 5, 1952, pp. 301–348.
2. HICKS, R. M.; and MENDOZA, J. P.: Prediction of Aircraft Sonic Boom Characteristics From Experimental Near Field Results. NASA TM X–1477, 1967.
3. HICKS, R. M.; MENDOZA, J. P.; and HUNTON, L. W.: Some Effects of Mach Number and Geometry on Sonic Boom. NASA TN D–4214, 1967.
4. KANE, E. J.; and PALMER, T. Y.: Meteorological Aspects of the Sonic Boom. SRDS Rept. No. RD64–160 (AD 610 463), FAA, Sept. 1964.

Preliminary Investigation of Flow Field Analysis on Digital Computers With Graphic Display

HARVARD LOMAX
Ames Research Center, NASA

The problem of calculating the sonic boom amounts to the problem of tracing the discontinuities (shocks) through a piecewise continuous function space (the atmosphere as time proceeds). For axisymmetric bodies this problem can be formulated mathematically as that of finding solutions to the axisymmetric wave equation. The linearized form of this equation, modified so that the local characteristics have the proper slope and so that local shocks are introduced to satisfy uniqueness properties, has been shown (by Whitham) to give quite satisfactory results when compared with experiment. Further investigations have shown that airplane configurations of the type now being flown at supersonic speeds are sufficiently close to being axisymmetric (or, more precisely, are predominantly described by the first terms in an axial Fourier expansion) for the Whitham theory to be applicable with good results. A fundamental aspect of such studies is the question of whether or not any airplane configurations exist which have properties (in particular, produce sonic booms) that cannot be disclosed by the predominantly axisymmetric Whitham theory as it is now applied. This question has led, in one direction, to the study of multipoles, that is, higher order terms in the Fourier expansion; and in another direction, to the study of second-order effects, that is, higher order terms in the governing partial differential equations.

It seems reasonable that the basic premises of the Whitham theory are sufficient to serve for a mathematical model that will describe with sufficient accuracy the boom signature of any (practical) airplane. This means, simply, that the form of the linearized wave equation could be used, provided the characteristic surfaces were properly traced through space according to the local stream direction and Mach number. It is, of course, the coalescence of characteristics of the "same family" that forms the shocks, and the shocks further coalesce to form the final N-like wave which is the sonic boom. If a significant

unsymmetric twisting of the characteristics can be brought about by reasonable airplane shapes, there is a possibility that the effect would be significant in studies concerning the minimization of the boom pressure impulse.

Unfortunately, the local adjustment of characteristics in three-dimensional flow is not as simple as for the axisymmetric case. The characteristics lines, appearing in the Whitham theory, generalize to conoids developed about curving streamlines. Further, if the three-dimensional properties are significant, the direction cosine between the axis alined with the free stream and the local velocity vector will depend, to a first order, upon both of the cross-perturbation velocities. This effect, together with the locally corrected Mach number, which depends principally on the third perturbation velocity, determine the regions of coalescence and the shock structure.

Because of the complications mentioned above, an investigation was initiated for developing methods for the direct numerical calculation of the flow about airplanes moving at supersonic speeds. Here the word "direct" means that the basic partial differential equations are reduced at once to difference equations which are programed for a digital computer. This concept is not new; nevertheless, at this time the numerical methods that are available for such calculations are not in a satisfactory state. The principal difficulty lies in the fact that the reductions of the partial differential equations to difference schemes implies a continuity in the dependent variables that simply does not exist for the initial and boundary values that are pertinent. To help offset this difficulty a digital computer system was assembled which contained a cathode-ray tube connected directly to the high-speed core of the computer. Methods are now being constructed which will make use of the visual display in an attempt to isolate the shocks from the continuous portions of the flow and calculate both by their individually appropriate techniques. These developments are in a preliminary stage and no results can be presented that apply to actual sonic booms. The remainder of the paper is devoted to a brief discussion of the numerical analysis that has been developed so far under the consideration that immediate graphic representations are available.

One important aspect of adding graphics to the sort of problems being discussed is to throw open the possibility that old (precomputer) methods may compete favorably in the new environment. In this sense, the method of characteristics in three-dimensional supersonic flows can be considered to be much less used in present-day computing than the fixed-mesh methods made popular by Lax in the midfifties. Under the new conditions, it seemed appropriate to reexamine the

two possibilities. This reexamination led to the results discussed below.

Consider the two-dimensional wave equation

$$\frac{\partial u}{\partial x}=C^2\frac{\partial w}{\partial z}$$

$$\frac{\partial w}{\partial x}=\frac{\partial u}{\partial z}$$

If the method of characteristics is introduced, these reduce to the two ordinary differential equations

$$\mathrm{d}u\pm C\mathrm{d}w=0 \tag{2}$$

which apply along the two characteristics. If the notation

$$u_i^{n+1}=u(x+\Delta x,\ z)$$

and

$$u_{i+1}^{n}=u(x,\ z+\Delta z)$$

is adopted, equation (2) can be written

$$\begin{aligned} u_i^{n+1}-u_{i+1}^{n}+C(w_i^{n+1}-w_{i+1}^{n})=0\\ u_i^{n+1}-u_{i-1}^{n}-C(w_i^{n+1}-w_{i-1}^{n})=0 \end{aligned} \tag{3}$$

Solve for u_i^{n+1} and w_i^{n+1} and there results

$$\begin{aligned} u_i^{n+1}&=\frac{1}{2}(u_{i+1}^{n}+u_{i-1}^{n})+\frac{C}{2}(w_{i+1}^{n}-w_{i-1}^{n})\\ w_i^{n+1}&=\frac{1}{2}(w_{i+1}^{n}+w_{i-1}^{n})+\frac{1}{2C}(u_{i+1}^{n}-u_{i-1}^{n}) \end{aligned} \tag{4}$$

where the mesh must be chosen such that

$$\frac{C\Delta x}{\Delta z}=1 \tag{5}$$

Under the conditions imposed by equation (5), equations (4) are identical to those which result from the differencing scheme commonly referred to as the original Lax method. This and similar studies showed that when the Lax and Lax-Wendroff differencing schemes work best, they do so because they are very close to local applications of the method of characteristics.

Turning next to a consideration of the stability of a numerical method, consider the simplest wave equation

$$\frac{\partial u}{\partial x}=-C\frac{\partial u}{\partial z} \tag{6}$$

One form of numerical approximation is to represent the u dependence upon z by evaluating u along a discrete number of lines equispaced in z and continuous in x. In such a case the vector $\vec{w}$ is defined so that

$$\vec{w}^T=(u_1, u_2 \cdots u_M) \tag{7a}$$

and the partial derivative is replaced by

$$\frac{\partial u}{\partial z}=[B]\vec{w}+0(\Delta z^k) \tag{7b}$$

where $[B]$ is a matrix heavily clustered about the principal diagonal. If equations (7) are used in equation (6), there results

$$\frac{\mathrm{d}\vec{w}}{\mathrm{d}x}=-C[B]\vec{w} \tag{8}$$

which is a set of M coupled, ordinary, differential equations. The solution of such equations depends upon the eigenvalues of the matrix $-C[B]$. If $[B]$ is the matrix tridiag

$$\left[-\frac{1+\beta}{2\Delta x}, \frac{\beta}{\Delta x}, \frac{1-\beta}{2\Delta x}\right]$$

these eigenvalues are

$$\sigma_m=-\frac{C}{\Delta x}\left(\beta-i\sqrt{1-\beta^2}\cos\frac{m\pi}{M+1}\right) m=1, \cdots M \tag{9}$$

The point of this analysis can now be made. The order of accuracy in representing the derivative in equation (7b) is no worse than $k=2$ for any value of β. However, the stability of equation (8) is profoundly affected by the choice of β, and one can see from equation (9) that equation (8) is stable or unstable depending on whether β is greater than or less than 1. It is customary, in the study of ordinary differential equations, to regard the eigenvalues of equation (8) as fundamental numbers and to associate them with the physical interpretation of the phenomena being studied. Here we see that the eigenvalues are completely artificial. They may induce damping

("artificial viscosity"), bring about neutral stability (the central differencing scheme, for which $\beta=0$) or they may cause divergence. At any rate, they no longer have a fundamental connection with the physical problem.

The arbitrary nature of the eigenvalues of equation (8) depends, of course, on the approximation in equation (7b); an approximation which, in turn, depends upon the continuity implied in equation (7a). In flow fields with shocks this continuity does not exist everywhere. If it is assumed to exist where it does not, and if the resulting errors are forced to decay by choosing (in effect) a value of β which induces an artificial viscosity, the results cannot, always, be justified. The entire flow field will be forced to decay, and this is not, in general, acceptable.

In conclusion, the ability to compute flow fields about airplanes traveling at supersonic speeds with the aid of an immediate visual display of the calculations as they proceed opens the possibility of devising new, or reviving parts of old, numerical techniques. In exploring these possibilities, preliminary studies indicate the following:

(1) Differencing schemes for hyperbolic partial differential equations governing discontinuous functions are good when they approach spacings that are equivalent to the method of characteristics, and this property is not necessarily connected to their stability.

(2) Artificially stabilizing methods based on continuous functions not only force errors to decay, but also can force the entire solution to (artificially) decay. Such methods do not appear to be appropriate for problems involving the sonic boom.

315-766 O—68——6

Report on Sonic Boom Studies

Part I—Analysis of Configurations

ANTONIO FERRI AND AHMED ISMAIL
New York University

INTRODUCTION

Present configurations selected for supersonic transport produce booms having maximum initial overpressure on the order of 2 lb/ft^2. A substantial part of the activities which has been carried out under NASA Contract NGR–33–016–119 has been directed toward the definition of future configurations that can reduce such values of maximum overpressure, without compromising too strongly other characteristics of the airplane. Several parameters affect the sonic boom, such as the weight of the airplane, altitude of flight, dimensions, etc. In this analysis the only parameter considered as variable is the configuration of the airplane. Therefore, the following assumptions have been made in the analysis:

(1) The length of the airplane is kept constant and equal to 300 feet.

(2) The weight, altitude, and Mach number of flight are kept constant and equal to 465 000 pounds and 60 000 feet and $M=2.70$.

(3) The variations of configurations investigated must not affect the drag too much at the required lift at the flight Mach number.

The analysis has been limited only to conditions corresponding to the maximum Mach number of the airplane. Therefore, the configurations obtained are possible configurations for cruise conditions and usually have acceptable transonic qualities. No attempt has been made to analyze subsonic cruise and low speed performance of such configurations.

In order to use realistic parameters in the analysis performed, a configuration proposed by industry for the supersonic airplane design has been used as a basis for comparison.

In the analysis, many of the design and aerodynamic data used have been selected on the basis of the values of equivalent parameters

selected in such configuration. However, the distribution of lift along the span has been modified. The analysis presented here shows that by conveniently selecting the shape of the equivalent area distribution much lower values can be obtained for the sonic boom than the lower bound obtained before for similar conditions of flight. Consider first the sonic boom given only by the lift. The expression corresponding to configurations used in reference 1 is given by:

$$\frac{\Delta p}{p}=\frac{0.60K_r\beta^{1/4}}{(h/l)^{3/4}}\sqrt{\frac{\beta}{2}\frac{C_LS}{l^2}} \tag{1}$$

This value corresponds, for example, to a lifting surface where the lift per unit span is constant and the integrated lift is proportional to the length from the leading edge, and therefore $L(x)=Kx$. A lower value of $\Delta p/p$ given by:

$$\frac{\Delta p}{p}=\frac{0.53K_r\beta^{1/4}}{(h/l)^{3/4}}\sqrt{\frac{\beta}{2}\frac{C_LS}{l^2}} \tag{2}$$

is possible with a configuration having large lift in the front part of the wingspan (ref. 2). Such values correspond to a maximum overpressure of the order of 1.20 to 1.31 lb/ft^2 for the conditions specified above, and a value of K_r equal to 1.8. The value of $\Delta p/p$ given by equations (1) and (2) are determined by assuming far-field effects. This assumption is correct for the configurations analyzed in reference 1 and for the configurations selected for the supersonic transport designs. However, lower values can be obtained for the conditions of flight selected and for the size of the airplane selected by the U.S. design. For these conditions, substantial reduction on maximum overpressure can be obtained if configurations are used that utilize near-field effects. This can be attained by introducing an appropriate distribution of lift that emphasizes such near-field effects. In order to prove this possibility, three steps are considered in the analysis presented here. First, the present selected configurations are reviewed in order to determine the reason for the difference between the minimum values given by equation (2) and the actual values of $\Delta p/p$ of practical configurations selected. As a second step, the lift distribution and therefore the equivalent cross-sectional area distribution for a given lift and length is changed. The third step, to reduce the value of max $\Delta p/p$, analyses the implications on the actual airplane design of the differences between such equivalent area distributions and the area distribution used in the actual configurations.

SONIC BOOM ANALYSIS

In figure 1, the equivalent cross-sectional area of the supersonic transport selected for the competition is presented. Curve 1 corresponds to the complete airplane; curve 2, to the lifting surface alone. Curve 3 corresponds to a distribution as required by the values of equation (1) for the same lift.

In figure 2, the sonic boom signatures obtained for the three distri-

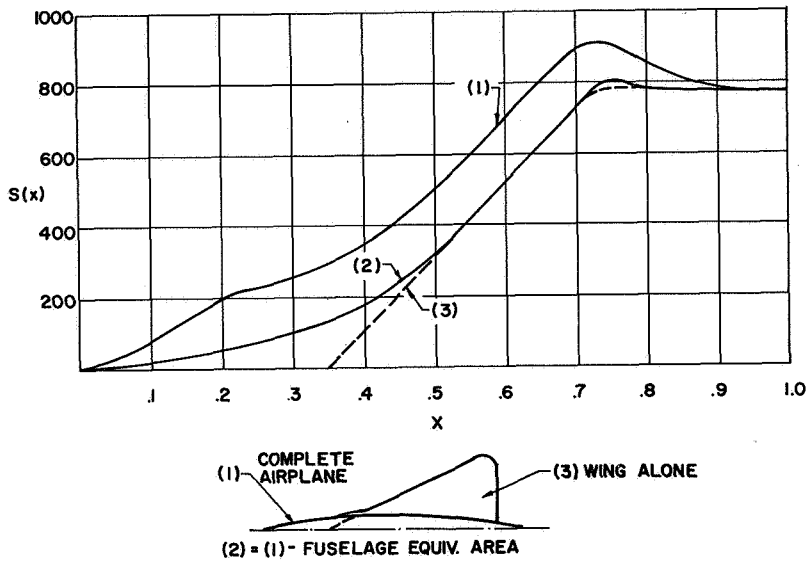

FIGURE 1.—Equivalent cross-sectional area of a present supersonic transport configuration.

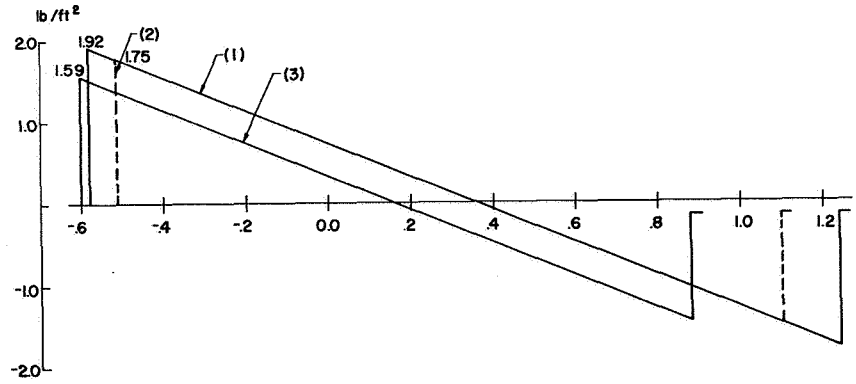

FIGURE 2.—Sonic boom signatures for conditions of figure 1.

butions are shown. All the values of the sonic boom presented here have been obtained with a numerical program developed by H. W. Carlson and associates at the Langley Research Center of NASA and made available to New York University. The sonic boom of the complete airplane gives a $\Delta p_{max}=1.92$ lb/ft^2, which agrees with the value calculated by others for the same configuration, while the wing alone is responsible for Δp of 1.59 lb/ft^2. The reflection coefficient value K_r, assumed here and in the following results, corresponds to 1.8. These results are far from the optimum considering the lift is concentrated only in a small fraction of the length (about 42 percent), while the length of the airplane is 300 feet. To indicate the sensitivity of sonic boom to the lift distribution and equivalent cross-sectional area distribution along the length, selected shapes of several equivalent area distribution have been considered as shown in figure 3.

Curve 2 of figure 3 is close to the distribution required for minimum boom. Curve 1 corresponds to a constant distribution of lift distribution for unit length of the airplane. If C_L is the local lift coefficient, referred to the span C at the given station considered, then

$$\frac{dL}{dx}=C_LC=2\int_{-C}^{+C}\Delta Cp\,dy$$

where the quantity ΔCp is the local pressure rise in the lower surface of the wing at a given station y along the span of the position x. Such distribution could be obtained by a sweptback wing with sonic

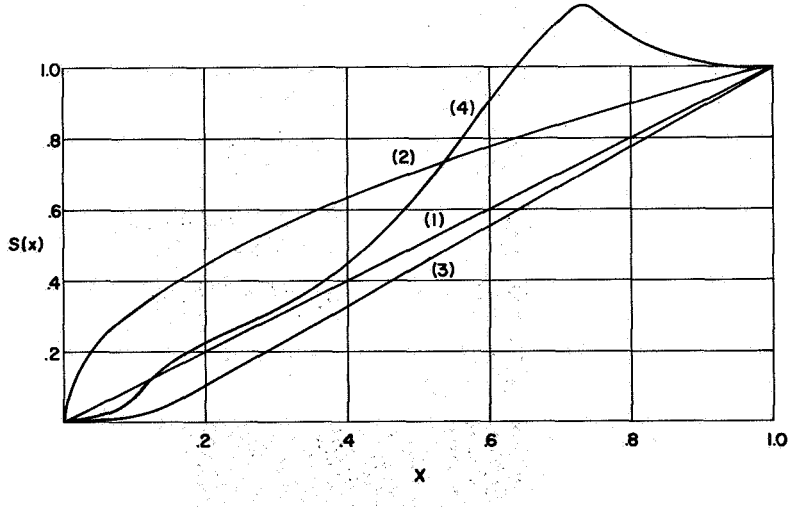

FIGURE 3.—Equivalent area distributions corresponding to a given value of total lift.

edges. Curve 3 corresponds to a wing that is initially triangular and has appropriate camber. Curve 4 corresponds to present airplane configurations. The sonic booms obtained are shown in figure 4. The results are of interest because they indicate that a large departure of $S(x)$ distribution from the optimum value affects the maximum pressure of the sonic boom only slightly, provided that the lifting surface has an actual length equal to 300 feet, and that the lift is produced in the front part of the airplane. It must be noted that for the lift distributions of curves 1, 2, and 3, the sonic boom signature has still near-field effects while the boom signature given by the area distribution of curve 4 has no near-field effects in spite of the fact that the total lift, the altitude of flight, and length of the airplane are the same in all cases.

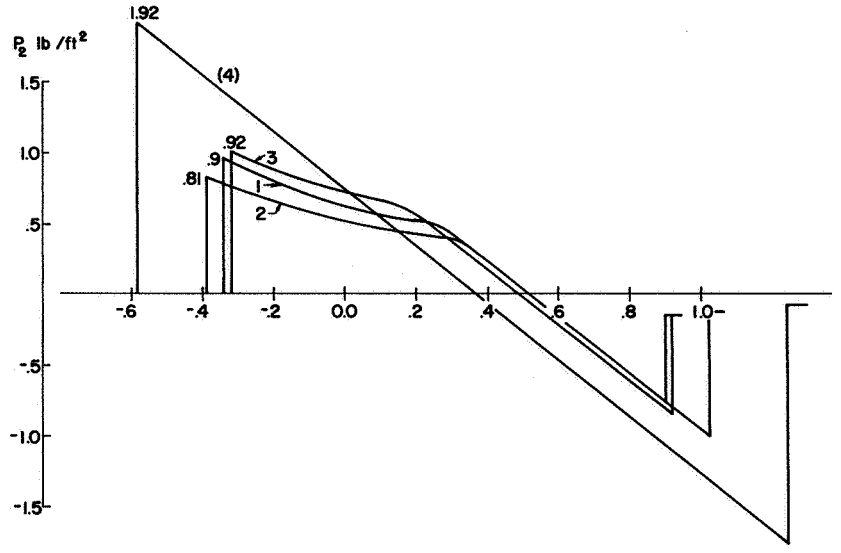

FIGURE 4.—Sonic boom signatures for the equivalent area distribution of figure 3.

The maximum overpressure given by the far-field solution for the curves 1, 2, 3, and 4 corresponds to 1.35 lb/ft² for curve 1, 1.28 lb/ft² for curve 2, 1.37 lb/ft² for curve 3, and 1.92 lb/ft² for curve 4.

These results are important because they indicate that the lower values given by equations (1) and (2) for far-field solutions are not indicative of the present problem, provided that large amount of lift is concentrated in the front part of the airplane. In addition, the results show that conventional configurations do not utilize the effect of near-field solutions in spite of the fact that the dimensions of the airplane are sufficiently large to make near-field effects usable.

MULTIPLANE CONFIGURATIONS

These results indicate that in order to reduce sonic boom, the airplane must have additional lifting surface in the front part of the airplane and therefore imply the use of highly sweptback wings. To have some indication of the minimum amount of lift required in the front part of the airplane to obtain near-field effect, a preliminary investigation has been performed of a tandem lifting system having different proportions of lift on the front wing and rear wing. The configurations considered are shown in figures 5, 7, and 8. The conditions of curve 5 correspond to a lift in the front wing on the order of one-sixth of the total. The shape of the equivalent cross-sectional area for figure 5 is shown in figure 6. Curve 1 in the figure corresponds to the equivalent area of the SST configuration selected as a comparison. In figure 7, the lift of the front wing has been increased to one-fourth of the total lift and in figure 8 to one-third of the total lift. The root cord of the front wing of figure 6 is 45 feet long. The wing starts at the nose. In figure 7, the root cord of the front wing is 85 feet; in figure 8, the root cord is 95 feet. Figures 5, 7, and 8 indicate the sonic boom signature for the configurations shown. The results of this analysis give some interesting indications. A small amount of lift or equivalent nonsectional area in front is ineffective for reducing the sonic boom. In addition, any increase of length is ineffective unless the lift is better distributed. The difference in signature between two configurations, one 154 feet long and the other 300 feet long, is very small as shown in figure 5. However, if the lift of the front wing is increased, the value of the maximum overpressure decreases as shown in the results of figures 7 and 8.

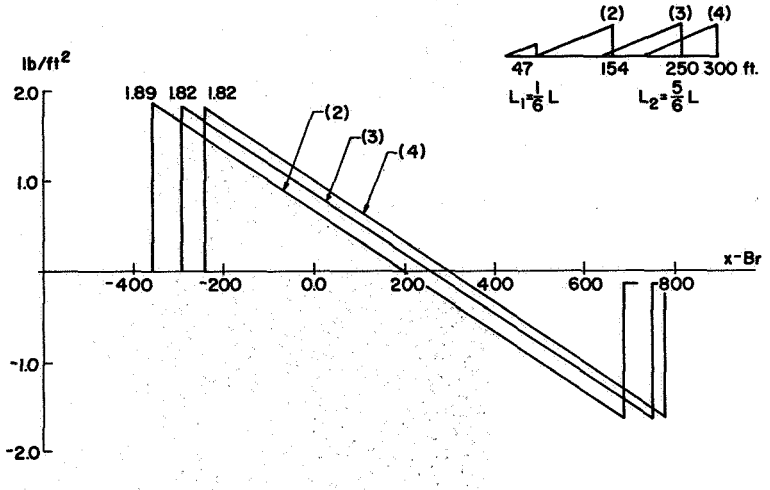

FIGURE 5.—Signature of tandem configuration shown.

The following interesting conclusions can be reached from the results of figures 7 and 8. For lengths of the order of 300 feet, near-field signature is obtained if one-fourth to one-third of the lift is used in the front part of the airplane. Then, the value of the first shock can be kept to values of overpressure of the order of 1 lb/ft^2. In addition, this result indicates a possible direction for producing gradual pressure rise without increasing the length of the airplane.

A comparison of the results in figures 7 and 8 indicate that the Δp of the first step of the overpressure depends mainly on the lift of the front wing when near-field effects are obtained. This value can be decreased by increasing slightly the length of the airplanes. From the results presented, it can be inferred that a larger airplane of the order

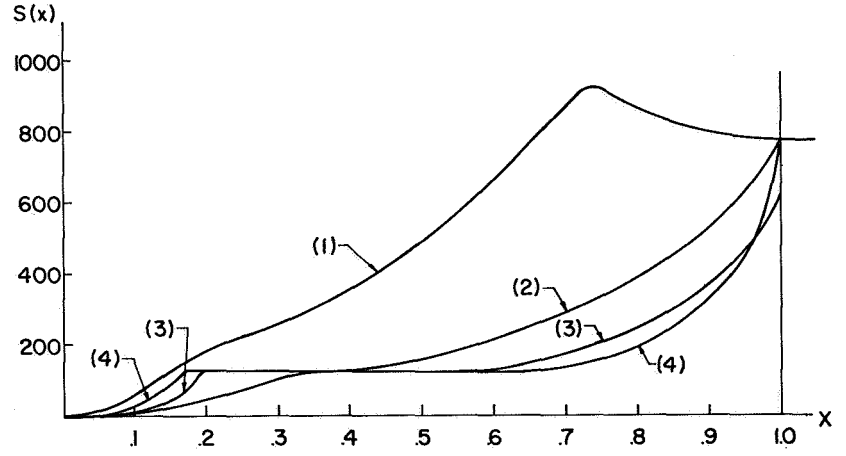

FIGURE 6.—Equivalent cross-sectional area of configurations shown in figure 5.

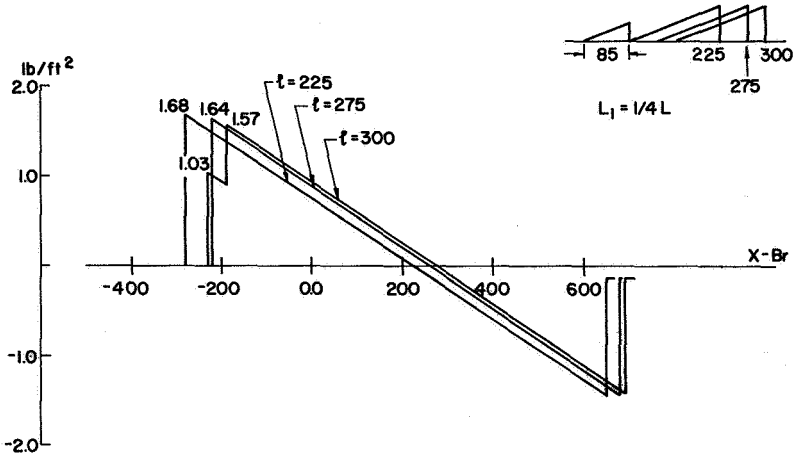

FIGURE 7.—Sonic boom signature of the configuration shown.

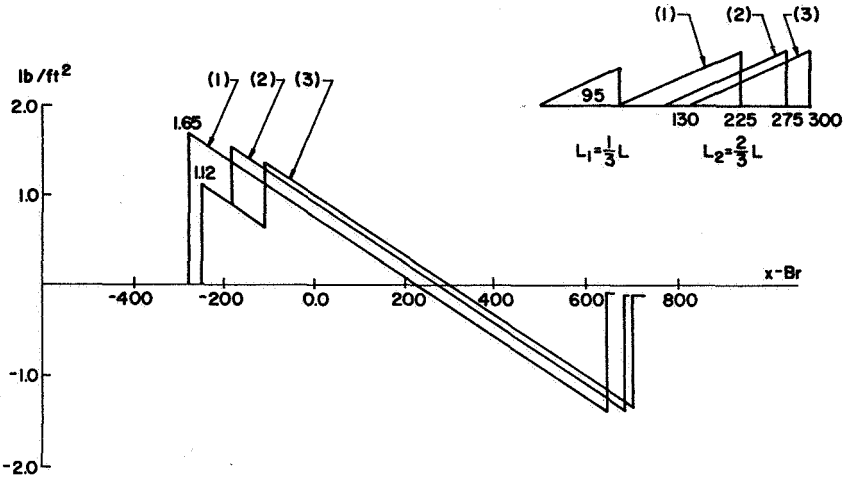

FIGURE 8.—Sonic boom signatures of the configurations shown.

of 350 to 400 feet long can have sonic boom signatures where the first step can be below 1 lb/ft².

PRACTICAL CONFIGURATIONS

The distribution of lift along the length of the airplane is an effective parameter in order to decrease the maximum overpressure attributed to the sonic boom. However, the effect of such distribution on the drag attributed to the lift must be investigated. Usually in order to maximize the L/D of the airplane, two steps are considered. First, the drag for zero lift is minimized, then the drag attributed to lift is minimized. In order to reduce the sonic boom, interference effects must be utilized. The introduction of lift in the front part of the airplane makes the equivalent area distribution similar to the cross-sectional area distribution of a blunt body. This effect could be erroneously interpreted as equivalent to a corresponding increase of the drag attributed to lift. That this is not so can be easily seen by using the theorem of equality of drag attributed to lift in direct and reversed motion. The theorem states that within the approximation of the linear theory, the drag of a given distribution of lift is unchanged by a reversal of the direction of motion. The reversal of the direction of motion for a given lift distribution produces large variation of the equivalent area distribution in spite of the fact that it does not change the drag. This effect is illustrated in figure 9. A triangular wing is considered in the upper left side of figure 9. When the direction of flight without changing the distribution of lift is reversed, a wing having the same spanwise and cordwise distribution of lift is obtained, figure 9 left. Then the drag attributed to lift does

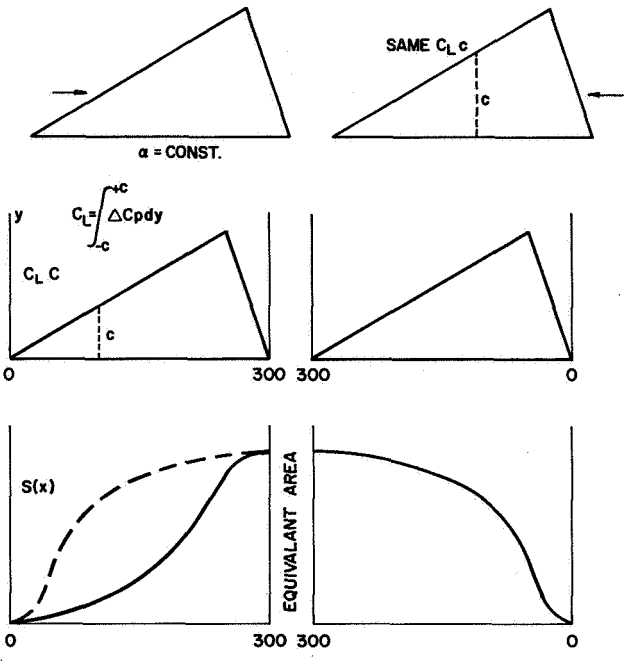

FIGURE 9.—Equivalent area distribution of a given lift distribution in direct and reverse motion. The drag attributed to a given distribution of lift is unchanged by a reversal of the direction of motion.

not change by reversing the flow, and the value of C_LC of the two wings remains the same in the two cases because the lift distribution must remain the same. The equivalent cross-sectional area for the two cases is quite different in spite of the fact that the lift and drag are the same because the direction of integration changes sign. This consideration indicates that the drag attributed to lift does not introduce any limitation to the requirement of large lift in the front part of the airplane.

The other consideration that can be made is related to the effect of volume. Again, the contribution of volume can be incorporated in the effect of lift. The fuselage, if considered as an isolated body, can be represented by a line source sink distribution. If the fuselage is placed underneath a flat plate, with sonic edges, then the source distribution induces lift on the plate proportional to the source's strength, while the back part of the fuselage is placed above a plate, then the sink distribution induces lift proportional to the strength of the sink. This can be seen immediately by using Evvard's theory. The sources and sinks required for the lift can be used to redistribute the equivalent area of the airplane. In figure 10 the required source sink distribution for the transport is indicated. If the

fuselage is placed under a wing and the leading edges of the wing are sonic, then the inviscid L/D of the system for a given C_L is not substantially changed. This is shown in figure 11. In one case a 5° cone is placed symmetrically across the wing or in front of a wing. In the second case, twice the same cross-sectional area is produced on the same length, by increasing the cone angle, and only half of the cone is used and placed underneath the wing. The pressure field of the cone extends under the wing and produces lift. The curves show that L/D in the absence of viscous drag is about the same in the two cones, in spite of the fact that the drag for zero lift is higher for the second case. The presence of the fuselage under the wing increases the lift of the front part of the lifting surfaces. The fuselage is closed in the rear on the top of the wing as indicated in figure 12. Assume that the wing area considered for the configuration is the same as for the configuration selected for the supersonic airplane. In the SST configuration used, the wing area is of the order of 8000 ft^2, while the fuselage wetted area is of the order of 8300 ft^2. In the configuration of figure 12, the wetted area of the fuselage is reduced substantially, because the fuselage is incorporated with the wing and the additional wetted area attributed to the fuselage is reduced

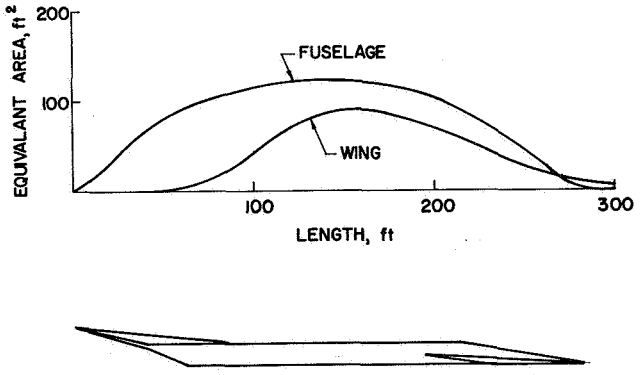

FIGURE 10.—Schematic utilization of volume to produce lift.

Schematic of Utilization	*Equivalent area, ft²*
Lift to be produced	780
Sources	780
Sinks	780
Sources available attributed to thickness	220
Sinks available attributed to thickness	220
Total attributed to lift if interference is utilized:	
Sources	560
Sinks	560

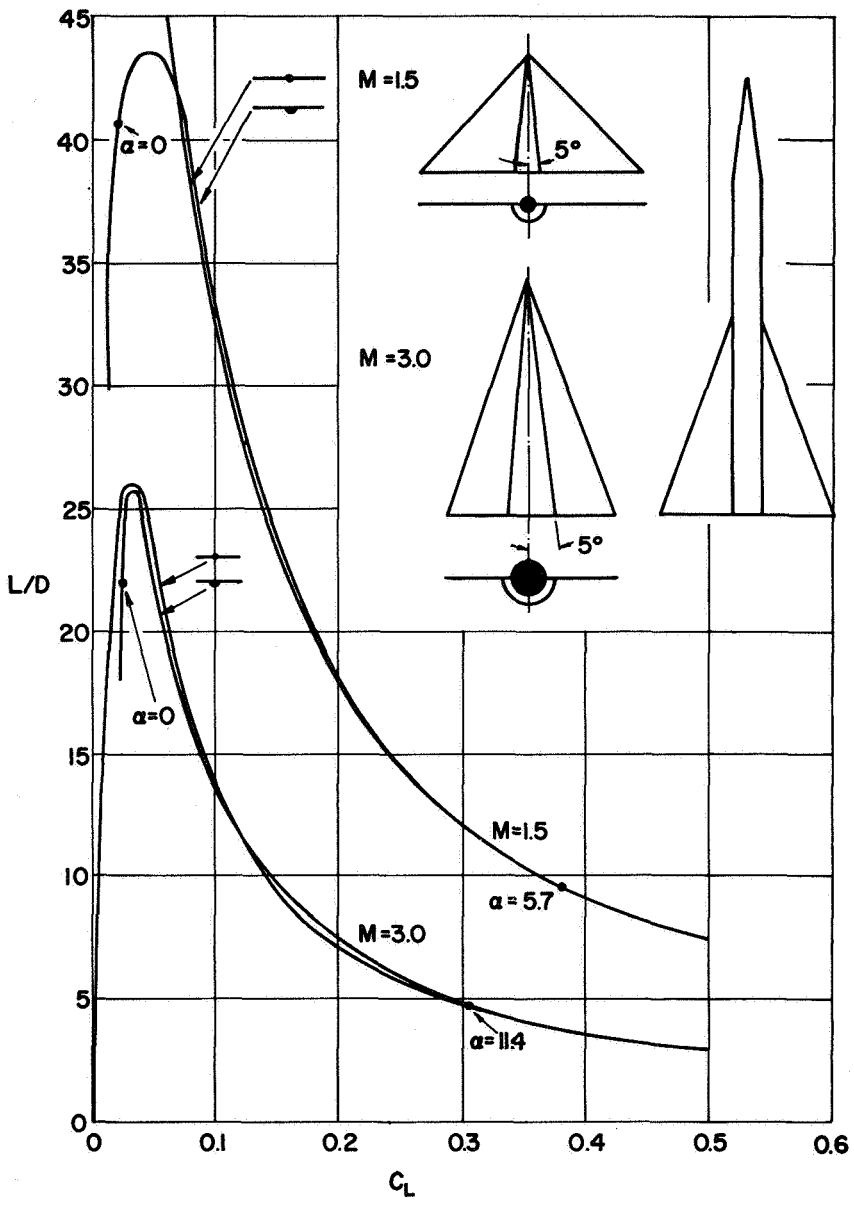

FIGURE 11.—L/D attributed interference.

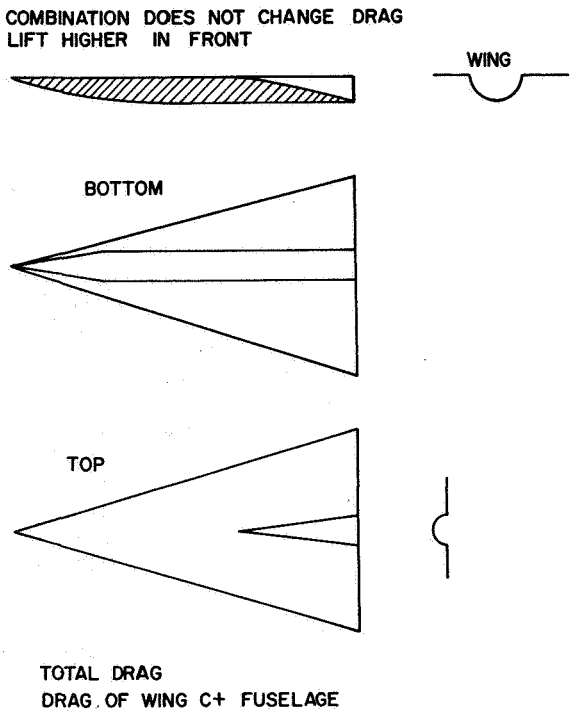

FIGURE 12.—Schematic design of fuselage integrated with lifting surfaces.

substantially. Therefore, if the wing area is kept the same, a reduction in drag can be obtained. An analysis indicates the wing area could be increased by 3000 ft^2 to a value of 11 000 ft^2 without increasing the drag at a given lift. Figure 13 gives the polar diagram for the SST configuration. The wave drag of the airplane is a small part of the drag and is of the same order of the skin friction drag of the fuselage; therefore, the reduction of skin friction drag of the fuselage can balance some increase in wave drag. In addition, any decrease of wetted area corresponds to a decrease in weight of the airplane. If the surface area is increased and the total wetted area of the airplane is kept constant, then the shock drag of the wing is decreased because the percent thickness of the wing decreases, and the drag attributed to lift is also decreased. For a given weight of the airplane, $C_L S$ is constant (S is the area of the wing). The total drag of the wing is given by three components.

$$SC_{D\,\text{wing}}=SC_{D\,\text{wave}}+SC_{D\,\text{friction}}+SC_{D\,\text{lift}}$$

and for constant lift and span, it is

$$SC_{D\,\text{wing}}=K/S+C_{D\,\text{friction}}\,S$$

For actual conditions, an increase in S decreases the total value of $SC_{D\,\text{wing}}$

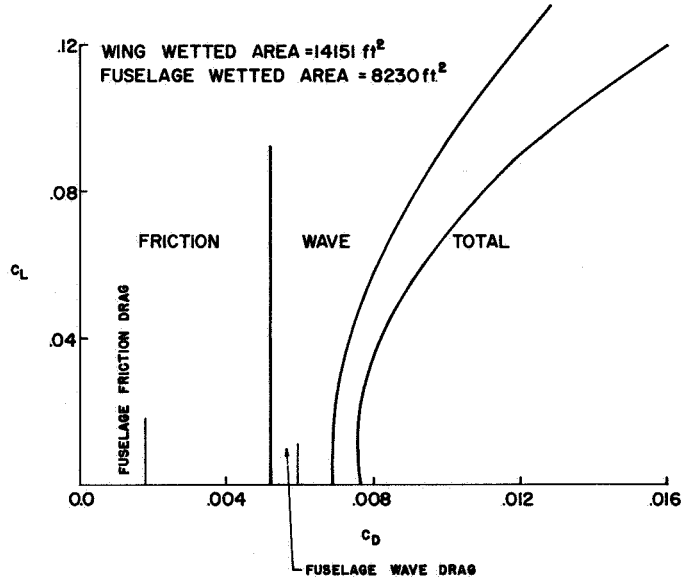

FIGURE 13.—Polar diagram for present supersonic transport design.

POSSIBLE CONFIGURATIONS

In order to indicate possible configurations, the analysis of three airplane designs is presented here. These configurations have been selected on the basis of being not too different from present configurations. Many other configurations having more radical changes could be considered. The configurations have approximately the same L/D at $M=3$. The configurations are shown in figures 14, 16, and 17.

Figure 14 is a triangular wing airplane with higher sweptback wing than present configurations. The fuselage and wing thickness are used to increase the lift in the front part of the airplane. The sonic boom of such an airplane is shown in figure 14. The maximum

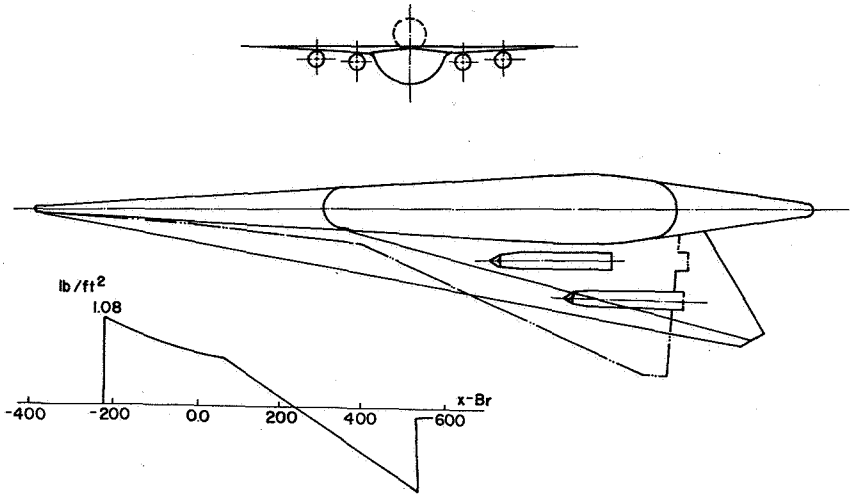

FIGURE 14.—Possible configuration for supersonic airplane.

overpressure is of the order of 1 lb/ft². The lift distribution of the airplane is indicated in figure 15. The quantity C_L is an average value integrated along the span of the wing (not along the cord). Figure 16 indicates the same configurations having larger wing area and the same sonic boom.

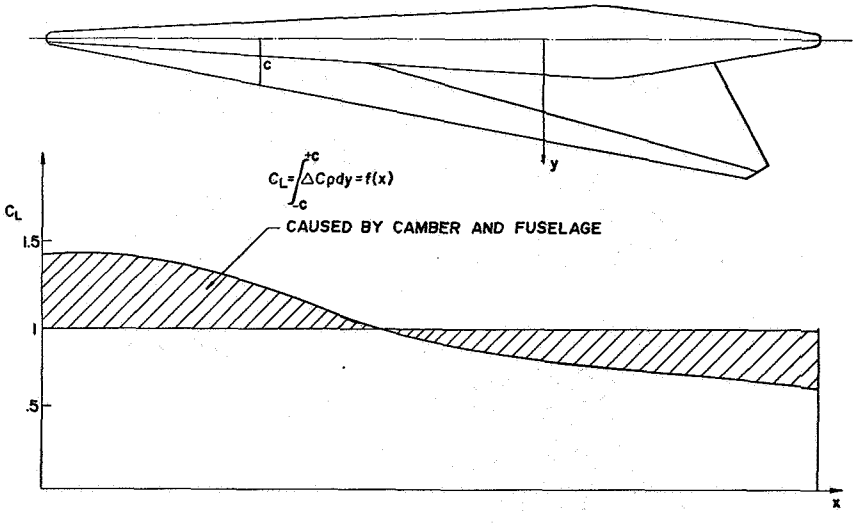

FIGURE 15.—Distribution of lift along the length.

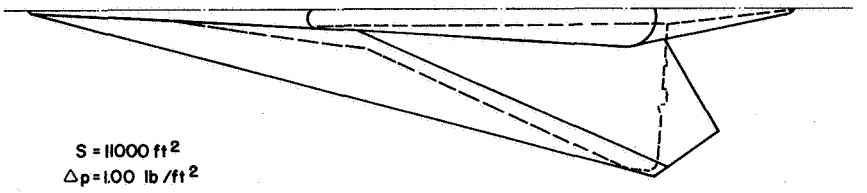

FIGURE 16.—Schematic design of airplane having large wing area.

Figure 17 indicates another possible configuration, and the corresponding sonic boom. The same type of C_LC distribution is used in this configuration.

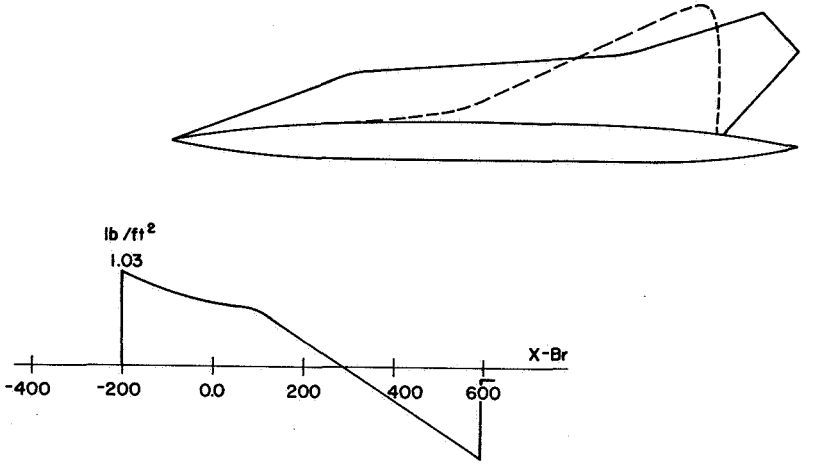

FIGURE 17.—Possible configuration for low boom supersonic airplane.

SUMMARY

Configurations have been investigated for supersonic transport which meet present SST design and requirement. It is shown that optimization on the waves of far-field analysis is not satisfactory. For a 300-foot airplane length, near-field effects can be obtained when sufficient lift is generated near the nose of the airplane. Because of near-field effects, sonic boom maximum overpressure on the order of 1 lb/ft² can be obtained with configurations that do not penalize the L/D of the airplane at cruise. Large improvements can be expected by limited increase of airplane dimensions.

315-766 O—68——7

CONCLUDING REMARKS

From these preliminary considerations, it appears that airplanes having lifting surfaces extended to the front of fuselage, and utilizing interference effects can be effective in reducing maximum sonic boom overpressure, because it utilizes near-field effects.

REFERENCES

1. CARLSON, HARRY W.: The Lower Bound of Attainable Sonic-Boom Overpressure and Design Methods of Approaching This Limit. NASA TN D–1494, Oct. 1962.
2. JONES, L. B.: Lower Bounds for Sonic Bangs, J. Roy. Aeron. Soc., vol. 65, June 1961, pp. 433–437.

Part II—Incidence of N-Waves on Structures

L. TING AND Y. S. PAN
New York University

INTRODUCTION

When an N-wave hits a structure, two aspects of the reaction are of interest. One is the intensification factors and the locations where the transient pressure variation becomes a maximum. The other is the assessment of the transient load or pressure distribution on the structure. The transient maximum pressure rises usually occur at a concave corner facing the incident N-wave. The intensification factor at the corner in certain instances can be determined directly by making use of the reflection principle, the conical solution (ref. 1), or the averaging principle (ref. 2) without the knowledge of the solution to the entire flow field even its neighborhood. However, for the determination of the transient load on the structure, it is necessary to obtain the history of the pressure distribution on the structure.

A procedure for the determination of the transient pressure distribution on a two-dimensional structure in the shape of a rectangular block by an incident N-wave is developed in the next section by the superposition of the solution of a unit plane pulse incident on the structure. When the plane pulse hits the first convex corner, the pressure distribution is given by a conical solution (ref. 1). When the conical flow field propagates to the next convex corner, the diffracted flow field, which is no longer conical, is obtained by the method developed for the diffraction of a general disturbance by a right convex corner (ref. 3). This method has to be employed whenever a disturbance attributed to diffraction at a convex corner propagates to its adjacent convex corner. A numerical program is developed to compute the pressure distribution on the two-dimensional structure incident by a plane pulse or by an N-wave.

The problem of an N-wave incident on a three-dimensional structure is very complicated. Even the basic conical solution of a plane pulse incident on the corner of a cube is not yet available. In the last section, the transient intensification factors at several corners of a three-dimensional structure are computed when the averaging principle (ref. 2) is applicable. The results are used to demonstrate the dependence of the intensification factors on the direction of the incidence.

TWO-DIMENSIONAL PROBLEM

When the structure is represented by a rectangular block in the x–y plane and the incident waves can be represented by superposition of parallel plane pulses inclined at an angle α to the horizon and with its normal in the x–y plane, the pressure disturbance and the velocity potential are governed by the linearized theory, the simple two-dimensional wave equation

$$\frac{1}{C^2}\varphi_{tt}-\varphi_{xx}-\varphi_{yy}=0$$

where C is the speed of sound at the ambient condition. The shape of the N-wave, i.e., the function $G(C\tau)$, is assumed to be given from the sonic boom calculations where G is the overpressure nondimensionalized with respect to the strength of the front shock and $C\tau$ is the distance behind the front shock. If $f(s,t)$ represent the overpressure on the surface of the structure at an instant $t>0$ attributed to a unit plane pulse incident at the front top corner o at the instant $t=0$ (fig. 1), the overpressure on the structure attributed to the N-wave is given by the integral

$$\begin{aligned}\frac{\Delta p(s,t)}{(\Delta p)_{th}}&=\int f(s,t-\tau)\,\mathrm{d}G(C\tau)\\&=\sum_{i=1}^{n} f(s,t-\tau_i)[G(C\tau_i)]\\&\quad+C\sum_{i=1}^{n}\int_{t-\tau_{i+1}-o}^{t-\tau_i+o} G'(Ct-Ct')f(s,t')\,\mathrm{d}t'\end{aligned}\qquad(1)$$

where s is the arc length along the front, top, or the rear sides; n is

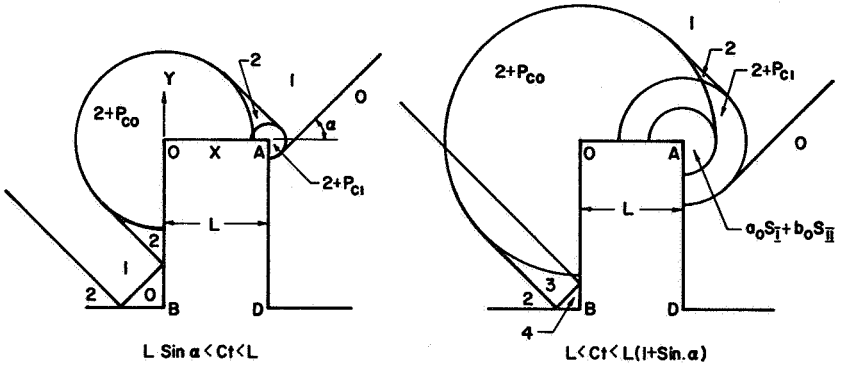

FIGURE 1.—Pattern of diffracted waves.

number of shock waves in the N-wave; and $[G(C\tau_i)]$ is the jump of G across the ith shock at τ_i. According to the definitions, it should be noted that $[G(C\tau_i)]=1$ and $f(s,t)=0$ for $t<0$. The problem now reduces to the determination of the function $f(s,t)$, the overpressure attributed to the incident of a unit plane pulse.

Immediately after the plane pulse incident at the corner o (fig. 1), i.e., $t>0$, the diffracted wave is given by a conical solution, $p_{CO}(x/t,y/t)$ (ref. 1), originated at O. The plane pulse and its reflected wave travel across the top surface and arrive at the rear corner A at the instant $t_1=L\sin\alpha/C$. For $t>t_1$, the diffracted wave at the corner A is given by another conical solution, p_{C1} $[(x-L)/(t-t_1),\ y/(t-t_1)]$, originated at point A.

At the instant $t_2=L/C$, the conical solution p_{CO} arrives at the corner A. For $t>t_2$, the diffracted wave at corner A is no longer a conical solution. The solution for diffraction of a general incident wave by a convex right corner was presented in ref. 3. To facilitate the numerical evaluation of the solution, the incident conical solution p_{CO} along the extended top surface can be approximated as

$$p_{CO}(x/t,\ O)=a_O\sqrt{1-x/(tc)}+b_O[1-x/(tc)]^{3/2}$$

The conical solution and the coefficients a_O, b_O depend on the incident angle α. The diffracted waves can be written as $a_OS_{\mathrm{I}}\ (x,\ y,\ t)+b_OS_{\mathrm{II}}$ $(x,\ y,\ t)$, where S_{I} and S_{II} are the parts attributed to $\sqrt{1-x/(tc)}$ and $[1-x/(tc)]^{3/2}$, respectively, and are independent of the incident angle α. S_{I} and S_{II} can therefore be computed by subroutine. At the instant $t_3=L\ (1+\sin\ \alpha)/C$, the conical solution p_{C1} originated as corner A travels back across the top surface and reaches corner O. For $t>t_3$, the conical solution along the extended top surface can be approximated by

$$p_{C1}[(x-L)/(t-t_1),\ O]=a_1\sqrt{1-x'/(Ct')}+b_1[1-x'/(Ct')]^{3/2}$$

where $x'=(L-x)$ and $t'=t-t_1$ and a_1 and b_1 are constants depending on α. The diffraction at corner O for $t>t_3$ is then given by $a_1S_{\mathrm{I}}+b_1S_{\mathrm{II}}$ with appropriate shift of time scale, and shift and rotation of the x and y variables.

When $t_4=(L\sin\alpha+H)/C$, the conical solution p_{C1} travels across the rear surface and reaches the ground. For $t>(L\sin\ \alpha+2H)/C$, the reflected wave travels upward and passes the corner A. The additional diffracted waves can again be represented by the linear combination of the fundamental solutions S_{I} and S_{II} with appropriate changes in the variables x, y, and t.

It should be pointed out that for $t>0$, the plane pulse and its

reflection will travel down the front surface, be reflected by the ground when $t>H\cos\alpha/C$, and be diffracted by the corner O when $t>2H\cos\alpha/C$ with the addition of a conical solution. The conical solution p_{co} will travel down the front surface, be reflected by the ground for $t>H/C$, and be diffracted by the corner O again when $t>2H/C$. It is clear that the intensification factor at the lower front corner B is 4 for the duration $H\cos\alpha/C\leq t\leq H/C$.

With the conical solutions and the fundamental nonconical solutions computed by subroutines, the additional solution attributed to diffractions and reflections at corners O, A, B, and D can be computed and added at the appropriate instant, and the numerical program for overpressure $f(s,t)$ on the surface of the structure is thereby constructed.

Figure 2 shows the pressure variation $f(s,t)$ on the surface of a square block ($L=H$) attributed to a unit plane pulse incident at 45° ($\alpha=45°$). From the discontinuities in the curves, the propagation of the waves and the additions of reflected or diffracted waves can be observed. As t increases from zero to $3L/C$, the pressure variations on the front, top, and rear surfaces increase from zero and finally approach the uniform value of 2.

With the aid of the solution $f(s,t)$, the pressure variation on the same block attributed to an N-wave incident at 45° to the same structure can be obtained by equation (1). Figure 3 shows the numerical results for an N-wave with a front and rear shock of the same strength; the thickness of the N-wave is L, i.e., $n=2$, $[G(O)]=[G(1)]=1$, and $G'=-2$ for $O<C_T<L$. The pressure variation gradually returns to the ambient value for $t>3L/C$.

With the same procedure, the pressure variation on a rectangular block ($L=2H$) attributed to the incident of the same N-wave is computed and shown in figure 4.

Figure 5 replots the pressure variation at the front bottom corner B from the preceding two figures to demonstrate the influence of the geometry of the structures. The front shock arrives at $t=H\cos\alpha/C$ and is followed by a linear expansion wave. Further expansion occurs after $t=H/C$, when the diffracted waves from the top corner O arrive. The rear shock arrives at $t=(H\cos\alpha+L)/C$ because $C_{T_2}=L$. Afterward, the pressure returns to the ambient value rapidly. The basic differences in these two curves are attributed to the shift of time scale for the different ratio of H/L. Additional small differences are attributed to the different time of arrival of the diffracted waves from the top corner O.

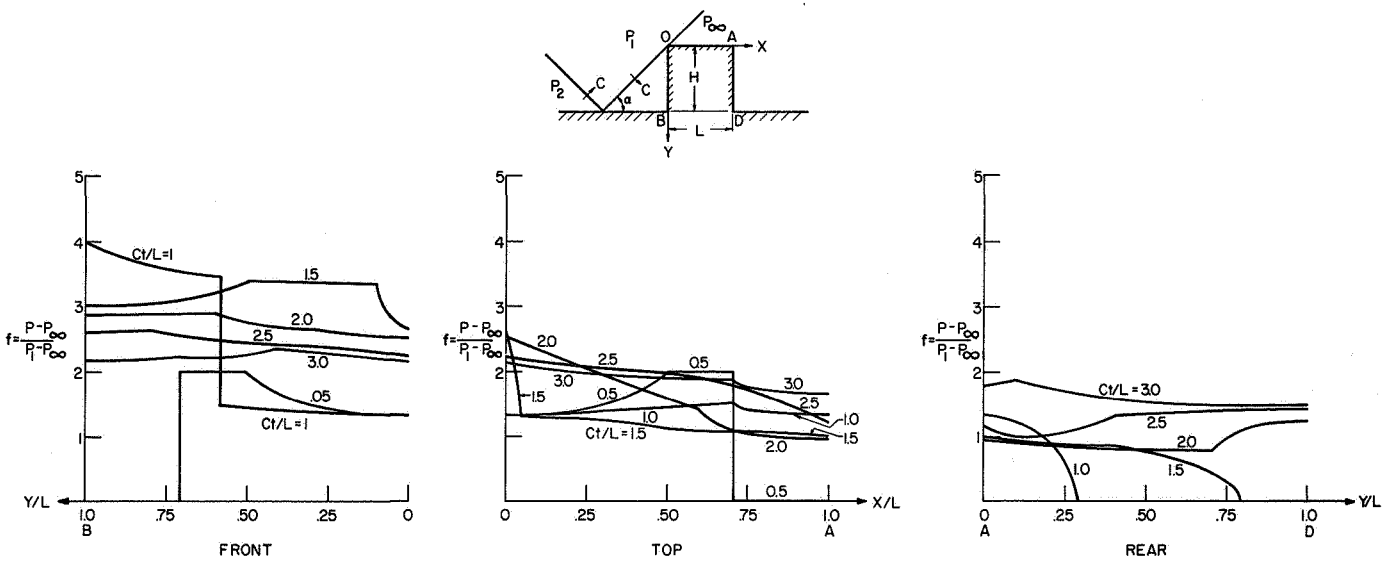

FIG.2 PRESSURE VARIATIONS ON THE SURFACES DUE TO OBLIQUE INCIDENE OF A WEAK SHOCK (H=L, α=45°)

FIGURE 2.—Pressure variations on the surfaces attributed to oblique incidence of a weak shock ($H=L$, $\alpha=45°$).

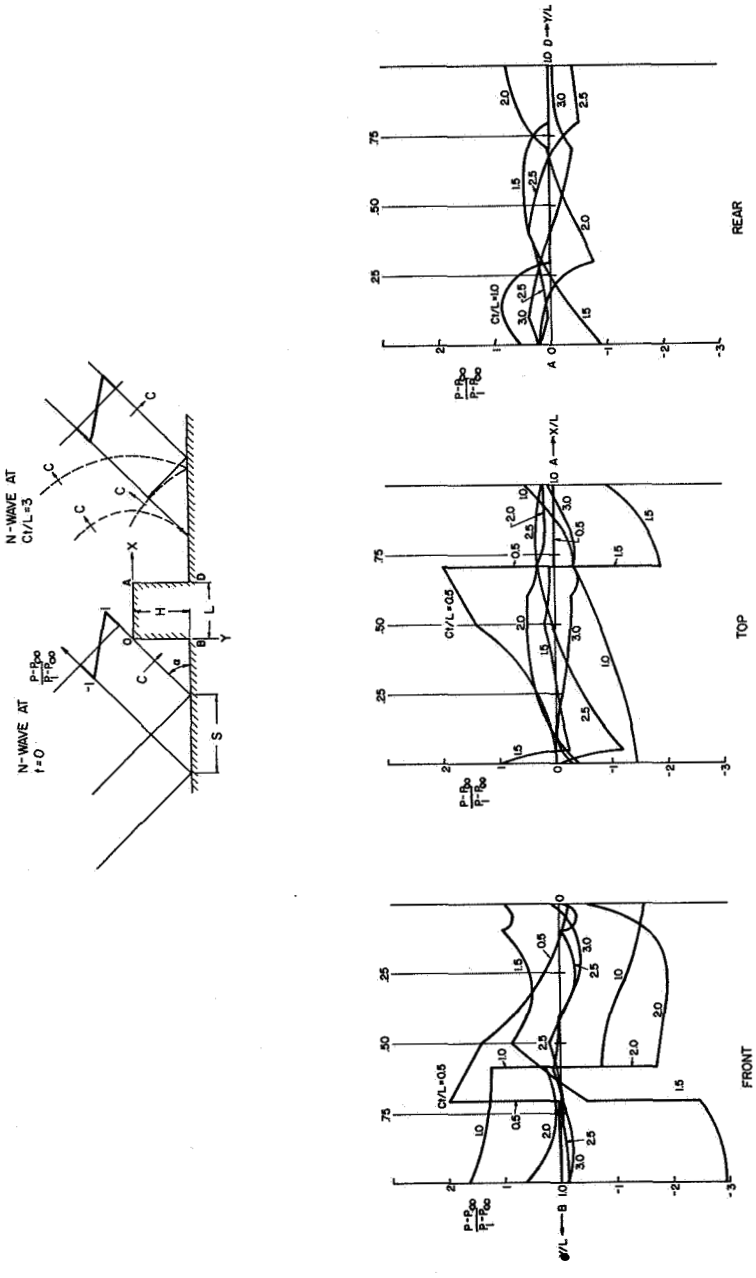

FIGURE 3.—Pressure variations on surfaces attributed to incidence of N-wave ($L=H$, $\alpha=45°$, $S=\sqrt{2}L$).

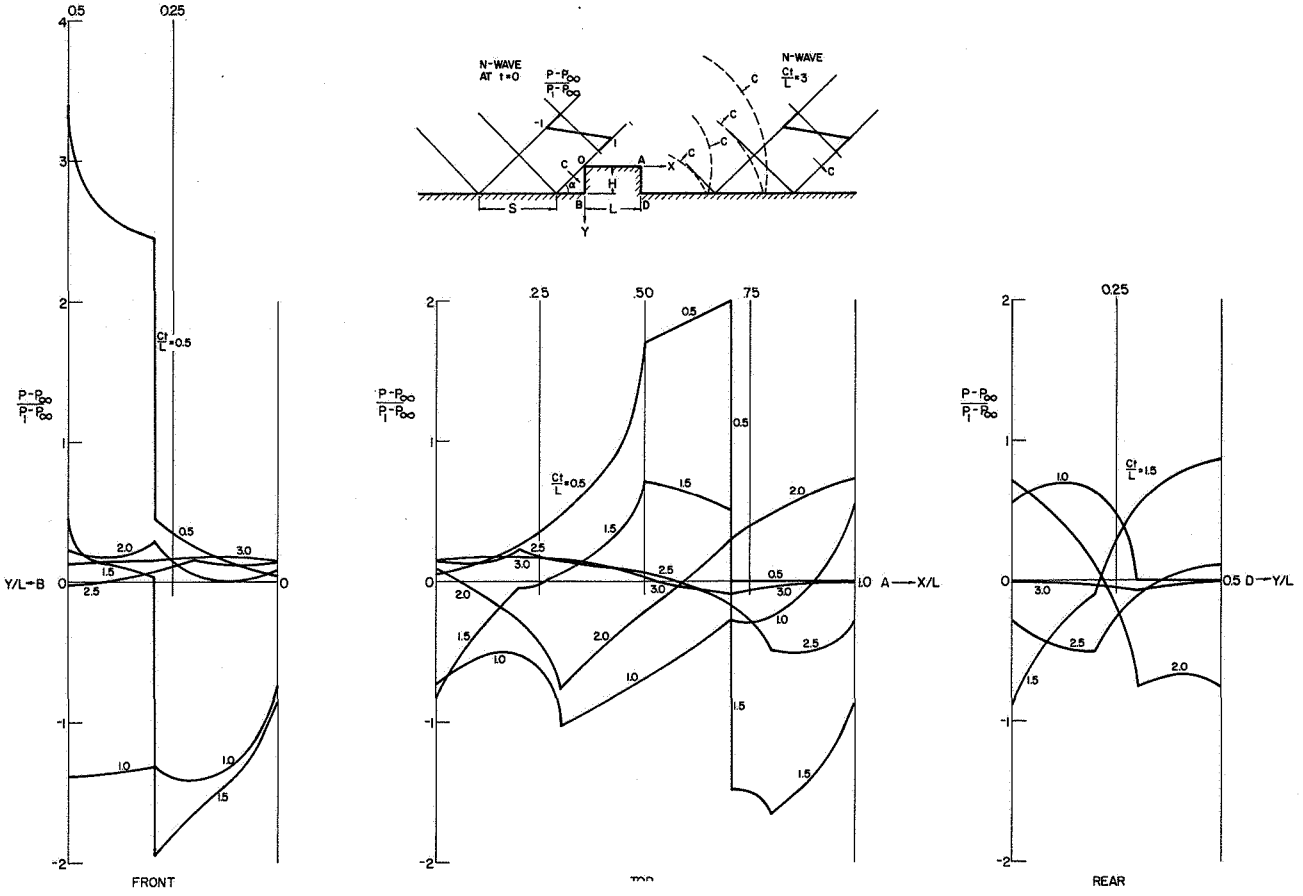

FIGURE 4.—Pressure variations on surfaces attributed to incidences of N-wave ($L=2H$, $\alpha=45°$, $S=\sqrt{2}L$).

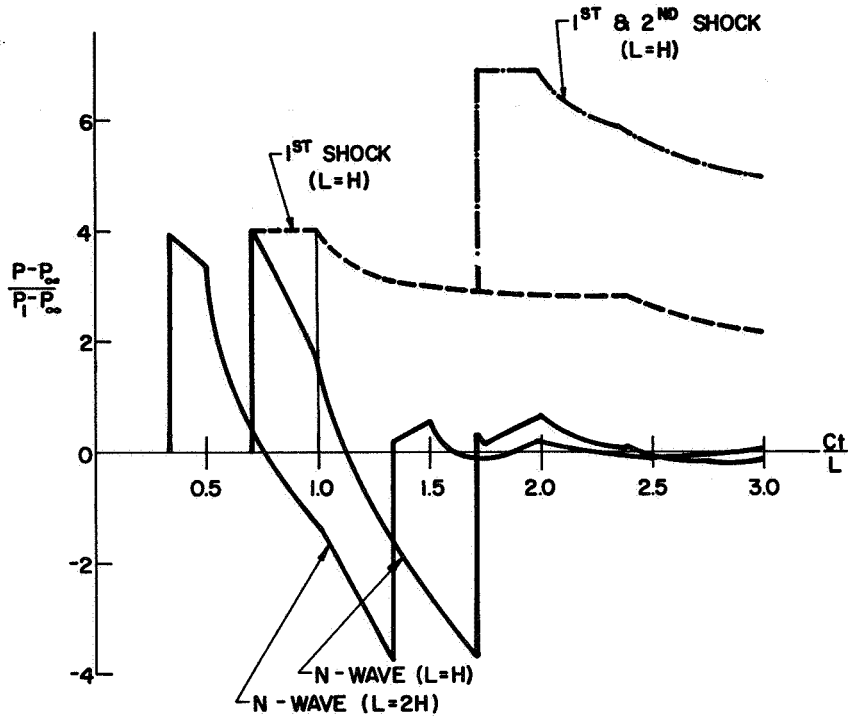

FIGURE 5.—Pressure variation at the front bottom corner.

Intensification Factors (I.F.)

Corners	Flight path					
	I		II		III	
	I.F.	$\lambda=\pi/2$	I.F.	$\lambda=\pi/2$	I.F.	$\lambda=\pi/2$
A	$4\pi/\lambda$	8	$4\pi/(2\lambda)$	4	[a]	[a]
B	$4\pi/(2\pi+\lambda)$	8/5	$4\pi/(2\pi+\lambda)$	8/5	$4\pi/(2\pi+\lambda)$	8/5
A′	[a]	[a]	$2\pi/(2\pi-\lambda)$	4/3	$4\pi/(2\pi-\lambda)$	8/3
B′	$4\pi/(4\pi-\lambda)$	8/7	$4\pi/(4\pi-\lambda)$	8/7	$4\pi/(4\pi-\lambda)$	8/7

[a] Reached by diffracted waves from adjacent corners and edges.

THREE-DIMENSIONAL PROBLEM

Because the near-field solution for the diffraction of a plane wave by a three-dimensional body is not yet available, only some partial information at corners will be obtained by the averaging principle (ref. 27). The principle states that the intensification factor at the vertex of a cone with solid angle Ω is equal to the ratio of the solid angle of the flow field at the vertex without and with the cone, i.e., $4\pi/(4\pi-\Omega)$. In the proof, the conical properties of the boundary are employed, but the solution of the flow field is not restricted to

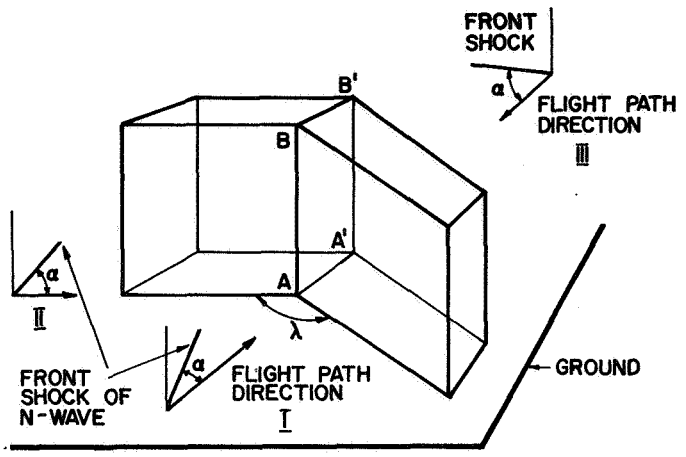

FIGURE 6.—Three-dimensional diffraction of incident wave.

conical flow. Near the vertex or corner of a body it is locally a conical surface, and the averaging principle can be applied to compute the overpressure until the arrival of the disturbances from the nonconical portion of the body. This principle is now applied to a V-shaped building with a concave angle λ (see fig. 6). For a given airplane flying at given Mach number and altitude, the N-wave signature and the incident angle to the ground are the same. The diffracted waves and the pressure distribution on the building depend also on the direction of the flight path. Three distinct types of flight path are considered, and the intensification factor at the corners and vertices are computed by means of the averaging principle.

Flight path I approaches the concave side of the V-shaped building and makes a finite angle with the two legs of the V. Flight path II is parallel to one leg of the V. Flight path III is opposite to that of I and is approaching the convex side of the V. The ratio of overpressure to the value of incident N-wave for various corners and vertices is tabulated also in figure 6.

For paths I and III the reflections of waves from the ground and the two vertical surfaces are assumed to be regular reflections (ref. 4). For path II, there is no reflection from one of the vertical surfaces, i.e., a degenerated case of Mach reflection. The intensification factor at the lower concave corner of the V is $4\pi/\lambda$ for flight path I and is $2\pi/\lambda$ for flight path II; they are 8 and 4, respectively, when $\lambda=\pi/2$. In between flight path of types I and II it will be necessary to admit Mach reflections from one of the vertical walls. On the other hand, the intensification factor at the convex lower corner for flight path III is $4\pi/(2\pi-\lambda)$, i.e., $\frac{4}{3}$ for $\lambda=\pi/2$. The lower concave corner is much

lower than $4\pi/\lambda$ times the value of incident wave. These examples clearly illustrate the importance of flight path direction. It should be pointed out again that the intensification factors, i.e., the ratio of overpressure to that of incident wave, given in the table are valid prior to the arrival of diffracted or reflected waves from the adjacent edges and corners. For a complete pressure distribution on the surfaces of the buildings it is necessary to develop the near-field solutions. The first step will be the construction of a conical solution for the diffraction of a plane pulse by a convex corner of a cube.

CONCLUSIONS

A numerical program for the pressure distribution of an N-wave incident on a two-dimensional structure in the shape of a rectangular block is completed. For a three-dimensional structure, the averaging principle is employed to compute the intensification factors for corners and vertices for certain durations and to demonstrate the importance of the flight path direction.

REFERENCES

1. Keller, J. B.; and Blank, A.: Diffraction and Reflection of Pulses by Wedges and Corners. Commun. Pure Appl. Math., vol. 4, no. 1, June 1951, pp. 75–94.
2. Ting, L.: On the Diffraction of an Arbitrary Pulse by a Wedge on a Cone. Quart. Appl. Math., vol. 18, no. 1, April 1960, pp. 89–92.
3. Ting, L.: Diffraction of Disturbances around a Convex Right Corner with Applications in Acoustics and Wing-Body Interference. J. Aero. Sci., vol. 24, no. 11, November 1957, pp. 821–831.
4. Courant, R.; and Friedrichs, K. O.: Supersonic Flow and Shock Waves. Interscience, New York, 1948, pp. 334–342.

Reduction of Sonic Boom Attributed to Lift

E. L. Resler, Jr.
Cornell University

INTRODUCTION

The expected sonic boom associated with presently planned supersonic aircraft, particularly the commercial supersonic transports, is not likely to be received graciously by the general public. To alleviate this problem, ways to modify the aircraft's configuration to reduce or eliminate the sonic boom would be highly desirable. Physical arrangements to eliminate completely the boom attributed to lift are discussed in this paper. The particular configurations discussed derive their lift by imparting downward momentum to the fluid in the vicinity of the aircraft and canceling the far-field effects by other means, namely, a reduced area stream tube that could be accomplished by special engine designs. These principles are most easily demonstrated in the two-dimensional case and then extended to three-dimensional cases.

TWO-DIMENSIONAL CONFIGURATIONS

The earliest and most famous example of an aerodynamic shape with thickness but no wave drag, and thus no boom associated with it, is the Busemann biplane and its counterpart with cylindrical symmetry. These configurations exhibit no boom because all the waves are confined to the internal flow and canceled by surface contours. The linearized version of a Busemann biplane is shown in figure 1. To continue the discussion, it is convenient to make use of the theory of H. Lomax (ref. 1). This reference relates equivalent cylinders in two dimensions or bodies of revolution in three dimensions to the cross-sectional area and normal forces on any aerodynamic configuration. In the far field the pressure disturbance attributed to the configuration is the same as would be caused by the equivalent bodies. The equivalent bodies may be different at different azimuthal angles depending on the configuration. Two-dimensional flows are particularly simple in that there are only two directions or angles of consequence, below $(-\pi/2)$ and above $(+\pi/2)$.

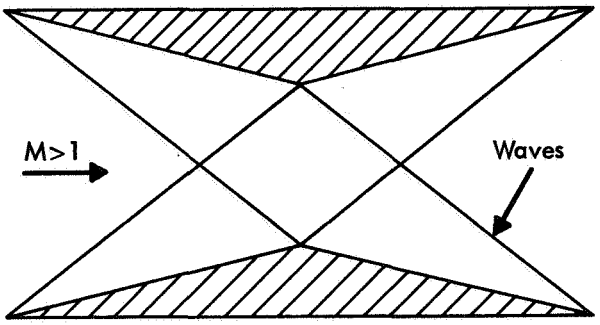

FIGURE 1.—Linearized Busemann biplane.

Using the theory of Lomax to analyze the two-dimensional Busemann biplane makes clear the reason for no wave drag in terms of equivalent cylinders. The forces acting on the biplane give an equivalent cylinder that identically cancels the equivalent cylinder because of thickness. There is another way to visualize the equivalent cylinders for the Busemann biplane which will be used later to discuss lifting bodies. Consider the stream tube that passes through the biplane and consider it a solid cylinder that extends from $-\infty$ to $+\infty$. This cylinder plus the solid parts of the Busemann biplane when superimposed (following the Lomax scheme) result in an equivalent cylinder of constant area that extends from $-\infty$ to $+\infty$ and again such a cylinder obviously does not disturb the flow at all and has neither wave drag nor boom (fig. 2).

Of course, there is another class of bodies that exhibit no boom but do have wave drag. Such bodies can be constructed from the equivalent bodies of the Busemann biplane. Such a body, which from the ground still looks like an infinite cylinder, is shown in figure 3. Any

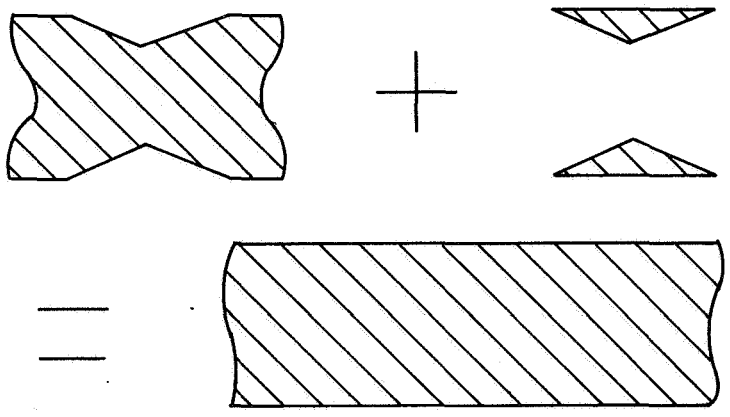

FIGURE 2.—Equivalent cylinders according to area rule for Busemann biplane.

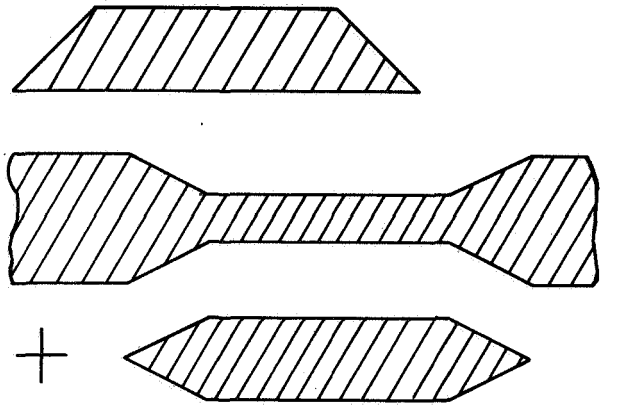

FIGURE 3.—Body with thickness, no sonic boom, but wave drag and equivalent cylinders from ground ($-\pi/2$).

two-dimensional shape with a streamline that is straight and parallel to the ground on the under side will give no two-dimensional boom but will have a wave drag. It is apparent that there are also three-dimensional counterparts of this class of body, namely, bodies with thickness, that are not hollow and would cause no pressure disturbance, and thus no boom directly beneath them, but would have a wave drag. These configurations would exhibit a moment but no net lift. Because skin friction is very important for supersonic flight conditions, the wave drag of these bodies may be a reasonable price to pay for boom reduction without having to cope with the large friction drag of a Busemann-type configuration which accomplishes the same boom reduction.

Suppose we now extend these considerations to construct a lifting body that would exhibit no boom. Again the two-dimensional case is most easily discussed. Begin with a flat plate at angle of attack which ordinarily would have waves extending above and below it. It is the downward directed waves that result in the two-dimensional boom. Thus the front compression wave must be intercepted with another plate as shown in figure 4. In this case, to maintain a horizontal streamline, the air in the stream tube between the plates must be processed to prevent "pluming" of the stream tube as it leaves the duct, which would cause a boom. The processing of the air in the cross-hatched region of figure 4 is such that the stream tube leaves the configuration at the correct ambient pressure (therefore preventing pluming) but with a reduced stream-tube area. The equivalent cylinders for this two-dimensional lifting configuration are shown in figure 5. These are found by replacing the stream tube where the air is processed by a solid cyclinder before applying the

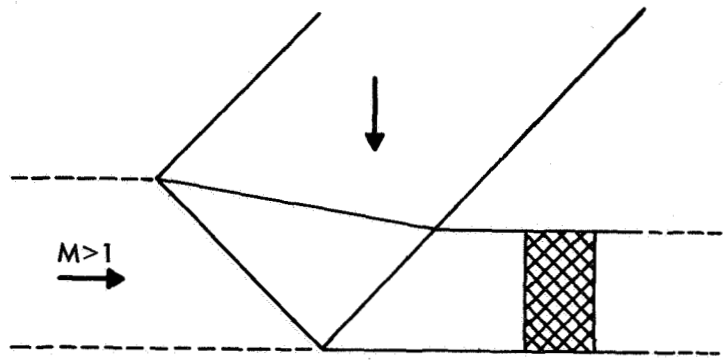

FIGURE 4.—Two-dimensional lifting configuration with no sonic boom.

area rules, because these rules were derived for flows where the Bernoulli constant is the same on all streamlines and the processing will change the Bernoulli constant in that particular stream tube. The equivalent cylinder because of lift just fills in the reduction in stream-tube area because of the processing and from below $(-\pi/2)$ the equivalent cylinder is, as in the case for the biplane, one that extends from $-\infty$ to $+\infty$ and has no boom. Above the configuration, however $(+\pi/2)$, the cylinder is different from the biplane and is shown in the figure. Thus in two dimensions the configuration discussed has lift but there is no boom resulting from it.

THREE-DIMENSIONAL CONFIGURATIONS

The three-dimensional bodies meeting the same conditions are now easily visualized in the following manner. Assume a body of revolution extending from $-\infty$ to $+\infty$ of constant area. This body

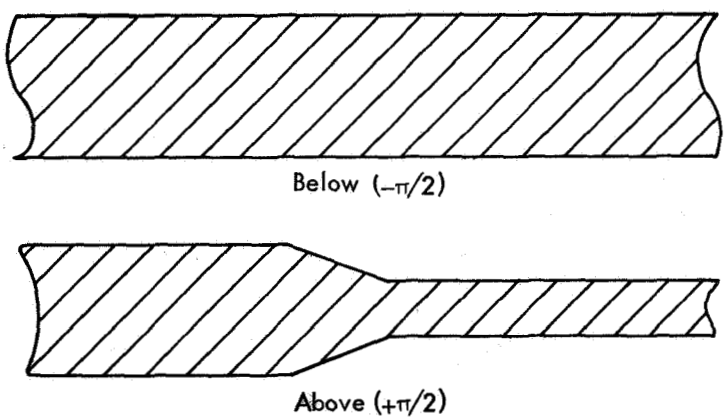

FIGURE 5.—Equivalent cylinders according to area rule for configuration in figure 4.

of revolution obviously has no boom associated with it. From this body of revolution remove the stream tube that contains the fluid that will be processed so that it will leave the configuration with a reduced stream-tube area. The difference in volume between the initial assumed body of revolution and the stream tube of reduced area can be used for a "lift body" so that from the ground at least there is no disturbance. This lift can be achieved with an ordinary wing located, of course, properly in accord with the area rules relative to the affected stream tube. This whole process is indicated schematically in figure 6. Thus boom attributed to lift can definitely be reduced by programing engine parameters appropriately if the engine is used to accomplish the required stream-tube area reduction.

In principle there is a class of configurations which have lift and no boom. Because this is accomplished by reducing a stream-tube area, in general there is a high velocity jet leaving the configuration. It should be realized that eventually dissipative processes will convert the kinetic energy of the jet into heat, and, as a result, the jet will eventually plume out to a larger area than at its origin at $-\infty$. However, because it is the dissipative processes that control this rate of energy conversion, it is expected that this pluming will take a very long distance in terms of aircraft lengths. Therefore while the pluming resulting from an expanding stream tube will cause a pressure disturbance on the ground beneath the aircraft, the rate of expansion is so slow that the equivalent body length will be very long and the ground disturbance will hardly be perceptible.

AERODYNAMIC PROPERTIES OF BOOMLESS CONFIGURATIONS

It is interesting to note that the configuration discussed above does not give the characteristic N-wave in the far field at any azi-

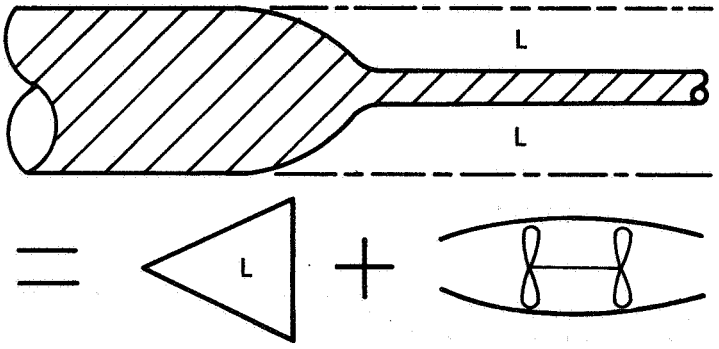

FIGURE 6.—Construction of three-dimensional configuration with lift and no sonic boom from equivalent body of revolution according to area rule.

315-766 O—68——8

muthal angle. In the far field at angles other than $-\pi/2$ (ground), the reduced stream tube more than compensates for the "lift volume." Thus the far-field pressure signature is an expansion followed by a shock and then the tail wave. For the case where the lift boom is completely canceled on the ground ($-\pi/2$), the shock wave is strongest above the configuration ($+\pi/2$).

It is also of interest to note that there is a drag penalty that is paid for the boom cancellation on the ground. Referring again to the two-dimensional case (fig. 4), it is obvious that the drag of this configuration is twice that of an ordinary flat plate at angle of attack giving the same lift. (Or alternatively the drag is the same as for the flat plate without the channel but one-half of the lift has been canceled by the bottom plate pressure rise, or the downward moving wave and its associated downward momentum has been intercepted.)

In the three-dimensional case, as suggested by Hayes at this conference, the factor is 3. That is, the drag for a given lift using this scheme is three times what it would be for an ordinary wing with the same lift. This can be computed as follows. Using Lighthill's result (ref. 2) that the wave drag of a body of revolution is just equal to an integral of the square of the F-function and Lomax's relation (ref. 1) between the lift and the equivalent body of revolution, namely

$$S_e''(y,\theta)=-\frac{\beta}{2q}\,l'(y,\theta)$$

where θ is the azimuthal angle, $\beta=\sqrt{M^2-1}$, q is the dynamic pressure, and $l'(y,\theta)$ is the streamwise (y-direction) gradient of the lift force in the proper obliquely cut sections and S_e'' the second derivative of the area of the obliquely cut sections. The F-function $F(y)$ for no boom on the ground is then:

(Lighthill's notation)

$$F(y)=\frac{1}{2\pi}\int_0^y\left\{-\frac{\beta}{2q}\frac{l(t)\sin\theta\,dt}{(y-t)^{1/2}}-\frac{\beta}{2q}\frac{l(t)\,dt}{(y-t)^{1/2}}\right\} \tag{1}$$

Thus for $\theta=-\pi/2$, $F(y)=0$. Note also that

$$F(y)\propto(\sin\theta+1) \tag{2}$$

so

$$F^2(y)\propto(\sin\theta+1)^2 \tag{3}$$

and integrating from $\theta=0$ to $\theta=2\pi$ gives a drag proportional to 3π. For the lifting element only which means keeping only the first term $\int_0^{2\pi}\sin^2\theta\,d\theta=\pi$. Thus the ratio of the drag of the boomless lifting

configuration to that of the wing above which gives boom on the ground is in the ratio of $3\pi/\pi=3$ regardless of the lift distribution with y. The same result is evident from George's work (ref. 3) using his formula (16) and in his notation noting that for no boom $B_1=A_0$ (eq. 13) so the wave drag is just

$$D_w=2D_0^{(A)}+D_1^{(B)} \qquad \text{and} \qquad D_0^{(A)}=D_1^{(B)} \tag{4}$$

In this formulation $D_1^{(B)}$ is just the drag attributed to a pressure dipole or the wing alone. Again the ratio is just 3, because this is the same calculation.

Fortunately this penalty is paid in wave drag alone. The drag of supersonic aircraft is chiefly viscous drag and the penalty paid in wave drag alone may not be large compared with the total drag.

ENGINE DESIGN

In another related paper (4) the possibility of using an engine to accomplish the stream-tube reduction is discussed. In particular, a ducted fan was used to effect the area reduction. By setting the thrust of this unit equal to the drag of the aircraft, it is found that the area reduction ΔA possible by this means is just

$$\frac{\Delta A}{A_R}=\frac{1}{1+A_R/A_i} \tag{5}$$

In equation (5), A_i is the inlet area of the unit and

$$A_R=\frac{W}{(L/D)\gamma p_i M^2}$$

where W=weight, L/D=lift-drag ratio, γ=ratio of specific heats, p_i=ambient pressure at cruise altitude, and M=flight Mach number. Note that even if $A_i\to\infty$ ΔA is at most A_R, so a limited amount of reduction is possible with this scheme. It is also shown in this reference that in order to produce the power aboard the aircraft with a turbine, the turbine exhaust stream-tube area necessarily is larger than the inlet stream-tube area. This effect reduces the net possible area reduction. If $\Delta A'$ is the area increase attributed to producing the fan power, one finds:

$$\frac{\Delta A}{A_R}=\frac{1}{\frac{2}{\gamma-1}\eta\frac{1}{M^2}\frac{\Delta A'}{A_R}\frac{T_t}{\theta}-1} \tag{6}$$

In this equation η is the turbine cycle efficiency, T_t is the turbine blade temperature and θ is the ambient air temperature at cruise

altitude. To be able to alleviate the boom it is necessary that $\Delta A > \Delta A'$ which implies that the cycle efficiency η be

$$\eta > (\gamma - 1) M^2 \left(\frac{\theta}{T_t} \right) \quad \text{for} \quad \Delta A > \Delta A' \tag{7}$$

The efficiency of the cycle used here is related to the temperature rise through the compressor ahead of the turbine, namely $\eta = 1 - \theta / T_c$, where T_c is the temperature of the air out of the compressor. Thus equation (7) dictates a certain compression ratio for the compressor. This analysis also identifies the important parameters involved in attempting to reduce sonic boom with an engine. Of course there are other schemes, some of which are better than the one described here.

SUMMARY

It has been demonstrated here that there are a class of supersonic configurations that have lift but no sonic boom. Using these principles, the sonic boom attributed to lift can be alleviated by integrating the engine design with the design of the rest of the aircraft.

REFERENCES

1. LOMAX, H.: The Wave Drag of Arbitrary Configurations in Linearized Flow as Determined by Areas and Forces in Oblique Planes. NACA RM-A-55A-18, Jan. 1955.
2. SEARS, W. R., ED.: General Theory of High Speed Aerodynamics. Princeton University Press, 1954, p. 449.
3. GEORGE, A. R.: Reduction of Sonic Boom by Azimuthal Redistribution of Overpressure. AIAA Paper No. 68-159, 1968.
4. RESLER, E. L., JR.: Lifting Aerodynamic Configurations with No Sonic Boom. Presented at proceedings of the AFOSR-UTIAS Symposium on Aerodynamic Noise (University of Toronto), May 1968.

ACKNOWLEDGMENTS

The author wishes to acknowledge many interesting discussions with his colleagues, Professors A. George, R. Seebass, and W. R. Sears. This work has been partially supported by the United States Air Force Office of Scientific Research under contract AF49(638)-1346, and by the National Aeronautics and Space Administration under NGR33-010-057.

The Approach to Far-Field Sonic Boom

F. K. Moore and L. F. Henderson
Cornell University

INTRODUCTION

In this study we have considered the approach to far field as described by the Whitham theory (ref. 1). Assuming that the observed signature would be nearly an N-wave, we have asked how the Whitham theory describes the first departure from that result as one moves toward the body. The hope is that, if attention is restricted to the approach to far field, signature improvements could be related in a simpler way to the aircraft configuration than would the description of changes throughout the entire flow field. If some such simplicity of influence could be found, perhaps effects of high Mach number, density stratification, and the like could also be simply expressed. It should be emphasized that in this problem the Whitham theory has been used without modification. The question is one of efficient presentation of results.

SYMBOLS

p	static pressure
h	miss distance
l	length of body
γ	ratio of specific heat
M	Mach number
β	$\sqrt{M^2-1}$
F	pressure on equivalent body
I	$\int_0^\tau F(\tau)\, d\tau$
τ	dimensionless distance along body axis
k	function of M (ref. 2)
ϵ	small parameter, equation (3)
$\bar{\epsilon}$	transformed version of ϵ
E	small parameter, equation (15)
x	streamwise coordinate

Subscript

0 evaluation where $F=0$ (smooth body) or just ahead of discontinuity of F passing through zero.

EXPANSION FOR APPROACH TO FAR FIELD

For purposes of discussion we may limit attention to the strength of the shock compression as given by the Whitham theory:

$$\left[\frac{\frac{\Delta p}{p}\left(\frac{h}{l}\right)^{3/4}}{\gamma\left(\frac{\sqrt{2}}{\gamma+1}\right)^{1/2}\beta^{1/4}}\right]_{\substack{\text{bow}\\\text{shock}}}=\sqrt{I(\tau)}$$

$$\left[\left(\frac{h}{l}\right)^{1/2}\right]_{\substack{\text{bow}\\\text{shock}}}=\frac{2}{k}\frac{I(\tau)}{F^2(\tau)} \tag{1}$$

where $F(\tau)$ is the customary integral of the curvature of an equivalent area function. In equations (1), τ can be regarded as the parameter enabling connection to be made between pressure jump and "miss distance." The ultimate N-wave is achieved when τ approaches τ_0, the axial location where the F-function passes through zero and the characteristic staying parallel to the free-stream characteristic originates.

To seek the description of the approach to the far field it would seem reasonable to expand the foregoing solution about τ_0, but eliminating explicit dependence on τ in the result. The following expansion results from this procedure.

$$\frac{\sqrt{I(\tau)}}{\sqrt{I_0}}=1+\frac{F_0}{2I_0}\epsilon+\frac{1}{4}\left[\frac{F_0'}{I_0}-\frac{F_0}{I_0}\left(\frac{\frac{F_0''}{F_0}-\frac{3}{2}\frac{F_0'}{I_0}+\frac{3}{4}\frac{F_0^2}{I_0^2}}{\frac{F_0'}{F_0}-\frac{1}{2}\frac{F_0}{I_0}}\right)-\frac{1}{2}\frac{F_0^2}{I_0^2}\right]\epsilon^2+\cdots \tag{2}$$

where

$$\epsilon\equiv\sqrt{2I_0}\frac{\left[\frac{1}{k}\left(\frac{l}{h}\right)^{1/2}\right]^{1/2}-\left(\frac{1}{2}\frac{F_0^2}{I_0}\right)^{1/2}}{F_0'-\frac{1}{2}\frac{F_0^2}{I_0}} \tag{3}$$

Subscripts 0 in the foregoing equations refer to quantities evaluated at τ_0.

Clearly, ϵ vanishes as $\tau \to \tau_0$, in view of equations (1), and $I \to I_0$ as it ought. Thus, ϵ is the small quantity governing approach to the far field, whether the equivalent body is smooth near τ_0 (so that $F_0=0$) or has a shoulder (so that F_0 has a positive value just ahead of the shoulder, as in fig. 1).

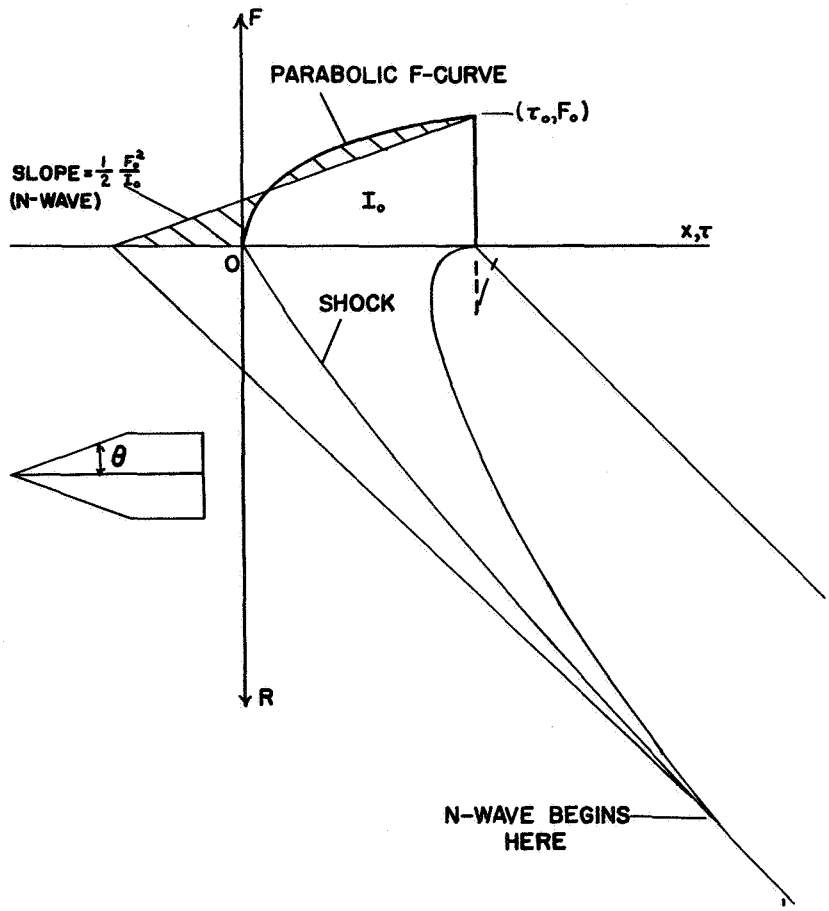

FIGURE 1.—F-curve and wave system for cone cylinder.

If one has a smooth body for which $F_0=0$, the asymptotic series just described contains no linear term in ϵ. For example, the first two terms of equation (2) would be

$$\frac{\sqrt{I(\tau)}}{\sqrt{I_0}}=1+\frac{(l/h)^{1/2}}{2kF_0''}+\cdots \tag{4}$$

This result is consistent with the equation cited by Lighthill (ref. 2) for pressure gradient in the far field, when the spreading of the N-wave is taken into account. If the body is not smooth, the linear term is present, and the N-wave is achieved at the finite distance defined by $\epsilon \to 0$.

REDUCTION OF SHOCK STRENGTH—SMOOTH BODY

For the moment, concentrating on the smooth body, we may ask if it may fairly be concluded that the strength of the shock given by equation (4) in the "almost-far" field may be reduced by making F_0' small (it is negative anyway). That is, we consider giving the F-function a pronounced S-shape near τ_0. A little study shows that this approach is not fruitful. The reason is that, apart from convergence problems, equation (4) is physically misleading in the following sense: If F_0' were zero then F would tend to remain near zero in the vicinity of τ, and the inclination of nearby characteristics would tend to remain the same as that emanating from τ_0 itself. This group of characteristics would therefore not overtake the shock, because they would not be spreading. Thus, although the signature would tend to have an S-shape, the inflection region would be confined to a band of characteristics which, going out from the body, would be a progressively smaller proportion of the signature width.

REDUCTION OF SHOCK STRENGTH—DISCONTINUOUS BODY

When the equivalent body is not smooth ($F_0 \neq 0$), then the series of equation (2) would appear to have a more useful application. Of course, when F passes discontinuously through zero, one expects an N-wave at a specific distance from the body, namely, when the numerator of ϵ goes to zero. Figure 1 is intended to illustrate this process for a cone cylinder. As explained in Lighthill's article, one may locate the beginning of the N-wave at the confluence of characteristics emanating from the endpoints of a line which cuts equal areas ahead of and within the F-curve, as shown shaded on the sketch. The slope of the line which cuts equal areas is $\frac{1}{2}F_0^2/I_0$, by simple geometry. Next, we ask if boom reduction can be expected when the denominator ϵ is small and negative:

$$F_0' \approx \frac{1}{2}\frac{F_0^2}{I_0}$$

In effect, one considers tilting the F-curve to reach τ_0 at nearly the same slope as the line cutting equal areas. Figure 2 illustrates this sort of change, in which, by the way, the area I_0 is kept the same.

Although again, we can hardly expect convergence when the denominator of ϵ goes to zero, we note that because there is a gradient of F, and F determines the spreading of the Mach waves, they can in fact undergo mutual interference. Figure 2 sketches this effect. The expansion emanating from τ_0 has a higher F, and therefore will spread more rapidly than will the compression emanating from just ahead at a lower value of F. Thus the compression will prevent the expansion from the shoulder from reaching the shock as soon as it otherwise would have done, and the N-wave formation is delayed.

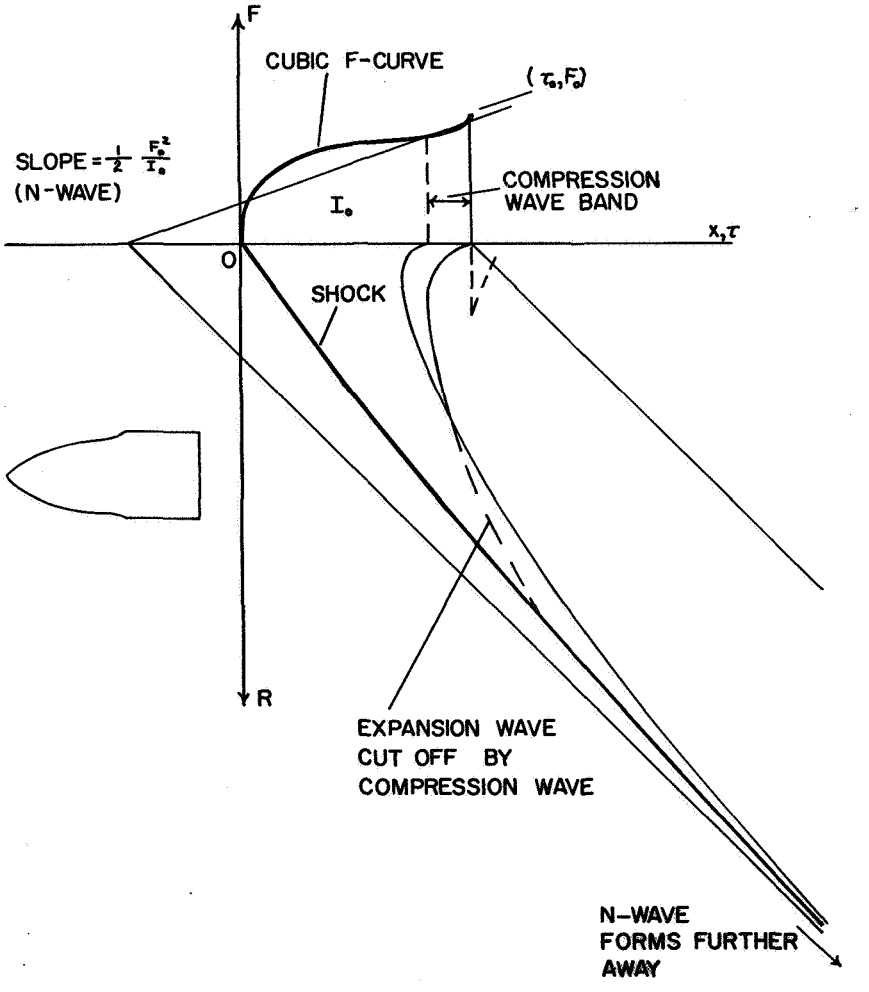

FIGURE 2.—F-curve and wave system for perturbed cone cylinder.

In consequence, if I_0 is conserved, the strength of the bow shock at a given location will be diminished. The overall energy in the N-wave would not be changed, though at a given location the shape would presumably be more S-shaped. It seems, then, that placing a compression ahead of the expansion corner may diminish the bow-shock strength for this shape.

IMPROVEMENT OF CONVERGENCE

Clearly, equation (2) does not converge fast enough to be useful in general circumstances. By considering certain specific cases, we can find an expansion parameter which gives better convergence than ϵ. We must distinguish, of course, between smooth and discontinuous F-functions.

(1) *Three-quarter-power body and cylinder.*—For this configuration, the F-function is a square wave, $F=F_0$, between $\tau=0$ and τ_0. The exact formula for $\sqrt{I}$ in this case is

$$\frac{\sqrt{I}}{\sqrt{I_0}}=\frac{F_0}{\sqrt{I_0}}\sqrt{\frac{k}{2}}\left(\frac{h}{l}\right)^{1/4} \tag{5}$$

and, from equation (3), the parameter ϵ is

$$\epsilon=\frac{2I_0}{F_0}\left[1-\frac{\sqrt{I_0}}{F_0}\frac{1}{\sqrt{\frac{k}{2}}\left(\frac{h}{l}\right)^{1/4}}\right] \tag{6}$$

Now, we ask, what parameter $\bar{\epsilon}$, expressed in terms of ϵ, would make the first two terms of equation (2) exact:

$$\frac{\sqrt{I}}{\sqrt{I_0}}=1+\frac{F_0}{2I_0}\bar{\epsilon} \tag{7}$$

Combining equations (5) and (7), and using equation (6) gives

$$\bar{\epsilon}=\frac{\epsilon}{1-\frac{F_0}{2I_0}\epsilon} \tag{8}$$

or

$$\frac{\epsilon}{1-\frac{\epsilon}{2\tau_0}}$$

Thus, the square-wave example suggests equation (8) as a Euler transformation to improve convergence.

(2) *Cone cylinder.*—The F-function is a parabola, $F=F_0\sqrt{\tau}/\tau_0$. Applying the foregoing procedure in this case gives

$$\bar{\epsilon}=\frac{2I_0}{F_0}\left[\frac{1}{\left(1-\frac{F_0'}{6I_0}\epsilon\right)^3}-1\right] \tag{9}$$

Actually, equation (9) supports use of the simpler expression, equation (8), because the two agree to first order in ϵ, agree at $\epsilon=-\infty$, and agree within 12 percent at $\epsilon=-I_0/F_0$.

(3) *Sine-wave F-function, $F\equiv A\sin\pi\tau/\tau_0$.*—We choose this as a simple "smooth" case, and ask, what ϵ would make the two leading terms of equation (2) exact in that case:

$$\frac{\sqrt{I}}{\sqrt{I_0}}=1+\frac{F_0'}{4I_0}\bar{\epsilon}^2 \tag{10}$$

we find,

$$\bar{\epsilon}^2=\frac{\epsilon^2}{1-\frac{\pi^2}{16}\frac{\epsilon^2}{\tau_0^2}} \tag{11}$$

Equation (11) might serve as a suitable variable for smooth bodies.

Now, if equation (8) is adopted, for discontinuous-slope bodies, the following formula results, using only two terms of equation (2):

$$\frac{\sqrt{I}}{\sqrt{I_0}}=\frac{F_0'-F_0^2/2I_0}{F_0'-\frac{1}{2}\left[\sqrt{\frac{2}{k}}\left(\frac{h}{l}\right)^{1/4}\right]\frac{F_0}{\sqrt{I_0}}} \tag{12}$$

Of course this formula has the feature previously discussed, that for the F-curve of figure 2, the numerator vanishes and the shock strength vanishes, except that when the N-wave is formed, numerator and denominator become equal, and I/I_0 is presumably one.

Returning to the complete expansion, equation (2), we may rederive the series in powers of a variable

$$\bar{\epsilon}\equiv\frac{\epsilon}{1-\epsilon}$$

chosen in place of equation (8) for simplicity, and because τ_0 is of unit order. This Euler transformation is evaluated on figure 3 for a particular cone cylinder for which the Whitham theory is in good agreement with experiment (ref. 3). It is seen that convergence of the transformed series is very good quite close to the body, even closer than $\epsilon=-1$. Equation (12) is not displayed on figure 3, but its accuracy is comparable to the three-term Euler series, for the body chosen.

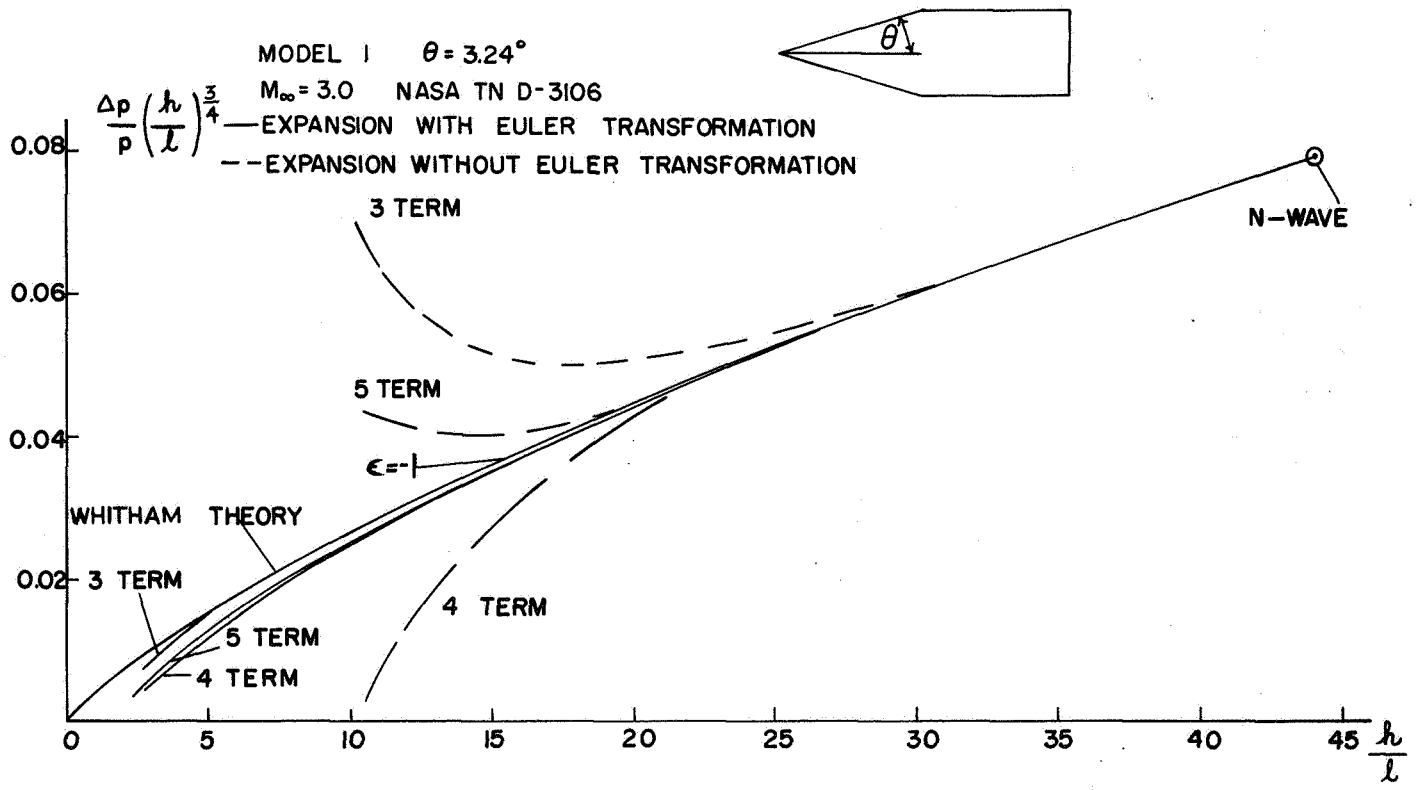

FIGURE 3.—Comparison of expansion formulas with Whitham theory for cone cylinder.

CONCLUDING REMARKS

It is clear that simple formulas can be derived by suitable choice of variable to give the shock strength quite accurately in the region of approach to far field and, as hoped, these formulas (e.g., eq. (12)) clearly suggest how changes in equivalent body shape can modify the signature in that region; the addition of a compression ahead of the expansion corner would improve matters, not everywhere in the flow, but as the N-wave is approached. The expansion method suggests that no modification is possible for smooth bodies which will favorably affect the nearly far-field shock strength.

The approach described here should be extended to consider the signature shape behind the bow shock, hoping to find simple formulas for rise time, for example. The series upon which this extension would be based is

$$\frac{\Delta p}{p}\left(\frac{h}{l}\right)^{1/2}=\frac{\gamma M^2}{\sqrt{2}\beta^{1/2}}\left\{F_0+\frac{F_0'}{1-k\left(\frac{h}{l}\right)^{1/2}F_0'}E+\frac{F_0''}{\left[1-k\left(\frac{h}{l}\right)^{1/2}F_0'\right]^3}\frac{E^2}{2}+\cdots\right\} \tag{14}$$

where

$$E=\frac{x}{l}-\beta\left(\frac{h}{l}\right)+k\left(\frac{h}{l}\right)^{1/2}F_0-\tau_0 \tag{15}$$

Geometrically, E is the distance that the characteristic from τ stands ahead of the front characteristic from τ_0.

SUMMARY

A series is derived for small departures from an N-wave for bodies of smooth and discontinuous slope. For the latter, the leading terms suggest that adding a compression just ahead of the shoulder reduces shock strength in the approach to far field. A Euler transformation is found to improve convergence of the series.

REFERENCES

1. Whitham, G. B.: The Flow Pattern of a Supersonic Projectile. Commun. Pure Appl. Math., vol. 5, 1952, pp. 301–348.
2. Lighthill, M. J.: General Theory of High Speed Aerodynamics. Vol. 6, Princeton Series, W. R. Sears, ed., 1954, pp. 345–489.
3. Carlson, H. W.; Mack, R. J.; and Morris, O. A.: A Wind Tunnel Investigation of the Effect of Body Shape on Sonic-Boom Pressure Distributions. NASA TN D-3106, Nov. 1965.

Nonlinear Effects on Sonic Boom Intensity

M. T. LANDAHL, I. L. RYHMING, and L. HILDING
The Aeronautical Research Institute of Sweden

INTRODUCTION

The purpose of the investigation is to study those higher order effects on sonic boom strength that are normally neglected in the currently used first-order Whitham theory. In this exploratory phase, the method of matched asymptotic expansions is employed to assess the importance of second-order effects on the flow field in some simple cases. The associated change in shock strength can then be calculated from the disturbance flow field by use of the ordinary shock relations.

TWO-DIMENSIONAL FLOW

A complete account of the second-order complete flow field pattern for the two-dimensional case has been presented by Lighthill (ref. 1). As an introduction to the more complicated axisymmetric case, the two-dimensional far field will be analyzed by continuing to second order the matched asymptotic expansion method developed to first order by Van Dyke (ref. 2). Accordingly, the perturbation velocity component u $(\xi, \eta; \epsilon)$ in the far field, where $\xi=x-By$, $\eta=By$, and ϵ is a thickness parameter, is expanded as follows:

$$u(\xi, \eta; \epsilon)=\epsilon U_1(\xi,H)+\epsilon^2 U_2(\xi,H)+ \ldots \qquad H=\epsilon\eta \tag{1}$$

By inserting the expansion into the partial differential equation for the velocity potential and equating terms of like powers in ϵ, one obtains

$$U_{1_H}+KU_1U_{1_\xi}=0 \tag{2}$$

$$U_{2_H}+K(U_1U_2)_\xi=\frac{1}{2}\varphi_{1_{HH}}+M^2\left(\gamma U_1U_{1_H}+\varphi_{1_H}U_{1_\xi}-\frac{1}{2}KU_1^2U_{1_\xi}\right) \tag{3}$$

where $U_1=\varphi_{1_\xi}$, $K=\frac{1}{2}M^2(\gamma+1)B^{-2}$, and $B^2=M^2-1$.

These equations can be solved most readily by employing the Monge theory (ref. 3). One finds that the solutions may be expressed parametrically as follows

$$U_1=G(z) \tag{4}$$

$$\xi=KHG(z)+z \tag{5}$$

and

$$U_2=\left[\frac{1}{2}K-(\Upsilon+1)M^2\right]G^2(z)+Ct^{-1} \tag{6}$$

where

$$t=B(1+KHG'(z)) \tag{7}$$

The lines $z(\xi, H)=$constant describe the characteristics. Matching to the inner first-order solution gives

$$G(z)=-\frac{1}{B}T'(z) \tag{8}$$

where $y=\pm\epsilon T$ gives the airfoil shape. For determination of the constant C, matching to the second-order inner solution is required.

AXISYMMETRIC FLOW

By employing a gage function analysis, it is found that the appropriate expansion for u in the far field in this case reads

$$u(\xi, \eta; \epsilon)=\epsilon^4U_1(\xi,H)+\epsilon^8U_2(\xi,H)+\ \ldots \qquad H=\epsilon^4\eta \tag{9}$$

The equations for U_1 and U_2 become

$$U_{1_H}+KU_1U_{1_\xi}+\frac{1}{2H}U_1=0 \tag{10}$$

$$U_{2_H}+K(U_1U_2)_\xi+\frac{1}{2H}U_2=\frac{1}{2}\varphi_{1_{HH}}+M^2\left(\gamma U_1U_{1_H}+\varphi_{1_H}U_{1_\xi}-\frac{1}{2}KU_1^2U_{1_\xi}\right)$$
$$+\frac{1}{2H}\varphi_{1_H}+\frac{M^2(\gamma-1)}{2H}U_1^2 \tag{11}$$

The solution for U_1 may be written

$$U_1H^{1/2}=G(z)$$
$$\xi=2KG(z)H^{1/2}+z \tag{12}$$

where $G(z)$ is a function to be found by matching with the inner solution. According to Van Dyke (ref. 4), the inner solution to second order is given by

$$\varphi=\epsilon^2\varphi_1+\epsilon^4\varphi_2 \tag{13}$$

where

$$\varphi_1=-\frac{1}{2\pi}\int_0^{x-Br}\frac{f(x_1)\,dx_1}{\sqrt{(x-x_1)^2-B^2r^2}} \tag{14}$$

$$\varphi_2=M^2\varphi_1\varphi_{1_x}+Kr\varphi_{1_r}\varphi_{1_x}-\frac{\epsilon^2M^2}{4}r\varphi_{1_r}^3 \tag{15}$$

and $\epsilon^2f(x)$ is the source strength. The last term in the expression for φ_2 must be included, because for $r=O(\epsilon)$, φ_{1_r} is of order ϵ^{-1}, and this term is hence of the same order as the others in the neighborhood of the body surface. For $r=O(1)$, however, the term may be neglected.

To the particular solution for φ_2 one could also have added a homogenous solution of the same form as φ_1. However, it is actually simpler to incorporate this term in φ_1 and instead assume f to have a correction term of order ϵ^2 (or, of order ϵ^2 ln ϵ for a slender body). Thus, it is assumed that

$$f=f_1+\epsilon^2f_2 \tag{16}$$

For the matching, the outer limit of the near-field solution is taken by replacing $\eta=Br$ by H/ϵ^4 in (13) and expanding in powers of ϵ. This yields

$$u=\epsilon^4[H^{-1/2}F(\xi)-2KF(\xi)F'(\xi)]+\epsilon^8\Big[-H^{-3/2}F^{(1)}(\xi)$$
$$+H^{-1}(4M^2-K)\Big(\frac{1}{4}F(\xi)^2+2F^{(1)}(\xi)F'(\xi)\Big)\Big]+\cdots \tag{17}$$

where

$$F(\xi)=-\frac{1}{2\pi\sqrt{2}}\int_0^\xi\frac{f'(t)\,dt}{\sqrt{\xi-t}} \tag{18}$$

and

$$F^{(1)}(\xi)=-\frac{1}{8\pi\sqrt{2}}\int_0^\xi f'(t)\sqrt{\xi-t}\,dt\equiv\frac{1}{8}\int_0^\xi F(\xi_1)\,d\xi_1 \tag{19}$$

If a homogenous term had been included in the solution for φ_2, the outer limit would have included a term of the form

$$\epsilon^6H^{-1/2}F_2(\xi) \tag{20}$$

which would have required, for matching, an additional term of order ϵ^6 in the outer solution. Comparing the two expressions (12) and (17) for u, one finds that

$$G(z)=F(z) \tag{21}$$

and the solution for U_1 is thus given by

$$\begin{aligned} U_1 &= F(z)H^{-1/2} \\ \xi &= 2KF(z)H^{1/2}+z \end{aligned} \tag{22}$$

To lowest order in ϵ for a slender body

$$f=\epsilon^{-2}S'=\overline{S}' \tag{23}$$

where $S(x)=\pi\epsilon^2R^2(x)$ is the cross-sectional area, and the solution (22) is found to be equivalent to that of Whitham (ref. 5). By inserting the expression for U_1 into the equation for U_2 and solving as above, one obtains

$$U_2H^{1/2}(1+2KF'H^{1/2})=K\left[K-M^2\left(\gamma+\frac{5}{2}\right)\right]F^2F'\log H$$

$$+(4M^2-2K)\left(\frac{1}{4}F^2+2F^{(1)}F'\right)H^{-1/2}-F^{(1)}H^{-1}+\text{const} \tag{24}$$

where $F(z)$ and $F^{(1)}(z)$ are the same functions as before. To determine the free constant, one needs to match to a third-order (of order ϵ^6) inner solution not presently available. The other terms match completely with the second-order inner solution.

To determine the relation between f and the body shape, we expand φ_1 for small r in the manner of slender-body theory. Hereby we find after some manipulations that

$$\varphi_{1_r}=\frac{f(x)}{2\pi r}+\frac{1}{2}B^2r\left(\varphi_{1_{xx}}-\frac{f''}{2\pi}\right)+\ldots \tag{25}$$

Inserting this expression into the formula for φ_2 and carrying out the differentiation with respect to r, one obtains

$$\varphi_r=\frac{\epsilon^2}{2\pi r}f(x)+\epsilon^4\left\{\frac{1}{2}B^2r\varphi_{1_{xx}}+\frac{M^2}{2\pi r}\frac{\partial}{\partial x}(f\varphi_1)\right.$$

$$\left.+\frac{K}{(2\pi)^2r}ff'+\frac{M^2}{2}\left(\frac{f}{2\pi}\right)^3\frac{\epsilon^2}{r^2}-\frac{B^2r}{4\pi}f''\right\} \tag{26}$$

The tangency condition at the body surface requires that

$$(1+\varphi_x)\varphi_r=\epsilon R' \qquad \text{at} \qquad r=\epsilon R(x) \tag{27}$$

By introducing the expansion (16) for f, and iterating by employing the lowest order approximation f_1 in the second-order terms, one obtains

$$f_2=B^2\left[\frac{1}{4\pi}\overline{S}\overline{S}'''-\left(\overline{S}\varphi_{1_x}\right)_x\right]-M^2\left[\varphi_1\overline{S}''+\pi R\,(R')^3\right]-\frac{K}{4\pi}(\overline{S}^2)_x \quad (28)$$

in which $f=f_1$ should be used in the calculation of φ_{1_x}.

One finds that f_2 has the finite value of $-M^2\varphi_1\overline{S}''$ at the rear end of the body. Hence, the modified source strength will have a discontinuity similar to what would appear in the first-order source strength for a body with a corner. Because corners have not been allowed for in the above simple analysis, the calculation of the second-order correction to the flow field for regions influenced by the aft end of the body cannot yet be carried out.

From f_1 and f_2 one may then determine the second-order Whitham function, F_W,

$$F_W=\epsilon^2F=\epsilon^2F_1+\epsilon^4F_2 \quad (29)$$

by inserting $f=f_1+\epsilon^2f_2$ into equation (18).

As an example, the first- and second-order source strengths and Whitham F-functions are computed for a parabolic body of revolution of thickness ratio $\epsilon=0.07$. As seen in figures 1 and 2, the second-order effects are fairly small near the forward portion of the body but quite noticeable toward the rear. Hence one would conclude that the higher order effects would have most influence on the rear shock.

THREE-DIMENSIONAL FLOW

Three-dimensional nonaxisymmetric flow is most conveniently treated in cylindrical coordinates x, r, and θ. The small parameter ϵ in this case is assumed to be the thickness ratio of a body of revolution having the same cross-sectional area distribution as the three-dimensional body. For the far field one then assumes

$$u=\epsilon^4U_1(\xi,H,\theta)+\epsilon^8U_2(\xi,H,\theta) \quad (30)$$

with ξ and H defined as before. Upon introduction into the differential equation for the velocity potential, one finds that the ilnear term $r^{-2}\varphi_{\theta\theta}$ will only appear in the equation for U_2 and that consequently, the equation for U_1 will be the same as for the axisymmetric case. Hence, the solution for U_1 may be expressed as

$$U_1H^{1/2}=F(z;\,\theta) \quad (31)$$

$$\xi=2KF(z;\,\theta)H^{1/2}+z \quad (32)$$

Matching to the inner first-order solution shows that F is given to lowest order by (18) as before, but with $f(x;\theta)$ calculated from the equivalent body of revolution for each θ as determined by the standard supersonic area rule procedure. Thus the correctness of the commonly employed sonic boom calculation method for lifting wing-body combinations is verified to first order. The second-order solution is found to be

$$U_2H^{1/2}(1+2KF_zH^{1/2})=\left\{KF^2F_z\left[K-M^2\left(\gamma+\frac{5}{2}\right)\right]+2K^2F_z\left(FF_{\theta\theta}+F_\theta^2\right)\right\}\log H$$
$$-\left[\left(F^2+F_z\int F\,dz\right)\left(\frac{K}{2}-M^2\right)+2K\left(FF_{\theta\theta}+F_\theta^2\right)+2KF_z\int F_{\theta\theta}\,dz\right]H^{-1/2}$$
$$-\left(\frac{1}{8}\int F\,dz+\frac{1}{2}\int F_{\theta\theta}\right)H^{-1}+\text{const} \quad (33)$$

where subscripts θ and z indicate partial derivatives. The solution

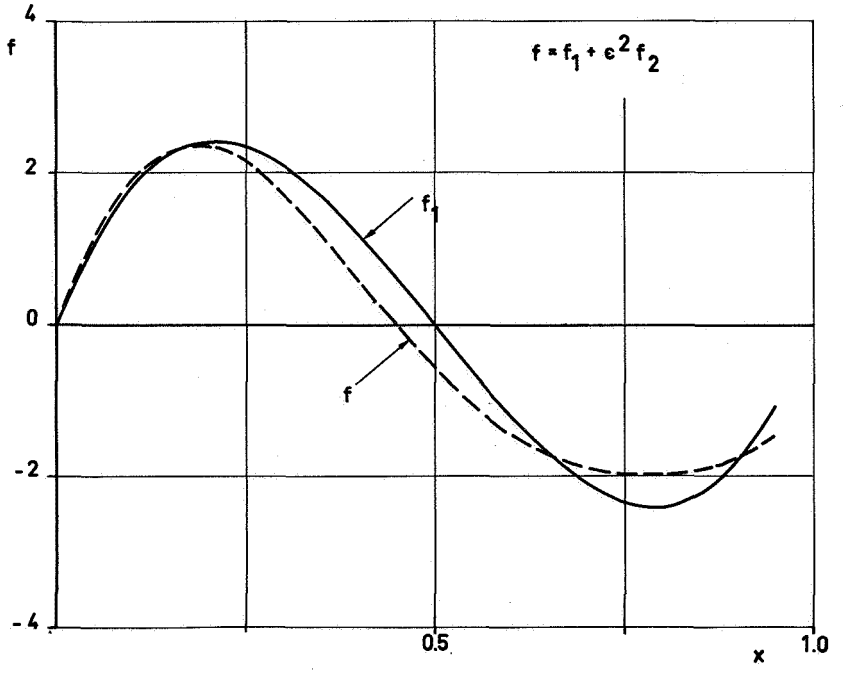

FIGURE 1.—First- and second-order source strength distribution for a parabolic body of revolution of thickness ratio $\epsilon=0.07$. Radius function, $R=2x(1-x)$, $M=2.5$, $\gamma=1.4$.

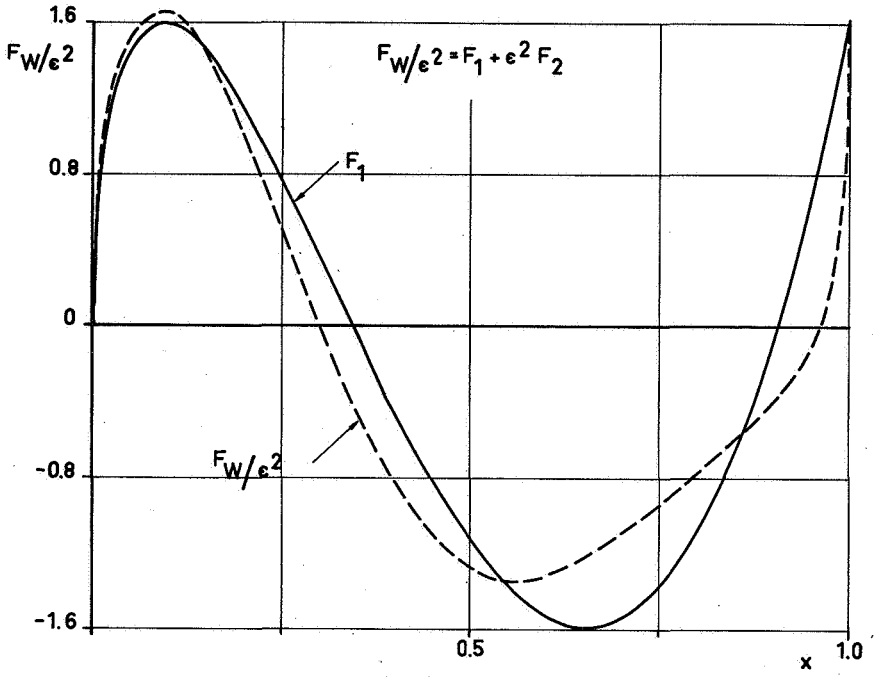

FIGURE 2.—First- and second-order Whitham function for parabolic body of revolution in figure 1.

differs from the one for axisymmetric flow by the terms containing derivatives with respect to θ, which all are generated by the term $r^{-2}\varphi_{\theta\theta}$. For the nonaxisymmetric case no second-order near-field solution is readily available, and the matching cannot therefore be completed. Hence, the second-order correction to the Whitham function cannot be calculated at present.

CONCLUSIONS

It was found in the analysis that for three-dimensional flow the first-order equation describes the far-field wave structure very accurately with a relative error of only $O(\epsilon^4)$ (the second-order term is of order ϵ^8 as compared to ϵ^4 for the first-order term). As a consequence the dominating higher order effect is that attributed to the nonlinear relationship between body slope and disturbance velocities at the outer boundary of the near field, which produces a second-order correction to the Whitham F-function. A calculation of source strength change, and hence the correction to the Whitham function, for a slender axisymmetric body indicates that the second-order contribution may be quite noticeable, particularly for regions toward the rear of the body. Also, the correction term increases in magnitude with

the Mach number approximately as M_2, so that it becomes more important at high supersonic speeds.

For three-dimensional configurations of general shape, no simple second-order solution for the near field is available, and one would then have to resort to some suitable approximate method. One such method, which has been employed recently (ref. 6) with considerable success for bodies of revolution with and without angle of attack, is the method of parametric differentiation (ref. 7) in its "local approximation" and work to apply this method has been initiated.

The possibility also exists to determine the near field from experiments. The theory indicates that by employing the measured disturbance flow field along a cylindrical surface at the edge of the near field, one should be able to predict very accurately the far-field flow pattern and shock strength.

In the analysis for the axisymmetric body the slender-body approximation was employed. To be valid the slender-body theory requires that the body is smooth without slope discontinuities. For a body with sharp corners there exists no simple relationship between body slope and source strength, and, in addition, the expansion for the far field will need to be modified. Another failure of the slender-body theory was that it produced a finite correction on the source strength and hence a jump in the source strength at the rear-pointed end of the body, thus precluding the calculation of the Whitham F-function for characteristics that meet the body axis downstream of the body. Consequently, the second-order effects on the rear shock cannot be analyzed until the slender-body approximation is removed.

REFERENCES

1. LIGHTHILL, M. J.: Higher Approximations, in General Theory of High Speed Aerodynamics. Princeton. 1954.
2. VAN DYKE, M.: Perturbation Methods in Fluid Mechanics. Academic Press, 1964.
3. SAUER, R.: Anfangswertprobleme bei Partiellen Differentialgleichungen. Julius Springer, 1952.
4. VAN DYKE, M.: A Study of Second-Order Supersonic Flow Theory. NACA Rept. 1081, 1952.
5. WHITHAM, G. B.: The Flow Pattern of a Supersonic Projectile. Commun. Pure Appl. Math., vol. 5, 1952, p. 301.
6. KACPRZYNSKI, J. J.; and LANDAHL, M. T.: Recent Developments in the Supersonic Flow Over Axisymmetric Bodies With Continuous or Discontinuous Slope. AIAA Paper 67–5, 1967.
7. RUBBERT, P.; and LANDAHL, M. T.: Solution of Nonlinear Flow Problems Through Parametric Differentiation. Phys. Fluids, vol. 10, no. 4, 1967, p. 831.

The Feasibility of Large Sonic Boom Reductions

ADOLF BUSEMANN
University of Colorado

INTRODUCTION

Small sonic boom reductions can be achieved by a large variety of changes in the airplane design until the optimization reaches the limits of absolutely rigid constraints; the possibility of finding new tricks to deal with the laws of nature may be remote in fields where our knowledge is well established and where the connection of all effects with the laws of nature is rather transparent. Supersonic flight and even supersonic aerodynamics do not have a long history as yet, but linearized theories in both two-dimensional and axially symmetric flow have existed for about 40 years and have lost their initial opaqueness with the years. Nevertheless, the central problem of this meeting, the sonic boom itself, came as a surprise with the beginning of supersonic flying some 20 years ago, though projectile waves and their investigations as Mach waves and shock waves count almost a century. Such historical facts may encourage our hopes for a compensatory surprise, or they may discourage us on account of the clarity of the supersonic theory. A linearized theory wins in time an apparent clarity, but can develop a widespread superstition as a result of its oversimplification. A nonexistence proof is still a different matter from a generally accepted transparency.

INVERSE RELATIONS

The sonic boom, as the footprint on the ground of a supersonic airplane in steady flight, seems to create more trouble than the benefits of high-speed transport can outweigh. Under such conditions the permissible footprint is getting the status of the independent variable or "master," while the shape of the airplane becomes the dependent function or "slave." Such reversal of a mathematical relation is the daily occurrence in engineering problems where "on second thought" everything is interdependent; but one should never forget that the seemingly trivial inversions of the simplest arithmetical operations created great mathematical revolutions which brought our number system or number space to perfection.

Because the pressure distribution in the far field, according to linearized supersonic aerodynamics, consists of a half differential with respect to the distribution of the cross-sectional area combined with the lifting forces along the airplane length, the inverse relation is simply a half integral (actually it is a 3/2 differential inversed to a 3/2 integral). As the name implies, the half integral is nothing but a half differential of an ordinary integral, which makes the mutual relations more or less equal. The trouble with noninteger differential or integral relations, however, is that the master function (in our case the airplane) may only be different from zero within a finite piece of the abscissa, while the slave function (the pressure in the far field) always gets a tail end stretching out to infinity. A complete reversal of such relations would attach the tail to the wrong partner. Imposing a tolerable footprint shape on an airplane of finite length must, therefore, lead to a compromise: prior to a given abscissa (say $x=0$) the footprint is the master and the airplane shape is the slave, but beyond that critical point the airplane is terminated and cannot play the slave anymore; thus the footprint falls back into its regular position as the slave with the tail. As long as infinite tales of decreasing strength are automatically unobjectionable, if started right, the proper precautions can be taken prior to the critical abscissa as a part of the prescribed footprint.

The result of such considerations combined with the fact that linearized relations permit the superposition of particular solutions leads to the following compromise plan:

Starting at a normalized abscissa prior to the terminal point (say at $x=-1$ prior to $x=0$) a delta-function and integer powers of $x+1$ are prepared for superpositions to a permissible footprint. For each particular function the half integral function $F_i(x)$ prior to the terminal point is established. Behind the terminal point $F_i(x)$ continues as a Taylor (Maclaurin) series with integer powers of x limited to 1/2 power below the power used in the starting portion of F_i. The tail created by this convention is less objectionable than the particular function in the pressure component $p_i(x)$ prior to the switching point. Out of the integer powers of x the rear portion of the superimposed total function $F(x)$ can be made to simulate the constant lift visible by the vortex wake behind the body, the zero cross section of the airplane body revised by a constant wake of cooled or heated air, and by positive or negative propulsion, if desired.

CENTERED LIFT

As soon as the F-function is determined, the area distribution of the body $A(x)$ and the accumulated lift $L(x)$ have to share the limited values of F along the abscissa. Because a resulting unbalanced

moment must be avoided, the center of mass and the center of lift have to coincide. This moment constraint can be seen clearly for the limit of a very soft body shell loaded with a constant specific weight throughout the body volume. In such a case the local lifting force $l(x)=\mathrm{d}L(x)/\mathrm{d}x$ has to be proportional to the local cross-sectional area $A(x)$ over the whole body length. The two relations, that $A(x)$ plus a constant (depending upon altitude and Mach number) times the lift $L(x)$ share the function $F(x)$, while $A(x)$ is proportional to $L'(x)$, makes the dividing of F into its parts A and L unique. If L is plotted first and A is the difference left between F and L, the slope of L must be made proportional to $F-L$. A hatchet with a given length of its shaft guided with the end of the shaft along the F-curve will cut automatically the L-curve (displaced by the length of the shaft in the abscissa). This so-called "pursuit curve" is the first step to divide F between A and L. Because the airplane shell is not really so soft as to require such a well-adjusted lift distribution, trading between local A's and L's can be made to improve the design of body and sweptwing. But the mass center and the lift center still have to coincide. Such constraint makes the footprint a genuine dictator for the complete airplane design.

UNCONVENTIONAL SHAPES

The considerations of the previous two sections of this paper are given in such detail because they can illustrate silent assumptions that have to be brought to light. Engineering compulsions and traditions very often introduce silent assumptions which we try to discover in "brainstorm" sessions. In case of severe restrictions, as they are imposed by sonic boom limitations, the conventional shape may not be able to survive. If, however, the details are exposed and the reasons for failing become obvious, the atmosphere for an unconventional exit is better prepared and the climate for a "breakthrough" may be created. The severe restrictions on the allocation of the given total $F(x)$ for area and lift are a combination of the necessity of making lift center and mass center coincide, but under the silent assumption that wing and body are in the same plane. If we were allowed to raise the wing high above the body (fig. 1), the mass center and the lift center would still be in the same vertical line, but the wing abscissa and the body abscissa that create a combined footprint are inclined under the Mach angle. Disregarding the silent assumption that wing and body are coplanar makes it possible to interrupt the fighting between the body tip and the wing, which are additive in $F(x)$, and allow the wing to cooperate with the receding tail end of the body of opposite sign at the latter part of $F(x)$ by making fast exchanges without any pressure creation in the far field.

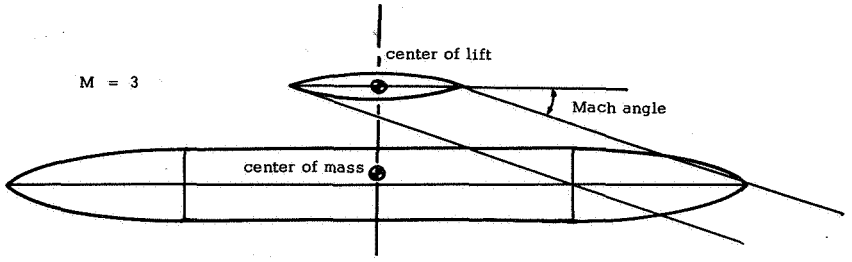

FIGURE 1.—Elevated wing configuration.

The proposal to remove the coplanar wing and to add the elevated wing may be called the addition of a "quadrupole" by inspecting the change in the lifting vortices. But, not worrying about the name, the application speaks for itself as an unconventional shape to remove severe constraints.

CONCLUSION

The present abstract shows in detail only a small part of the feasibility study for large sonic boom reductions which is underway. The author is well aware that one day the full account has to be given of all the roads that were found blocked. But since optimism is a prerequisite for success, the few positive findings may still get priority. To mention just the general field explored, the linearized theory was investigated with respect to the stratified atmosphere in the gravity field of the earth including the temperature differences for the cutoff at the sides and the changes of Mach number along the way. The next higher order terms, neglected in the linearized approach, were explicitly determined and investigated as to meaning. The Mach number range was not kept as close to Mach number 1 as in the Brooklyn paper [1] of 1955, in which the reflected shock wave was allowed to create a long Mach stem with the incoming shock. Because the pressure limits are in the order of one-tenth of a percent of the atmospheric pressure on the ground and because the altitudes reduce the pressures less than two orders of magnitude, the higher order terms are usually unimportant. Local superpositions of pressures high above the ground to speed up the decay without reaching the ground are hard to invent, but are not completely explored yet. Lower altitude flight with positive control over the finite slope in all pressure rises replacing the common N-shape of the footprint has advantages, if the ear responds much less, and if the airplane can sustain droplets and ice crystals or is allowed to change altitude on bad days.

[1] Busemann, A.: Relation Between Minimizing Drag and Noise at Supersonic Speed. Paper presented at High Speed Aeronautics Conference (Polytechnic Institute of Brooklyn), Jan. 1965, pp. 133–144.

Review of Second-Order Wave Structure

DAVID A. CAUGHEY and WALLACE D. HAYES
Princeton University

The study of the wave systems associated with a body in supersonic flight is both of practical importance as it relates to the intensity of the sonic boom produced by a supersonic aircraft, and of theoretical interest as it illustrates techniques useful in solving problems of weakly nonlinear wave propagation. As has long been recognized, the classical linearized theories of supersonic aerodynamics do not present an accurate description of these wave systems at large distances from the body. This is because cumulative nonlinear effects must be taken into account if we wish an accurate description of the wave after it has traveled a great distance. The nature of these effects has been considered by various writers (including Landau, Friedrichs, Whitham, and Lighthill), and Hayes has given the similarity variable governing the first-order wave structure (ref. 1).

The present study is concerned with determining the second-order corrections to this wave structure. Thus, we attempt to find the second term in an asymptotic series representation of the solution, valid to all distances from the body. This is accomplished by the method of matched asymptotic expansions, wherein the solution valid at large distances from the body is matched to a local solution valid near the body which satisfies the actual boundary condition. In the large-distance, or wave-structure solution, account is taken of these cumulative nonlinear effects and shocks are inserted according to the appropriate conservation laws. Although the flow field is irrotational to the order of accuracy considered everywhere in the flow field (except behind the trailing shock), and a velocity potential is used, entropy jumps at the shocks are important and must be considered if the resulting shock shapes are to be correct to second order.

The relationship of this theory to the other perturbation theories of high-speed aerodynamics is shown in figure 1. The first-order wave-structure theory is obtained by the inclusion of those nonlinear effects of second order which have a cumulative effect of first order.

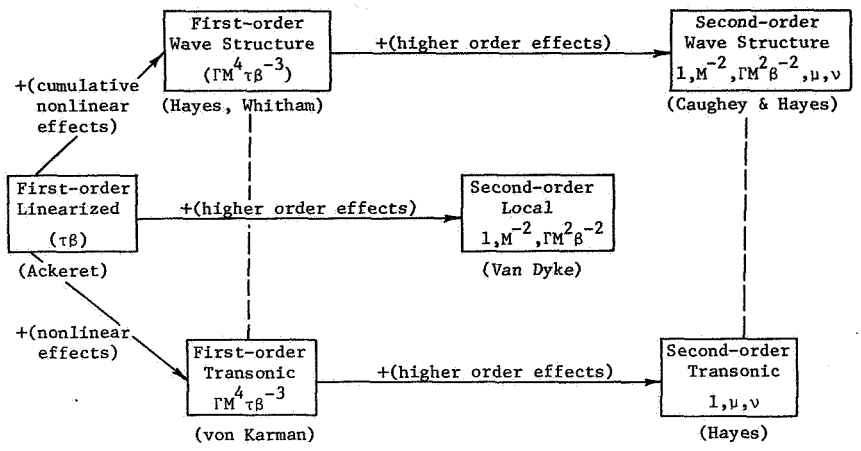

FIGURE 1.—Relationships between perturbation theories of high speed aerodynamics.

Similarly, third-order effects which exert a cumulative influence must be retained in the second-order wave-structure theory. The nature of the effects which exert a cumulative influence on the supersonic wave structure is similar to that which must be considered locally in the theories of transonic flow. This is suggested by the likeness of the similarity parameters in the respective theories.

The similitude for the second-order theory is not of the classical nature—i.e., it is not particularly useful for relating different flows while keeping a limited number of parameters fixed. Because the number of parameters obtained in the second-order theory is considerable, such a statement would be overly restrictive and of little or no practical value. Rather, a similitude like that of Van Dyke (ref. 2) for the local second-order theory is expressed: the important parameters of the problem are thought of as similarity coefficients, and are interpreted as giving the form of the second-order solution. Thus, the second-order potential is expressed as

$$\Phi_1=\psi_1+\frac{1}{M^2}\psi_2+\frac{\Gamma M^4}{\beta^2}\psi_3+\mu\psi_4+\nu\psi_5$$

where Γ, μ, and ν are thermodynamic properties (defined in ref. 3) of the (general) fluid, evaluated in the free stream, M is the free-stream Mach number, and $\beta=\sqrt{M^2-1}$. The ψ_i are functions invariant under the first-order similitude. Thus, the similitude given the form of the second-order solution and its explicit dependence upon these parameters.

The precise manner in which cumulative higher order effects are retained in the theory is by contracting the coordinate which measures

distance along the wave system (which is very nearly along the direction of the free-stream characteristics). The new contracted variable is found to be proportional to the so-called "age" variable in the analogous one-dimensional unsteady problems. These wave-structure variables are defined as

$$\xi=\bar{\xi}-\bar{\eta}$$

$$\eta=\frac{\Gamma M^4\tau}{\beta^3}\bar{\eta}$$

for planar flows and

$$\xi=\bar{\xi}-\bar{\eta}$$

$$\eta=\frac{2\Gamma M^4\tau}{\beta^3}\sqrt{\bar{\eta}}$$

for flows about finite bodies, where $(\bar{\xi},\bar{\eta})$ are the Prandtl-Glauert coordinates in the plane of the free-stream direction and the azimuth angle of interest, with $\bar{\xi}$ in the direction of the free-stream flow.

For planar flows, the wave-structure solution is uniformly valid to the body surface, and the boundary conditions may be applied directly without the intervention of a local solution. Complete solutions have been obtained in this case, and confirm the results of Friedrichs (ref. 4) as presented and corrected by Lighthill (ref. 5), when specialized to their case of a calorically perfect gas (ref. 6). In addition to allowing treatment of a general fluid more easily, the present method is easily extended to the case of flows about finite bodies, where the cylindrical nature of the problem precludes easy application of Friedrichs' simple wave concept.

For flows about finite bodies, the wave-structure solution must be matched with a local solution valid near the body surface. Here an intermediate solution (termed of $1^{1/2}$ order) must be inserted to match with the outer asymptotic behavior of the local second-order solution satisfying the homogeneous equation. In addition, the outer asymptotic behavior of the third-order local solution is required to determine the second-order wave structure solution. Complete particular integrals have been found for the second-order solution, however, and the wave-structure solution may be easily constructed once the appropriate inner boundary conditions are determined from the local solutions.

In the region behind the trailing shock, entropy and pressure disturbances are of the same order, and a velocity potential no longer exists. This region is important because the broad third-order pressure wave that is reflected from the shocks below the body even-

tually catches up with the rear shock above the body and alters its position. This effect must be considered if the theory is to be uniformly accurate to second order. The appropriate scaling for this region is

$$\hat{\xi}=\frac{\Gamma M^4\tau}{\beta^3}\xi$$

$$\hat{\eta}=\left(\frac{\Gamma M^4\tau}{\beta^3}\right)^2\eta$$

in the case of planar flows, and

$$\hat{\xi}=\left(\frac{2\Gamma M^4\tau}{\beta^3}\right)^2\xi$$

$$\hat{\eta}=\left(\frac{2\Gamma M^4\tau}{\beta^3}\right)^4\eta$$

for flows about finite bodies. The rotational method of characteristics gives the strength of this wave, which is convected along lines parallel to the free-stream characteristics. In the region defined by the above scaling (which we term the Lighthill region, ref. 5), vorticity is again negligible, and the velocity potential exists to the required order.

REFERENCES

1. Hayes, W. D.: Pseudotransonic Similitude and First-Order Wave Structure. J. Aeron. Sci., vol. 21, 1954, pp. 721–730.
2. Van Dyke, M. D.: The Similarity Rules for Second-Order Subsonic and Supersonic Flow. NACA Rept. 1374, 1958.
3. Hayes, W. D.: La seconde approximation pour les écoulements non visqueux. J. Méchanique, vol. 5, 1966, pp. 163–206.
4. Friedrichs, K. O.: Formation and Decay of Shock Waves. Commun. Pure Appl. Math., vol. 1, 1948, pp. 211–245.
5. Lighthill, M. J.: Higher Approximations in Aerodynamic Theory. Princeton University Press, 1960 (reprinted from General Theory of High Speed Aerodynamics, Sec. E, W. R. Sears, ed., Princeton University Press, 1954).
6. Caughey, D. A.; and Hayes, W. D.: Second-Order Wave Structure: Planar Flows. Presented at Proceedings of AFOSR–UTIAS Symposium on Aerodynamic Noise (University of Toronto), May 1968.

Multipoles, Waveforms, and Atmospheric Effects

A. R. George and A. R. Seebass
Cornell University

MULTIPOLES

The azimuthal distribution of the pressure field about an aircraft in supersonic flight has been investigated by analyzing the various multipole contributions to this pressure field. In brief, it has been shown that for supersonic flows multipole effects are important in the far field, and that there are reasonably efficient ways of using multipole contributions to reduce sonic boom overpressures.

The primary disturbances attributed to the flow about a supersonic aircraft propagate outward near a Mach cone originating at the aircraft. The pressure and momentum of the disturbance flow are concentrated near this cone and in the wake. Thus, in contrast to subsonic flow where a disturbance effect is felt over a large ground area, a supersonic aircraft's weight and volume effects are concentrated at the ground primarily between the intersections of the fore and aft Mach cones and the ground.

There is no fundamental reason the motion of a closed volume at supersonic speeds need cause far-field flow disturbances and boom, as can be seen from the examples of the Busemann biplane or the analogous ring wing with central body. However, there appears to be no applicable way of eliminating the far-field disturbances attributed to lift without involving a net source or sink of energy or mass. However, the boom attributed to volume and lift can be significantly reduced by other methods.

This section reports on a detailed analysis of the possibility of redistributing the variation of an aircraft's pressure field around the Mach cone to reduce the overpressure directly below practical aircraft configurations (ref. 1). The utility of this idea is based on two factors affecting the propagation of disturbances in different azimuthal planes. First, disturbances in other than the vertical θ plane will travel a longer distance before intercepting the ground and will thus have decayed somewhat more. If the dependence of portions of the flow field

is arranged properly, the maximum strength of the disturbances felt on the ground can be reduced. The second factor is the lateral cutoff of the "boom corridor," which is attributed to the "total reflection" of waves traveling along rays inclined at more than the critical angle to the sound speed (temperature) gradient of the atmosphere.

Previous analyses did not consider multipole effects explicitly because undue importance was ascribed to the fact that the disturbance from any slender configuration is essentially axisymmetric away from the axis. This need only be true for slender bodies. Nonslender configurations generally excite significant multipole contributions. An analysis of multipole solutions and the closure conditions that they must satisfy to be physically realizable leads to the conclusion that for any given azimuth angle a zero net dipole or quadrupole distribution may be used to cancel the far-field disturbance of a closed nonlifting body. The boom attributed to a positive lift which corresponds to a positive net dipole distribution can only be completely canceled by canceling the lift or by a negative net equivalent source distribution. (An example of such an approach is given by E. L. Resler, Jr., in "Reduction of Sonic Boom Attributed to Lift" in this volume.) However, the effects of lift can be reduced using multipole effects. An additional zero net lift distribution can be used to reduce boom but is generally not practical because of the moments introduced. On the other hand, additional quadrupole distributions can be practical. They can be looked upon as equivalent to zero net lift distributions where the lifting elements have been moved along Mach planes to give zero net moment. This also reduces the physical length of the aircraft compared to the length of the equivalent singularity distribution as discussed in reference 1.

As was shown and discussed in more detail in reference 1, certain conditions must be met in order to excite significant multipole effects. The region where the boundary conditions are applied must satisfy

$$\Delta x << \beta r \tag{1}$$

where Δx is the axial extent of the boundary condition and r its radial coordinate. Using this concept one can see that only the initial leading edge region of the "ducted quadrupole" reported by H. W. Carlson in "Laboratory Sonic Boom Research and Prediction Techniques" in this volume would be expected to excite significant quadrupole effect. Indeed the initial peaks of the $\Delta p/p$ curves given for that configuration show a significant difference between the side and below and both of these initial peaks decay by the same factor of about 0.54 between the two values of h/l shown. The relative inefficiency of the tetrahedron model shown by Carlson is also easily

understood. Here the effect of the small portion of the leading edge which satisfies $\Delta x << \beta r$ is obliterated by the large volume of the model. A related test of a thin wing, having a much smaller volume (ref. 2), does show quadrupole effects clearly.

For any given airplane configuration the equivalent multipole distributions are obtained by simply Fourier analyzing in θ the far-field effective area or F-curve distributions. An aircraft generally has a source distribution corresponding to its volume and engine stream-tube area changes, a dipole distribution corresponding to its lift, and quadrupole and higher order multipole distributions corresponding to the off-axis positioning of various aircraft elements such as wing volume, pods, etc. For example, figure 1 shows the approximate source, dipole, and quadrupole contributions to the Whitham function for a version of the NASA SCAT 15F. As is discussed in detail in reference 1, additional quadrupole distributions can be used to reduce boom on lifting configurations. Also, because the wave drag can be related to the multipole distributions, boom reductions are made with consideration of wave drag changes. At present the possibilities for wave drag reduction are being studied. Examples of applications to boom reduction are given in reference 1. A sample calculation gave a 9.5-percent reduction in boom on the SCAT 15F at the expense of a 14-percent increase in wave drag. Figure 2 shows the modifications made to achieve this reduction.

WAVEFORMS

In steady level flight an aircraft's weight is ultimately transferred by the atmosphere to the ground in the form of a pressure field there. When the aircraft's speed is greater than the speed of sound at the ground, then the main area of the ground available to the aircraft for its support is limited to the region between the intersection of the front and rear shock surfaces with the ground; the larger region behind the rear intersection contains the tail pressure wave left behind by these shock waves. Unfortunately, the primary region contains relatively large positive and negative contributions which, when they are combined with the negative tail wave pressures, nearly cancel: the difference is the pressure field that is required to support the aircraft. For radial distances that are large compared to a characteristic aircraft dimension, this pressure difference becomes negligible compared to the pressures that constitute the overall signature. Indeed, the term that must be present in order to provide a net force on the ground is proportional to $r^{-5/4}$, while the leading terms in the overpressure signature are proportional to $r^{-5/4}$ and $r^{-7/8}$. These terms provide no net force on the ground. The classical waveform formulas, which give a negative force on the ground, have been corrected so

315-766 O—68——10

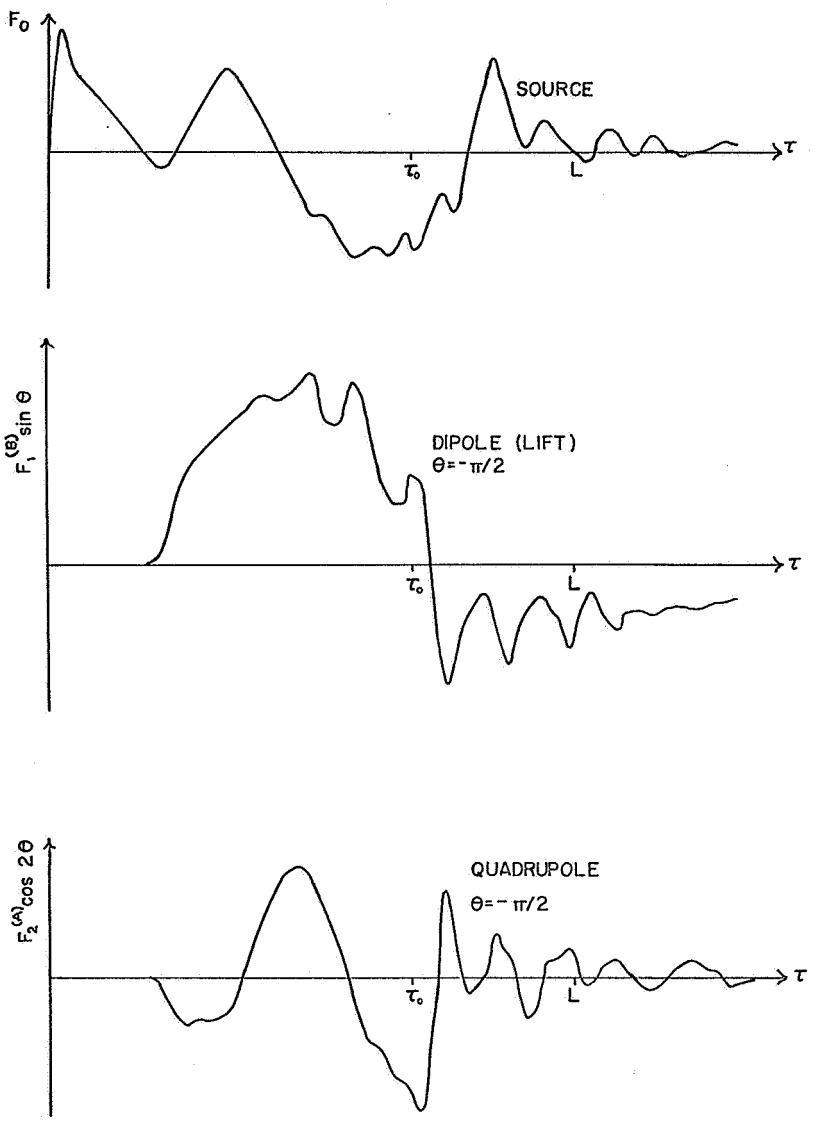

FIGURE 1.—Source, dipole, and quadrupole contributions to the F-function.

that the leading terms yield, as they should, no net force on the ground (ref. 3). The further extension of this result to the order necessary to account for the net positive force on the ground is only of academic interest. Here we outline the derivation of the results; further discussion of their meaning and the difference between these results and the classical ones may be found in reference 3. It should be noted that

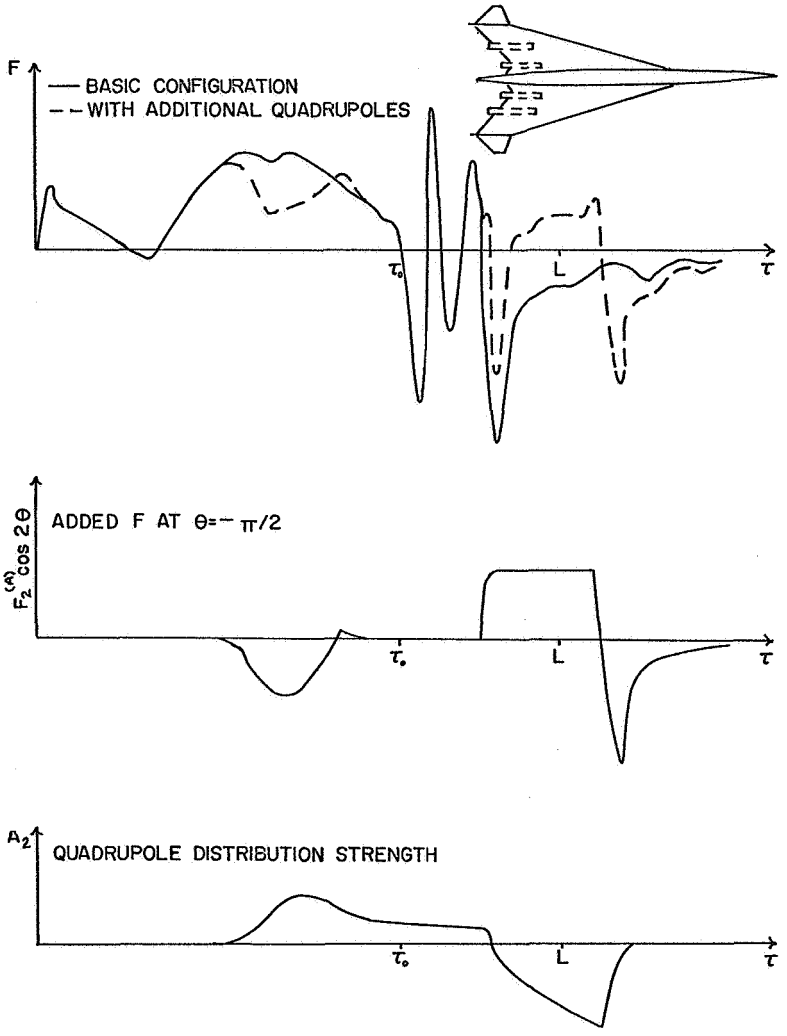

FIGURE 2.—Modification to the F-function for lower far-field boom.

these results must be reinterpreted for an inhomogeneous atmosphere. The shape to which the signature for a homogeneous atmosphere has evolved in $\pi/2$ real atmospheric scale heights is the shape that will persist to any greater distance. In a real atmosphere the decay of the overpressure signature is not the $r^{-3/4}$ law given here. For example, below the aircraft in an isothermal atmosphere the asymptotic decay law is $(p/r)^{1/2}$. This point is discussed further in the submitted comments.

For any finite body, the linearized pressure field at a given azimuthal

angle and radial distance can be integrated over the entire extent of the axial coordinate with the result

$$\int_{\beta r}^{\infty} C_p\,(x, r, \theta)\,\mathrm{d}x = R^2 \sin\theta/\beta r \tag{2}$$

Here C_p is the pressure coefficient and $R|\sin\theta|^{1/2}$ is the ultimate base radius of the equivalent body of revolution, which is related to the lift by $\pi R_2 = \beta$ lift$/\rho_\infty U^2$. One way to arrive at this result is to consider the solution for the velocity potential,

$$\varphi\,(x, r, \theta) = \frac{1}{2\pi}\sum_{n=0}^{\infty} \sin n\theta \int_0^{x-\beta r} \frac{\sigma_n(\xi)\,\cosh^{-1}\left(n\cosh\dfrac{x-\xi}{\beta r}\right)}{[(x-\xi)^2-\beta^2 r^2]^{1/2}}\,\mathrm{d}\xi,$$

for various n-tuple distributions $\sigma_n(\xi)$, perform the indicated integration and apply the closure conditions appropriate to the various distributions. If the result (2) is then integrated over the infinite lateral extent of the hyperbola formed by the intersection of the body's fore Mach cone with a horizontal plane, then the lift is indeed equal to the force on the horizontal plane. After the attendant quasi-linear correction is applied to the linear theory, the resulting sonic boom waveform, when integrated over a horizontal plane, must again give a force that is equal to the lift: the quasi-linear correction simply relocates the pressure disturbance and introduces shock waves so that the value of the integral $\int_{-\infty}^{\infty} C_p(x, r, \theta)\,\mathrm{d}x$ is preserved.

Because we are interested in the leading terms in far field overpressure signature, and as we have mentioned earlier, these dominate the right-hand side of equation (2), we use the asymptotic form of the linear result

$$\int_{\beta r}^{\infty} C_p(x, r, \theta)\,\mathrm{d}x = \sqrt{\frac{2}{\beta r}}\int_0^{\infty} F(y)\,\mathrm{d}y = 0 \tag{3}$$

Here we have introduced the F-function of Whitham and the variable

$$y = x - \beta r - kF(y)r^{1/2} \tag{4}$$

where $k = 2\Gamma M^4/\beta\sqrt{2\beta}$; the parabolas y=constant are characteristics with their location corrected for quasi-linear effects. In those regions of the flow where characteristics of the same family intersect one another, the solution is now triple valued; the condition that determines the position of the shock wave that renders the solution unique is simply that

$$\int_{-\infty}^{\infty} C_p\,\mathrm{d}x$$

be invariant. As a consequence the locations of the front and rear shock waves are given implicitly by

$$\int_0^{y_f} F(t)\,\mathrm{d}t=\frac{1}{2}kF^2(y_f)r^{-1/2} \tag{5}$$

and

$$\int_{y_r}^{y_t} F(t)\,\mathrm{d}t=\frac{1}{2}k[F^2(y_t)-F^2(y_r)]r^{1/2} \tag{6}$$

where y_t is the characteristic on which the rear shock terminates.

To determine the asymptotic behavior of the overpressure signature, we note that as $r\to\infty$, y_f and $y_r\to y_o$ but that $y_t\to\infty$; thus we expand y_f and y_r in Taylor series about y_o, where $F(y_o)=0$. It is easy to verify that

$$y_{f,r}=y_o-\left(4r^{5/4}\frac{\mathrm{d}y_{f,r}}{\mathrm{d}r}\right)_{r=\infty}r^{-1/4}+O(r^{-3/8})$$

and that

$$y_t=\left(4r^{3/4}\frac{\mathrm{d}y_t}{\mathrm{d}r}\right)_{r=\infty}r^{1/4}+O(r^{1/8})$$

The derivative $\dfrac{\mathrm{d}y}{\mathrm{d}r}$ is obtained from equation (4):

$$\frac{\mathrm{d}y}{\mathrm{d}r}=\frac{\dfrac{\mathrm{d}x}{\mathrm{d}r}-\beta+\dfrac{RF(y)}{2r^{1/2}}}{1-kF'(y)r^{1/2}}$$

Now at a shock wave we can write, to first order,

$$\frac{\mathrm{d}x}{\mathrm{d}r}-\beta=\tan\sigma=\frac{k}{2r^{1/2}}\Delta F \tag{7}$$

where σ is the shock angle and ΔF is the jump in $F(y)$ attributed to the jump in the flow deflection angle. Substituting the result into the expressions for $\mathrm{d}y/\mathrm{d}r$ and carrying out the limiting process, we find:

$$y_f-y_o=I\left[\frac{1}{kr^{1/4}F'(y_o)}\right]+O(r^{-1/2})$$

$$y_r-y_o=-I\left[\frac{1}{kr^{1/4}F'(y_o)}+\frac{R^2}{2I^{5/2}r^{3/8}F'(y_o)}\right]+O(r^{-1/2})$$

$$y_t=I\left(r^{1/4}-\frac{7kR^2r^{3/8}}{4I^{5/2}}\right)+O(1)$$

where

$$I=\left[2k\int_0^{y_o}F(t)\,\mathrm{d}t\right]^{1/2}$$

For simplicity we have tacitly assumed that $F'(y_o) \neq 0$ and that $F(y)$ is continuous at y_o.

Finally, making use of the fact that

$$\int_0^\infty F(t)\ \mathrm{d}t = 0,$$

we may reexpress (5) and (6) as

$$r^{1/4}F(y_f) = \left[\frac{2}{k}\left(\int_0^{y_o} - \int_{y_f}^{y_o}\right) F(t)\ \mathrm{d}t\right]^{1/2}$$

and

$$r^{1/4}F(y_r) = -\left[\frac{2}{k}\left(\int_0^{y_o} + \int_{y_o}^{y_r} + \int_{y_t}^{\infty}\right) F(t)\ \mathrm{d}t\right]^{1/2}$$

The second integral in each formula is evaluated by expanding $F(y)$ in a Taylor series about y_o:

$$F(y) = F'(y_o)(y-y_o) + F''(y_o)(y-y_o)^2/2 + \ \ldots$$

The third integral in the second result is evaluated by using the asymptotic behavior of $F(y)$ for large y. This gives

$$kF(y_f) = I\left[1 + \frac{1}{kF'(y_o)\,r^{1/2}} + O(r^{-3/4})\right]^{1/2} r^{-1/4}$$

$$kF(y_r) = -I\left[1 + \frac{1}{kF'(y_o)\,r^{1/2}} - \frac{kR^2}{I^{5/2}r^{1/8}}\right]^{1/2} r^{-1/4}$$

and

$$kF(y_t) = -\frac{kR^2}{4I^{3/2}r^{3/8}}$$

In an earlier derivation we expanded the square roots indicated in the first two formulas. In many instances the third term in the second formula is not sufficiently small for such an expansion to be valid. Consequently we shall leave the roots as they stand in these formulas. Furthermore, in computing the actual position $x-\beta r$ of the shock waves, we combine y_r with $-kF(y_r)r^{1/2}$ by first expanding the roots and then recasting the results back in to the form of a square root. This preserves the simple structure of the formulas and avoids using an expansion that is marginally valid.

The correct first-order results, which are given below, locate the rear shock wave so that the departure of the main portion of the signature from the final N-wave form compensates for the tail pressure wave to the extent that if l is a typical length for the configuration, then

$$\int_{x_f}^{\infty} C_p(x, r; \theta)\, dx = O\left[\left(\frac{R^2}{l}\right)\left(\frac{l}{r}\right)^{3/4}\right]$$

It is important to note that these corrections apply only to the asymptotic waveform formulas and follow directly from the basic theory as given by Whitham (ref. 4).

The correct first-order results for the location of the front and rear shock waves, the pressure behind the front shock, the linear decrease with x to its value ahead of the rear shock wave and the pressure in the tail wave behind the rear shock follow directly from the results given above and are tabulated below.

FAR-FIELD WAVEFORMS

Front shock wave:

$$x-\beta r = y_o - I\left[1-\frac{1}{kF'(y_o)r^{1/2}}\right]^{1/2} r^{1/4}$$

$$k\sqrt{\frac{\beta}{2}}\, C_p = I\left[1+\frac{1}{kF'(y_o)r^{1/2}}\right]^{1/2} r^{-3/4}$$

Between the shock waves:

$$k\sqrt{\frac{\beta}{2}}\, C_p = -(x-\beta r-y_o)\left[1+\frac{2}{kF'(y_o)r^{1/2}}\right]^{1/2} r^{-1}$$

Rear shock wave:

$$x-\beta_r = y_o + I\left[1-\frac{1}{kF'(y_o)r^{1/2}}-\frac{kR^2\sin\theta}{I^{5/2}r^{1/8}}\right]^{1/2} r^{1/4}$$

$$k\sqrt{\frac{\beta}{2}}\, C_p = -I\left[1+\frac{1}{kF'(y_o)r^{1/2}}-\frac{kR^2\sin\theta}{I^{5/2}r^{1/8}}\right]^{1/2} r^{-3/4}$$

Tail wave:

$$k\sqrt{\frac{\beta}{2}}\, C_p = \frac{-kR^2\sin\theta}{4r^{1/2}(x-\beta r-y_o)^{3/2}}$$

where

$$I = \left[2k\int_0^{y_o} F(t)\, dt\right]^{1/2} \qquad \text{and} \qquad k = 2\Gamma M^4/\beta\sqrt{2\beta}$$

The NASA Langley computer program (ref. 5) has been used to determine the sonic boom waveforms in the azimuth planes below and above the B–70 aircraft ($\theta=+\pi/2$; $\theta=-\pi/2$). Figures 3 and 4 compare the computed pressure signatures given by the formulas above, and the uncorrected results. Excellent agreement between the far-field formulas and the actual waveform is obtained.

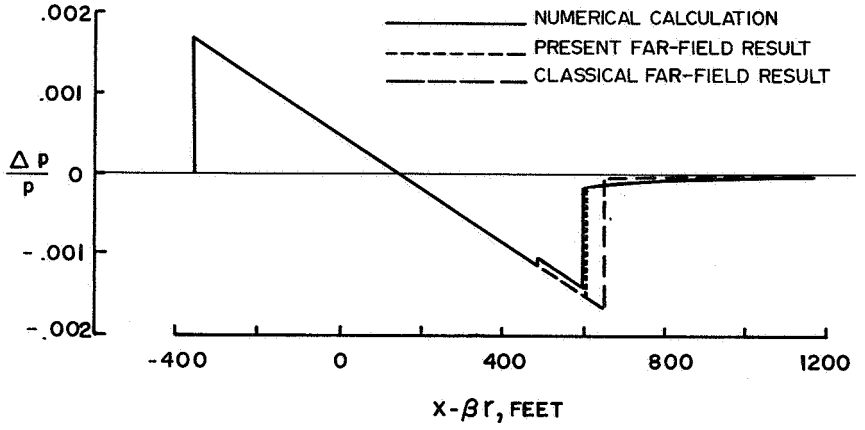

FIGURE 3.—A comparison of the waveforms for the B–70 aircraft at a Mach number of $M=2.6$, an altitude of 63 360 feet, a gross weight of 372 000 pounds, and $\theta=\pi/2$.

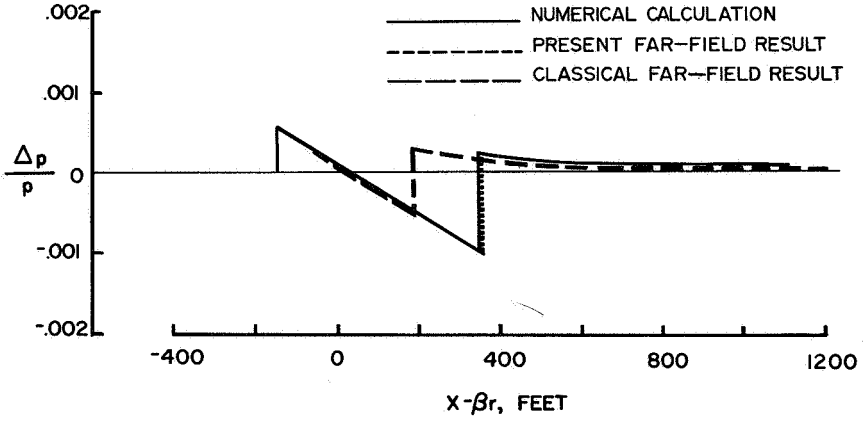

FIGURE 4.—A comparison of the waveforms for the conditions used in figure 3, but with $\theta=-\pi/2$.

ATMOSPHERIC EFFECTS

Upon initiating an investigation of the turbulent dispersion of sonic boom signatures, it became apparent that the simple problem of propagation in a layered atmosphere was not universally understood. Results of various investigators were in disagreement. To clarify this situation a short study was made by Plotkin (related in a private communication) of the simplest possible case: the effect of a steady, horizontally stratified atmosphere on the overpressure directly below the airplane. Our analysis agrees with the results of Randall (ref. 6). The resulting correction factors were computed to better than 1 percent accuracy and compared with those of other investigators. We agree with Randall when we use his model atmosphere and essentially agree with the results of Kawamura and Makino (ref. 7) for a standard atmosphere. There are significant differences from some of the earlier published results (refs. 8 and 9). A comparison of various results is shown in figure 5.

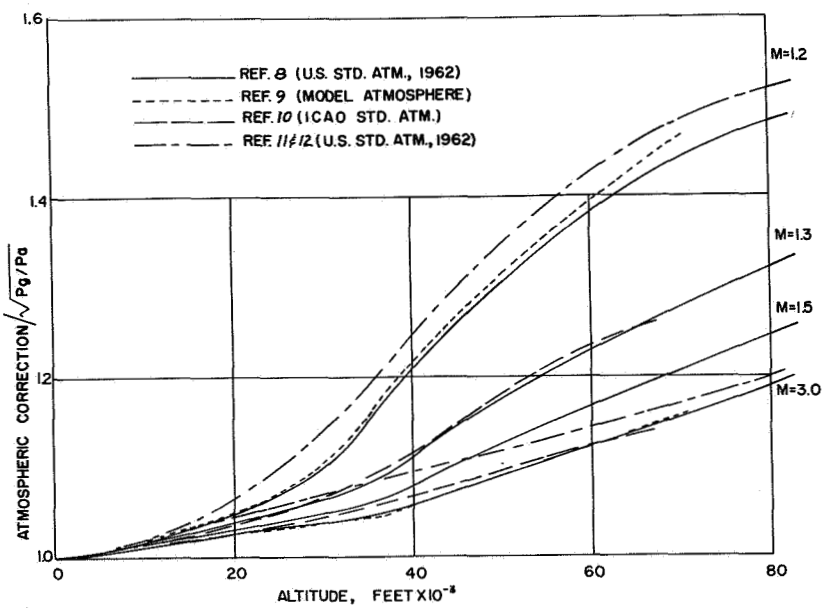

FIGURE 5.—A comparison of the atmospheric correction factors reported by various authors.

REFERENCES

1. GEORGE, A. R.: Reduction of Sonic Boom by Azimuthal Redistribution of Overpressure. AIAA Preprint No. 68–159 (1968).
2. CARLSON, H. W.: Correlation of Sonic-Boom Theory with Wind-Tunnel and Flight Measurements. NASA Technical Rept. TR R–213, 1964.
3. SEEBASS, R.; and MCLEAN, F. E.: Far-field Sonic Boom Waveforms. AIAA Journal, vol. 6, 1968, pp. 1153–1156.
4. WHITHAM, G. B.: The Flow Pattern of a Supersonic Projectile, Commun. Pure Appl. Math., vol. 5, 1952, pp. 301–348.
5. MIDDLETON, W. D.; and CARLSON, H. W.: A Numerical Method for Calculating Near-Field Sonic-Boom Pressure Signatures. NASA TN D–3082, 1965.
6. RANDALL, D. G.: Sonic Bang Intensities in a Stratified Still Atmosphere. Royal Aircraft Establishment TR 66002, 1966.
7. KAWAMURA, R.; and MAKINO, M.: The Effect of Atmospheric Nonuniformity on Sonic Boom Intensities. University of Tokyo. ISAS Rept. 416, 1967.
8. KANE, E. J.: Some Effects of Nonuniform Atmospheric on the Propagation of Sonic Booms. J. Acoust. Soc. Amer., vol. 39, no. 5, Part 2, 1966.
9. KANE, E. J.; and PALMER, T. Y.: Meteorological Aspects of the Sonic Boom. Boeing Aircraft Co. SRDS Rept. RD64–160, 1964.

Uniform Ray Theory Applied to Sonic Boom Problems

M. B. Friedman and M. K. Myers
Columbia University

The subject of the present research is the propagation of shock waves from a slender body of revolution moving at supersonic speed through a stratified medium in which the ambient sound speed is a monotonically decreasing function of altitude. The problem is treated using a first-order Whitham correction to the linear field. The major difficulty arising in such a procedure is the development of a uniformly valid asymptotic expansion of the linear field which is appropriate as a basis for the Whitham technique. Such an expansion must take account of the interaction between diffraction effects attributed to the medium and the motion of the body and the primary disturbances. It must also account for the subsequent occurrence of focusing in the field attributed to refraction of the signal by the medium.

The uniform linear field may be obtained in a parametric form using a ray technique which is a generalization of classical geometric acoustics. In recent years the subject of asymptotic solutions using rays has undergone wide development. However, the major portion of the existing theory of uniform expansions is concerned with problems involving time-harmonic wave propagation. Thus, a major effort in the present work has been to derive corresponding generalizations of geometric acoustics to describe the propagation of arbitrary pulses. These uniform asymptotic representations serve to correct certain anomalies occurring in the simplest theory of geometric acoustics. In particular, the classical theory predicts infinities in the field at points of focusing where the ray family forms an envelope, and also it predicts an infinite value for the field at points on the boundary between the region of the main signal and the diffracted field. From a study of certain exact solutions to typical problems of this type, it can be seen that such points in the field are located in regions where the linear solution varies most rapidly, and the anomalies above are a reflection of the failure of the geometric approximation to describe such regions.

These notions suggest that the problem of focusing is best analyzed by considering it as a stage in the transient development of the disturbance field. From this point of view, the process of developing an asymptotic theory for the treatment of a general problem involves several stages employing different asymptotic expansions. The first significant stage is governed by diffraction effects. A second is associated with the formation of ray envelopes in the field as a result of these interactions. Under certain circumstances, i.e., the presence of boundaries, the first stage of propagation is of major interest in itself. In any event, it provides the knowledge necessary to study the onset of focusing.

It is characteristic of modern ray techniques associated with asymptotic solutions to linear partial differential equations that certain functions appearing in the solution are left undetermined in the general formalism. A basic element of these theories is the hypothesis that these functions are determined by comparison of the asymptotic expansions with exact solutions of certain canonical problems. A canonical problem is one which is sufficiently simple to be solved exactly, and which is locally similar to the more general problem being considered. Consequently, for each stage in the development of asymptotic expansions for a general problem, it is necessary to identify and solve uniformly the appropriate canonical problem.

UNIFORM RAY EXPANSION FOR STAGE ONE

A canonical problem for the asymptotic development of the first stage is a two-dimensional point source set impulsively into uniform supersonic motion in a medium in which the sound speed is a constant; the source strength may be an arbitrary function of time. The geometry of the disturbance front is apparent and consists of a Mach envelope issuing from the source and an elementary initial disturbance front. The Mach envelope is tangent to the initial front. At the points of tangency, the potential $\varphi(x, y, t)$ of the point source has a directional singularity, and classical (nonuniform) ray theory predicts infinite values for the field at these points.

A study of the exact solution has established that a uniformly valid ray expansion for φ exists of the form

$$\varphi(X, t)=\sum v_n F_n\left[\left(\frac{s-\bar{s}}{s}\right)^{1/2}\right] s^n+\sum \bar{v}_n \bar{s}^{n+1/2} \tag{1}$$

Here, $s(X, t)=0$ represents the characteristic Mach envelope in space-time and $\bar{s}(X, t)=0$ represents the characteristic elementary cone of

the initial disturbance.[1] The quantities v_n and $\bar{v}_n$ represent the strength factors which propagate along the two sets of rays corresponding to the main rays (bicharacteristic of $s=0$) and the diffracted rays (bicharacteristics of $\bar{s}=0$). The canonical function F_0 is given by

$$F_0=\frac{\pi}{2}-\sin^{-1}\left(\frac{s-\bar{s}}{s}\right)^{1/2}-\left(\frac{\bar{s}}{s-\bar{s}}\right)^{1/2}$$

the functions F_n, $n=1, 2, \ldots$ are essentially successive integrals of F_0.

The first terms of the series may be written explicitly:

$$\varphi\sim v_0H(s)+\left\{\bar{v}_0\bar{s}^{1/2}-\left[v_0\sin^{-1}\left(\frac{s-\bar{s}}{s}\right)^{1/2}-\left(\frac{s}{s-\bar{s}}\right)^{1/2}\right]\right\}H(\bar{s}) \qquad (2)$$

$H(s)$ is the unit step function. For $\bar{s}<0$, the leading term provides the usual first-order geometric acoustic approximation. As $s\to\bar{s}\to 0$, the region of validity of the geometric approximation becomes vanishingly small. For a uniformly valid result, all three terms in equation (2) must be maintained. On the other hand, if only $\bar{s}$ is close to zero, an approximation can be obtained across the initial disturbance front, namely,

$$\varphi\sim\bar{v}_0(\bar{s})^{1/2}$$

where $\bar{v}_0=\dfrac{\text{const}}{\cos\theta-\cos\theta_0}$; θ_0 corresponds to the polar angle of the point of tangency. This is precisely the first-order geometric approximation across the initial disturbance front and becomes infinite along $\theta=\theta_0$, the ray (shadow boundary) through the point of tangency. However, if all three terms are maintained to form the uniform expansion (2), then this expansion of φ is continuous across the shadow boundary and has the correct directional singularity at the point of tangency.

This uniform expansion provides the information necessary to develop the asymptotic solution involving an arbitrary variation of sound speed. Consider a point source set into uniform supersonic motion in a medium in which the sound speed is described by a monotonically decreasing function of altitude $c(y)$. The potential $\varphi(X,t)$ which describes the field attributed to the point source satisfies the equation

$$\varphi_{xx}+\varphi_{yy}-\frac{1}{c^2(y)}\varphi_{tt}=-f(t)\delta(x-Vt, y) \qquad (3)$$

where $f(t)\equiv 0$ for $t\leq 0$ and $\varphi(X,O)=\varphi_t(X,O)=0$.

[1] Because the canonical function F_n are functions only of characteristic variables, extension to similar problems involving more space dimensions is straightforward.

The solution is postulated to be of the form

$$\varphi=\sum v_n F_n\left[\left(\frac{s-\bar{s}}{s}\right)^{1/2}\right]s^n+\sum \bar{v}_n \bar{s}^{n+1/2}$$

where the functions s, $\bar{s}$, v_n, $\bar{v}_n$ are to be determined. The wave equation (3) implies a set of differential equations to be satisfied by these unknown functions. The first few equations are

$$s_x^2+s_y^2-\frac{1}{c^2(y)}s_t^2=0; \qquad \bar{s}_x^2+\bar{s}_y^2-\frac{1}{c^2(y)}\bar{s}_t^2=0 \tag{4}$$

$$\begin{gathered}(v_0)_x s_x+(v_0)_y s_y-\frac{1}{c^2(y)}(v_0)_t s_t=0 \\ (\bar{v}_0)_x \bar{s}_x+(\bar{v}_0)_y \bar{s}_y-\frac{1}{c^2(y)}(\bar{v}_0)_t s_t=0\end{gathered} \tag{5}$$

Equations (4) implies that s and $\bar{s}$ are characteristic surfaces of the wave equation (3). In the usual manner, they can be solved by the method of characteristics which constructs the surfaces s and $\bar{s}$ out of the bicharacteristics (rays, in spacetime). Equations (5) are easily shown to be ordinary differential equations along the bicharacteristics and are the transport equations which must be solved to determine the strength factors v_0, $\bar{v}_0$.

NONLINEAR CORRECTION

The availability of a uniform expansion permits the application of the Whitham method to many cases of interest. As an illustration, consider a two-dimensional, wedge-shaped airfoil set impulsively into uniform supersonic motion. In the case of arbitrary variations in sound speed, the corresponding nonlinear field is expressible in parametric form based on computations which determine the ray system and the associated uniformly valid linear field. In the special case of constant sound speed explicit results can be obtained which illustrate the importance of the uniform expansion as a basis for the nonlinear correction.

By assuming a steady state in this problem, the Whitham method predicts a straight shock of constant strength standing ahead of the Mach lines and extending from the leading edge to infinity. If the full transient problem is considered, classical geometric acoustics can be applied and predicts constant strength along the Mach lines through the leading edge and infinite values for the pressure at the points of tangency of the Mach envelope and the initial disturbance front from the leading edge. Thus the Whitham approach will fail to predict correct shock pressures in the neighborhood of these

points. However, the uniform ray expansion predicts finite values for the linear solution at the points of tangency and the Whitham correction may be applied to this linear field. When this is done, it is found that the shock strength decreases continuously along the straight portion of the shock in the neighborhood of the diffraction boundary and along the curved portion of the shock associated with the diffraction front.

The above results are valid until the onset of focusing. A canonical problem and the uniform ray theory for the next stage, which involves focusing, is presently under study.

The ARAP Sonic Boom Computer Program

WALLACE D. HAYES
Princeton University
and
RUDOLPH C. HAEFELI
Aeronautical Research Associates of Princeton, Inc.

Under the sponsorship of the NASA Langley Research Center, Aeronautical Research Associates of Princeton, Inc. (ARAP), has prepared a computer program for the calculation of sonic boom signatures on the ground. A NASA contractor's report entitled "Sonic Boom Propagation in a Stratified Atmosphere" (to be published) presents the program with instructions for its use, together with a review of the underlying theory. Here we briefly outline the computer program to indicate its theoretical basis and its special features.

GENERAL DESCRIPTION

The theory on which the computer program is based is an integrated "standard" theory (refs. 1 and 2), making only those simplifying assumptions which are made by all first-order theories on the subject. The atmosphere is assumed to be stratified with thermodynamic properties and horizontal winds functions of altitude alone. The signal leaving the aircraft is presumed known and must be specified as input to the present program in terms of an F-function. A discussion of the derivation of the F-function may be found, for example, in reference 3, and it is dependent on Mach number, lift coefficient, and direction. This signal and the aircraft maneuver provide initial conditions for the wave propagation which is given by the theory of geometric acoustics. (See Hayes' paper, "Geometric Acoustics and Wave Theory," in this volume.) The calculations provide ray trajectories for the signal, and also ray-tube areas to determine the strength of the signal. A modification of the signature is made with the help of an age variable to account for nonlinear distortion and the presence of shock waves. The atmospheric condi-

315-766 O—68——11

tions have an essential role in determining the age and degree of distortion.[1]

Particularly novel features of the computer program are that ray-tube areas are computed correctly according to geometric acoustics, with both arbitrary maneuvers of the aircraft and arbitrary stratification taken into account, and actual (midfield) signatures are computed without the common simplifying assumption of an N-wave (far-field signature). The calculations are made in the program for a set of selected rays originating at the aircraft at particular flight times and with specified initial azimuth angles (about the aircraft longitudinal axis).

As a caustic is approached, the ray-tube area approaches zero. The theory appropriate near a caustic is more complicated than that underlying the computer program, and the program simply stops when a caustic is reached. If a ray traveling downward becomes horizontal, no attempt is made to follow the propagation further, and the propagation computation is stopped.

PROGRAM INPUT DATA AND THEIR USE

Stratified Atmosphere

The temperature and pressure or density may be specified at a number of altitudes, together with the magnitude and direction of the horizontal wind. This input may be in English or metric units, and either geometric or geopotential altitude may be used. The program linearly interpolates these input tables. The input must be made consistent with hydrostatic equilibrium if such a condition is desired. The 1962 standard atmosphere is contained within the program and therefore may be specified as an alternate to the arbitrary atmosphere.

Aircraft Maneuvers

The aircraft Mach number, flight path direction, altitude, and bank angle must be specified for a succession of times during the flight of the aircraft. The aircraft maneuver equations then provide the initial location of the signal relative to the ground and also give values of the initial conditions and the time derivatives required by the ray-tube area equations. Two options are provided in the maneuver equations, depending on whether or not load factors are specified. In option 1, load factors are used, and time derivatives of

[1] For example, consider an aircraft in level, uniform flight without winds, comparing signal propagation in a uniform atmosphere (constant density) with propagation in an exponential atmosphere (density varies exponentially with altitude). Then the signal shape traveling through the exponential atmosphere at an infinite distance below the aircraft is the same as the shape occurring in the uniform atmosphere only $\pi/2$ scale heights (approximately 32 000 feet) below the aircraft (ref. 2).

velocity, Mach angle, and two flight path angles, which are required by the ray-tube area equations, are calculated explicitly. In option 2, these time derivatives are obtained using quadratic fits to tabular inputs, and the load factors are not needed. In the program, the differential equations of motion of the aircraft are integrated to give its location.

F-Functions

The *F*-function for the aircraft is input for different values of the azimuth angle of the initial ray direction and as a function of distance along the aircraft (aircraft station). The *F*-function input for the azimuth angle closest to that under investigation is chosen for the then current calculation.

Other Inputs

The height of the ground above sea level and the choice of azimuth angles for which propagation is to be investigated need to be specified. The aircraft wing loading and length are also required. A ground reflection factor (which multiplies the pressure) may also be selected.

PROGRAM OUTPUT INFORMATION

1. For each chosen azimuth angle and aircraft time, the ray trajectory (including time) is given at selected altitude intervals, starting at the aircraft altitude and continuing to the ground intersection or to an intervening stop in the program. The values of ray-tube area and age variable are also listed at these altitudes.
2. At each ground intersection, the signature in terms of pressure versus time is given without regard to shock waves. An auxiliary *S*-function versus time is also given which then provides the location of the shock waves in the actual pressure signature.
3. If a stop occurs because of a horizontal ray, the information of item 2 is given for the signal at that point.
4. Ground intersection and peak pressure information obtainable by interpolation from results from a number of rays is given.
5. The input information is listed in the output for the purpose of a data check.

SELECTED RESULTS

Some results obtained with the sonic boom computer program are illustrated in this section only. These results were obtained using zero wind speed, although the program can give results for any stratified wind profiles. In figure 1 comparisons are shown for four ray traces from an aircraft flying at 20 000 feet above sea level to the ground level at 2300 feet (Edwards Air Force Base). The location of the rays (wave front) at various times after leaving the aircraft is indicated on the traces. At Mach 1.4, the straight-line propagation in a uniform atmosphere may be compared with the diffraction

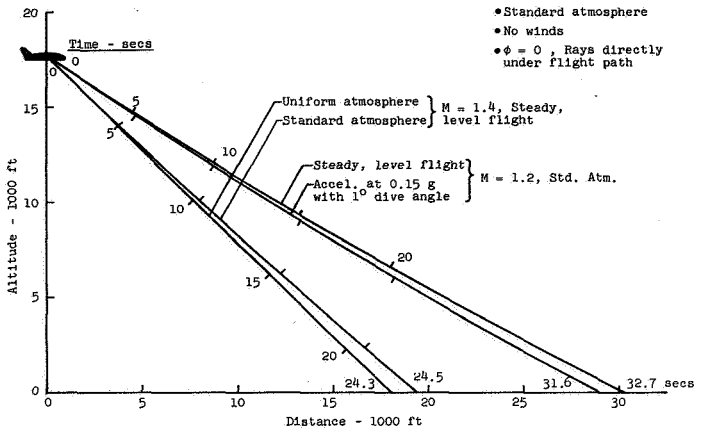

FIGURE 1.—Ray traces for four flight conditions.

in the 1962 standard atmosphere. The difference in ground intersection locations is 1370 feet. At Mach 1.2 the rays travel considerably farther, of course. Ray traces are shown here for comparing propagation from an aircraft in uniform level flight and in a shallow accelerating dive (n_T=0.15 g, $\gamma=-1°$). The ground intersection for the diving conditions occurs 1340 feet shorter and 1.1 seconds earlier.

Figure 2 shows an F-function for an F–104 aircraft as a function of aircraft station L/L_A (L_A=50 feet). This F-function has been used as an input to the sonic boom computer program with the above flight conditions. The complete pressure signature which results at the ground for propagation in a uniform atmosphere is shown in figure 3. The pressure increment $\Delta p=(p-p_{\text{ambient}})$ is plotted against a local time parameter ξ_1 which is proportional to the length of the signature. The shock structure has been drawn (heavy line) using information

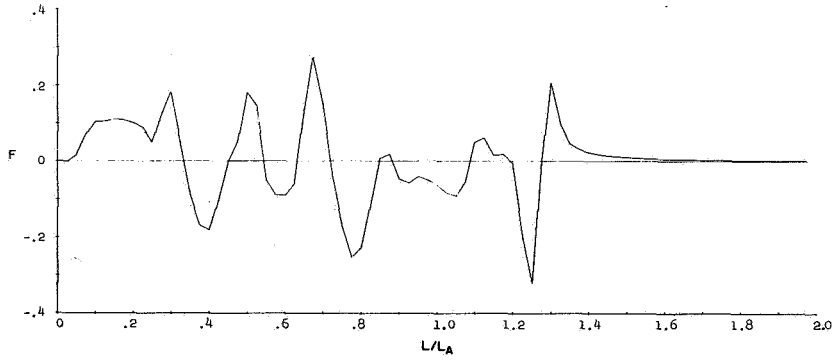

FIGURE 2.—An F-function for the F–104; Mach 1.4, $\phi=0$, $C_L=0.06$.

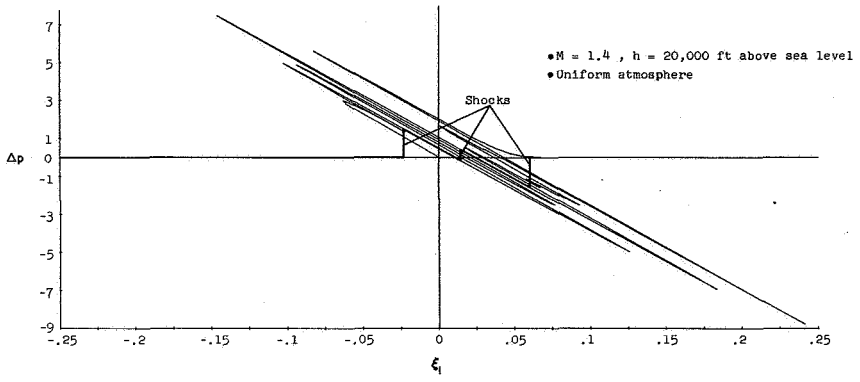

FIGURE 3.—Computed pressure signature at ground and resulting shocks.

on the location of the shock provided by the S-curve of figure 4. This auxiliary curve is an integral of the signature, making use of area balancing (mentioned, for example, in ref. 3) to remove the inadmissible multivalued pressures. Specific S-curve intersections, as indicated in figure 4, yield the shock locations.

Figure 5 shows pressure signatures for three flight conditions using the 1962 standard atmosphere. The shock strengths and the lengths of the signatures are compared in table I. Here the results at Mach 1.4 for uniform atmosphere and standard atmosphere are compared. The pressures in the uniform atmosphere (first column, values in parentheses) are multiplied by a factor of 1.50 commonly used to adjust for the standard atmosphere, and can be compared with the data for the standard atmosphere (second column). Although in this example the computed adjust pressure jumps would be the same in both cases, the lengths of the signatures are significantly shorter using the standard atmosphere solution (refer to previous footnote).

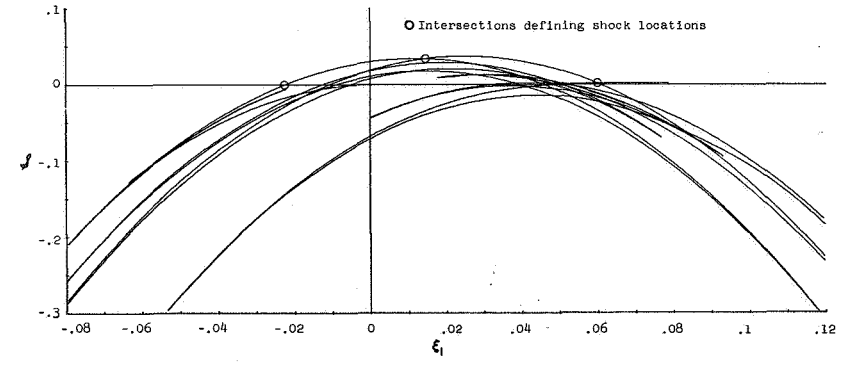

FIGURE 4.—S-curve for identifying shock locations.

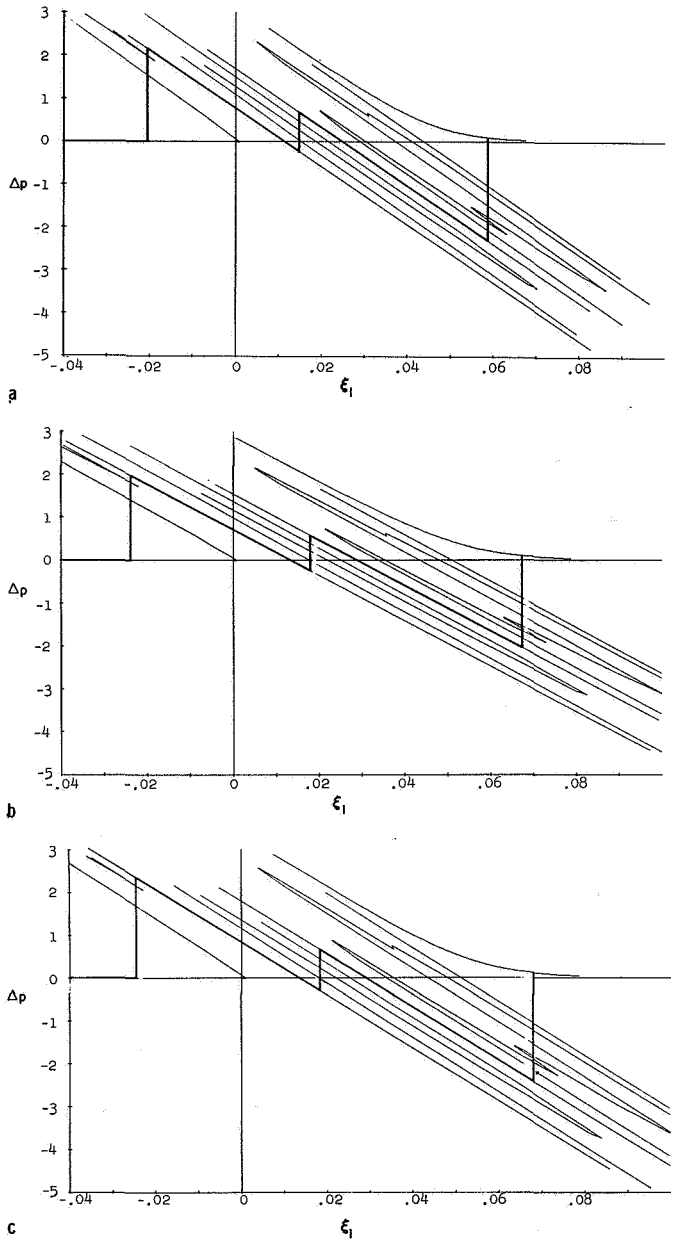

FIGURE 5.—Pressure signatures at the ground for three flight conditions: $M=1.4$, level flight (a), $M=1.2$, level flight (b), $M=1.2$, accelerating dive (c).

TABLE I.—*Shock Strength and Length of Signature*

[Estimated precision of data: $l \pm 0.5$ ft, $\Delta p \pm 0.03$ psf]

Parameter	$M=1.4$		$M=1.2$				
	Uniform atmosphere	Standard atmosphere	Standard atmosphere				
	Uniform level flight		Uniform level flight	Acceleration in level flight, $n_T=0.15$ g		Acceleration in dive, $n_T=0.15$ g, $\gamma=-1°$	
l_1, ft	119. 9	113. 8	114. 2	115. 4	[a] 1. 05%	116. 7	[a] 2. 19%
l_2, ft	131. 0	128. 3	128. 3	128. 8	0. 39%	130. 2	1. 46%
Δp_1, psf	1. 47, [b] 2. 20	2. 17	1. 99	2. 27	1. 41%	2. 36	1. 86%
Δp_2, psf	0. 60, [b] 0. 90	0. 90	0. 83	0. 91	0. 96%	0. 94	1. 33%
Δp_3, psf	1. 60, [b] 2. 40	2. 39	1. 95	2. 45	2. 56%	2. 53	2. 98%

[a] Percent increase over value for uniform level flight.

[b] Value of $k_A \Delta p$ where $k_A=1.50$ (commonly used factor to adjust to standard atmosphere).

Three sets of results for different maneuvers at Mach 1.2 are compared in table I: uniform level flight, accelerating level flight (0.15 g), and accelerating dive (0.15 g, $\gamma = -1°$). These latter two examples represent very mild maneuvers. The resulting sonic boom strengths, as shown in the table, are about 1 to 2.5 percent larger with acceleration only, and about 1.3 to 3 percent larger in the shallow dive.

These results have been presented to show some of the capabilities of the sonic boom program. It is well known that more severe overpressures occur for other conditions. Further calculations are being planned to obtain results for various combinations of maneuvers, atmospheres, and wind conditions.

REFERENCES

1. HAYES, W. D.: Brief Review of the Basic Theory. NASA SP–147, 1967, pp. 3–7.
2. HAYES, W. D.: Review of Sonic Boom Theory. Presented at Proceedings of the AFOSR–UTIAS Symposium on Aerodynamic Noise (University of Toronto), May 1968.
3. CARLSON, H. W.: Experimental and Analytic Research on Sonic Boom Generation at NASA. NASA SP–147, 1967, pp. 9–23.

Geometric Acoustics and Wave Theory

WALLACE D. HAYES
Princeton University

GEOMETRIC WAVE THEORY

The purpose of this note is to present the theory of geometric acoustics as it emerges as a special case of the geometric theory of general linear wave propagation. The study of geometric theory of wave propagation of any type starts with a study of linear solutions in a uniform medium which are proportional to functions (generally sinusoidal) of a phase variable $\phi=\boldsymbol{\kappa}\cdot\mathbf{r}-\omega t$, with $\mathbf{r}$ a distance variable in a suitable euclidean space and $\boldsymbol{\kappa}$ a vector wave number. The study yields a relation $\omega=\Omega(\boldsymbol{\kappa})$ term a dispersion relation. If ω is real when $\boldsymbol{\kappa}$ is real, the waves are termed nondissipative. The solutions obtained are termed solutions for plane waves, the waves being planar in the $\mathbf{r}$ space. A typical example is that of gravity waves in a flat ocean of uniform depth, with the $\mathbf{r}$ space two-dimensional.

In the general geometric theory for nondissipative waves, the strict conditions above are relaxed, and an asymptotic theory in a slowly varying nonuniform medium is sought for which the local solutions are very close to those obtained for plane waves, and ω and $\boldsymbol{\kappa}$ are considered large in some relative sense. The solutions are again proportional to functions (generally sinusoidal) of a phase variable $\phi(\mathbf{r},t)$, and also to slowly varying amplitude functions. The frequency and wave number are defined by

$$\omega=-\frac{\partial\phi}{\partial t} \tag{1a}$$

$$\boldsymbol{\kappa}=\nabla\phi \tag{1b}$$

and are themselves functions of $\mathbf{r}$ and t, and satisfy

$$\frac{\partial\boldsymbol{\kappa}}{\partial t}+\nabla\omega=0 \tag{2}$$

plus the condition that $\Delta\boldsymbol{\kappa}$ is symmetric.

The dispersion relation obtained for plane waves depends upon the medium, and when applied in the asymptotic theory to the quantities defined in equation (1) gives a dispersion relation

$$\omega=\Omega(\kappa,\mathbf{r},t) \tag{3}$$

defined in an augmented space $(\kappa,\mathbf{r},t)$. The dispersion relation (3) applied to equation (2) gives a first-order partial differential equation for κ alone. The method of characteristics gives then, in place of equation (2), the ordinary differential equation

$$\frac{d\kappa}{dt}+\nabla_{\mathbf{r}}\Omega=0 \tag{4}$$

holding along characteristics defined by

$$\frac{d\mathbf{r}}{dt}=\mathbf{c}=\nabla_{\kappa}\Omega \tag{5}$$

These characteristics are termed "rays." The symmetry of $\Delta\kappa$ is used in deriving equations (4) and (5). The quantity $\mathbf{c}$ is the group velocity (ref. 1), while the quantity κ/ω is the inverse phase velocity. The frequency ω obeys

$$\frac{d\omega}{dt}=\frac{\partial\Omega}{\partial t} \tag{6}$$

so that if the medium is steady, ω is constant along rays. The phase variable obeys the relation

$$\frac{d\phi}{dt}=\kappa\cdot\mathbf{c}-\omega=\kappa\cdot\nabla\kappa\Omega-\Omega \tag{7}$$

The rays may be parametrized by coordinates in a parameter space $\mathbf{a}$ of the same number of dimensions as the space $\mathbf{r}$. In the obvious analog with fluid mechanics in which $\mathbf{c}$ becomes the particle velocity and the rays become particle paths, the parameter space $\mathbf{a}$ becomes a Lagrangian variable space.

The slowly varying amplitude functions required for a quantitative solution may be obtained from separate equations. With the waves nondissipative this is best done through a conservation law, one in which volume integrals of an appropriate energy or wave action density are found to be conserved. In such a law the appropriate density times a measure V of an infinitesimal volume element is constant along rays. A convenient definition of V is as the determinant

$$V=|\nabla_{\mathbf{a}}\mathbf{r}| \tag{8}$$

The quantity V obeys the relation

$$\frac{\mathrm{d}\ln V}{\mathrm{d}t}=\nabla\cdot c \tag{9}$$

along rays.

NONDISPERSIVE WAVES

A dispersion relation is nondispersive if it is of the form

$$\omega=\kappa c_n(\mathbf{n},r,t) \tag{10}$$

where $\boldsymbol{\kappa}=\kappa\mathbf{n}$ and $\mathbf{n}$ is a unit vector. The group velocity is then

$$\mathbf{c}=\mathbf{n}c_n+\nabla_{\mathbf{n}}c_n \tag{11}$$

with $\nabla_{\mathbf{n}}$ a gradient (normal to $\mathbf{n}$) in the unit sphere, while the inverse phase velocity is $\mathbf{n}/c_n$. Plots of $\mathbf{c}$ and $\mathbf{n}/c_n$ are found to be dual in the sense that the procedure used to go from either plot to the other is the same.

The most significant special property of nondispersive waves is that the functions of phase need not be sinusoidal but may be arbitrary. A new phase variable which is a monotonic function of the old may be introduced, if desired, and the variables ω and κ are far less significant than they are in the general case. If the medium is steady, it is convenient to define the phase so that $\omega=-1$; the phase becomes then simply a time variable measured by a fixed observer, with a suitably defined zero point.

Another special property is that the right-hand side of equation (7) is zero, so that the phase is constant along rays. This has as one consequence the result that the phase ϕ may be used as one component of the parameter space $\mathbf{a}$, and $\mathbf{a}$ replaced by $(\mathbf{a}',\phi)$.

With $\mathbf{a}$ thus replaced, equation (8) may be rewritten

$$V=c_nA_n/\omega=A_n/\kappa \tag{12}$$

where

$$A_n=\left|\begin{matrix}\nabla_{\mathbf{a}'}\mathbf{r}\\ \mathbf{n}\end{matrix}\right| \tag{13}$$

is a measure of the area of a ray tube formed by rays for a given value of ϕ as cut by surfaces of constant ϕ. If the right-hand side of equation (9) is divided into normal and tangential parts, we can identify

$$\frac{\mathrm{d} \ln \kappa}{\mathrm{d}t} = -\mathbf{n} \cdot \nabla \mathbf{c} \cdot \mathbf{n}, \tag{14a}$$

$$\frac{\mathrm{d} \ln A_n}{\mathrm{d}t} = \nabla_t \cdot \mathbf{c} \tag{14b}$$

Here ∇_t is the tangential gradient, normal to $\mathbf{n}$.

GEOMETRIC ACOUSTICS

A study of linear inviscid acoustic theory following the approach outlined above leads to the conclusion that its geometric theory is of the nondissipative, nondispersive type. The perturbation velocity $\mathbf{q}$ and the perturbation pressure p' are related by

$$\mathbf{n}p' = \rho a \mathbf{q} \tag{15}$$

while the dispersion relation (10) is

$$c_n(\mathbf{n},r,t) = a(\mathbf{r},t) + \mathbf{n} \cdot \mathbf{u}(\mathbf{r},t) \tag{16}$$

where a is the speed of sound and $\mathbf{u}$ is the undisturbed fluid velocity (wind). Equations (4) and (6) are replaced by equation (13) and

$$\frac{\mathrm{d}n}{\mathrm{d}t} = -\nabla_t a - (\nabla_t \mathbf{u}) \cdot \mathbf{n} \tag{17}$$

$$\frac{\mathrm{d} \ln \omega}{\mathrm{d}t} = \frac{1}{c_n}\left(\frac{\partial a}{\partial t} + \frac{\partial \mathbf{u}}{\partial t} \cdot \mathbf{n}\right) \tag{18}$$

From equation (11) the group velocity is given by

$$\mathbf{c} = a\mathbf{n} + \mathbf{u} \tag{19}$$

The quantity constant along rays is $\rho q^2 c_n^2 A_n/\omega^2 a$. The ray-tube area A_n may be obtained by a quadrature, essentially that of equation (14b), after a differential equation for the wave-front curvature $\nabla_t \mathbf{n}$ has been solved.[1] If the medium is steady, so that ω is constant along rays, the result reduces to the classical result of Blokhintsev that $\rho q^2 c_n^2 A_n/a$ is constant along rays.

PROPAGATION IN A STRATIFIED MEDIUM

A stratified medium is one in which the dependence of Ω on $\mathbf{r}$ and t reduces to that in one Cartesian variable, here chosen to be z. We

[1] W. D. Hayes: The Energy Invariant for Geometric Acoustics in a Moving Medium. Phys. Fluids, vol. 11, 1968, to be published.

replace $\mathbf{r}$ by $\mathbf{r}'+z\mathbf{k}$ and $\boldsymbol{\kappa}$ by $\boldsymbol{\kappa}'+\kappa_z\mathbf{k}$. The general dispersion relation (3) takes the form

$$\omega=\Omega(\boldsymbol{\kappa}',\kappa_z,z) \tag{20}$$

Equations (4) and (6) give

$$\frac{d\boldsymbol{\kappa}'}{dt}=0 \qquad \frac{d\omega}{dt}=0 \tag{21}$$

A separate equation for κ_z may be given, but we may consider it given by equation (20) in terms of $\boldsymbol{\kappa}'$ and ω.

We use the term Snell's law for a refraction law, once integrated, for wave propagation in a stratified medium. The result, equation (21) gives directly the general Snell's law that $\boldsymbol{\kappa}'$ and ω are constant along rays. In particular, also, the horizontal component $\boldsymbol{\kappa}'/\omega$ of the inverse phase velocity is constant along rays.

It is convenient to replace t by z as a basic independent variable. The ray equations (5) then take the form

$$\frac{d\mathbf{r}'}{dz}=\frac{\mathbf{c}'}{c_z}=\mathbf{K}(\boldsymbol{\kappa}',\omega,z) \tag{22}$$

$$\frac{dt}{dz}=\frac{1}{c_z} \tag{23}$$

and can be integrated by quadratures to give the rays $\mathbf{r}'(z)$, $t(z)$.

When the wave propagation is nondispersive the dependence of $\mathbf{K}$ in equation (22) upon $\boldsymbol{\kappa}'$ and ω reduces to dependence upon the horizontal component

$$\frac{\boldsymbol{\kappa}'}{\omega}=\frac{\mathbf{n}'}{c_n}=\mathbf{N}(\mathbf{a}',\phi) \tag{24}$$

of the inverse phase velocity. The volume element V may be shown to be given by

$$V=c_zA/\omega \tag{25}$$

where A is a measure of the area of a ray tube formed by rays for a given value of ϕ as cut by planes of constant z. The area A may conveniently be defined

$$A=|\nabla_{\mathbf{a}'}\mathbf{r}'| \tag{26}$$

To evaluate A we apply the operator $\Delta\mathbf{a}'$ to equation (22). The total derivative d/dz in equation (22) is a partial derivative in a

$(\mathbf{a}',z)$ space, and commutes with the operator $\nabla_{\mathbf{a}'}$. Thus we obtain

$$\frac{\mathrm{d}\nabla_{\mathbf{a}'}\mathbf{r}'}{\mathrm{d}z}=\nabla_{\mathbf{a}'}\mathbf{K}=\nabla_{\mathbf{a}'}\mathbf{N}\cdot\nabla_{\mathbf{N}}\mathbf{K} \tag{27}$$

In this equation $\nabla\mathbf{a}'\mathbf{N}$ is constant, while with $\mathbf{N}$ given $\nabla_{\mathbf{N}}\mathbf{K}$ is a function of z alone. The solution of (27) is then

$$\nabla_{\mathbf{a}'}\mathbf{r}'=(\nabla_{\mathbf{a}'}\mathbf{r}')\ z_0+\nabla_{\mathbf{a}'}\mathbf{N}\cdot\int_{z_0}\nabla_{\mathbf{N}}\mathbf{K}\,\mathrm{d}z \tag{28}$$

The determinant then gives A according to equation (26).

In the acoustic case we take $\mathbf{u}$ to be horizontal and dependent only upon z. The horizontal vector $\mathbf{K}$ may be evaluated from equation (22),

$$\mathbf{K}=\frac{a^2\mathbf{N}+(1-\mathbf{u}\cdot\mathbf{N})\mathbf{u}}{a\sqrt{(1-\mathbf{u}\cdot\mathbf{N})^2-a^2N^2}} \tag{29}$$

We define the horizontal unit vector $\mathbf{i}$ and $\mathbf{j}$ so that $\mathbf{N}=N\mathbf{i}$ and $u_t\mathbf{j}=\mathbf{u}-\mathbf{ii}\cdot\mathbf{u}$. We introduce the angle θ such that $n_z=\sin\theta$, $\mathbf{n}'=\mathbf{i}\cos\theta$, and note that $c_z=a\sin\theta$. The derivative

$$\nabla_{\mathbf{N}}\mathbf{K}=N^{-3}\frac{\cos^3\theta}{a^2\sin^3\theta}\mathbf{ii}+N^{-2}\frac{u_t\cos^3\theta}{a^2\sin^3\theta}(\mathbf{ij}+\mathbf{ji})+N^{-1}\left(\frac{\cos\theta}{\sin\theta}+\frac{u_t^2\cos^3\theta}{a^2\sin^3\theta}\right)\mathbf{jj} \tag{30}$$

is obtainable from equation (29), and permits A to be calculated through equation (28). The conserved Blokhintsev quantity is $\rho q^2c_nc_zA/a=N^{-1}\rho q^2A\sin\theta\cos\theta$.

The theory given here is equivalent to that used [2] in a recently developed computer program for calculating sonic boom pressure signatures. In such a calculation, results are first obtained using geometric acoustics and then modified for nonlinear effects.

REFERENCE

1. Whitham, G. B.: Group Velocity and Energy Propagation for Three-Dimensional Waves. Commun. Pure Appl. Math., vol. 14, 1961, pp. 675–691.

[2] W. D. Hayes et al.: Sonic Boom Propagation in a Stratified Atmosphere, with Computer Program. NASA CR, to be published.

Similarity Rules for Nonlinear Acoustic Propagation Through a Caustic

WALLACE D. HAYES
Princeton University

BASIC EQUATIONS AND SIMILITUDE

A caustic in geometric acoustics is an envelope of rays, and also a locus of wave front cusps. A point on a caustic is one where a ray-tube area is zero, but corresponds to a lowest order type singularity for points of zero ray-tube area. A caustic has a characteristic scale R, which may conveniently be visualized as proportional to the inverse of the relative curvature of a ray with respect to the caustic (both rays and caustics may be curved). This scale will be defined in terms of wave front shape. We are interested in acoustic signals of characteristic length L, which may be the total length of a sonic boom signal, or which might be the spatial period of a periodic signal.

When the ratio L/R is sufficiently small, a boundary-layer approach is valid (ref. 1). Separate inner and outer analyses are carried out and are matched. The outer analysis is one for geometric acoustics, in which weak nonlinear effects may be taken into account. The inner analysis, in a thin region including the caustic, is a local analysis with stretched coordinates. The thin region is interpreted as the boundary layer. Our purpose here is to examine how weak nonlinear effects are to be taken into account in this local analysis.

One difficulty arises from the fact that rays are really trajectories in four-dimensional spacetime, with the caustic a hypersurface in this space. We use a particular moving coordinate system, one moving with velocity $a_0\mathbf{n}$ with respect to the fluid at a reference point on the caustic. Here a_0 is the speed of sound at this point. In this coordinate system the caustic will appear temporarily frozen. This procedure is analogous to that used with a general moving shock wave to reduce it to a temporarily stationary normal shock.

Another difficulty arises from the fact that the motion is, in general, not irrotational. This may be attacked by defining a reduced velocity potential, but is most easily resolved by taking advantage

of the fact that the analysis is local. We assume that the characteristic scale of the vorticity in the disturbed flow is at least of order R. Then the vorticity is properly neglected in our local analysis, and a velocity potential may be used.

We aline our x axis in the direction of the flow ($-\mathbf{n}$), and let the velocity potential be $a_0(x+\Phi)$. The linearized equation in a uniform sonic flow is

$$\Phi_{yy}+\Phi_{zz}-2a_0^{-1}\Phi_{xt}-a_0^{-2}\Phi_{tt}=0 \tag{1}$$

This equation must be modified is several ways. The term in Φ_{tt} will turn out to be negligible, and we drop it here. A term in Φ_{xx} times a linear combination of x, y, and z must be added to give the caustic behavior. The coordinate system is alined so that the coefficient of z is zero, and the term added is $-R^{-1}(y+bx)\Phi_{xx}$, where b is a dimensionless constant. Nonlinear effects are taken into account to lowest order with the term $-2\Gamma\Phi_x\Phi_{xx}$, with $\Gamma=\frac{1}{2}(\gamma+1)$ in a perfect gas. The resulting equation is

$$\Phi_{yy}+\Phi_{zz}-[R^{-1}(y+bx)+2\Gamma\Phi_x]\Phi_{xx}-2a_0^{-1}\Phi_{xt}=0 \tag{2}$$

The spatial coordinate system is illustrated in figure 1.

We assume next that the characteristic time scale of unsteadiness is $c^{-1}a_0^{-1}R$, and that the characteristic distance scale of z variations is $d^{-1}R$, with c and d constants of order no greater than one. The small parameter λ, defined by

$$\lambda=L^{1/3}R^{-1/3} \tag{3}$$

is introduced, and a transformation of the independent variables is made,

$$x=L\xi \tag{4a}$$

$$y=L\lambda^{-1}\eta=R\lambda^2\eta \tag{4b}$$

$$z=d^{-1}R\zeta \tag{4c}$$

$$t=c^{-1}a_0^{-1}R\tau \tag{4d}$$

Quantities of relative order λ^2 will consistently be neglected. Equation (2) is thereby transformed into

$$\Phi_{\eta\eta}+d^2\lambda^4\Phi_{\zeta\zeta}-(\eta+b\lambda\xi+2\Gamma L^{-1}\lambda^{-2}\Phi_\xi)\Phi_{\xi\xi}-2c\lambda\Phi_{\xi\tau}=0 \tag{5}$$

The errors in this equation are of relative order λ^2, and the z-derivative term in $\Phi_{\zeta\zeta}$ is here dropped. The Φ_{tt} term in equation (2) would appear here as of order $c^2\lambda^4$.

For reasons that will be apparent when we discuss boundary conditions, the transformation

$$\Phi=\epsilon L\lambda^{-1/2}\psi \tag{6a}$$

$$\Phi_x=\epsilon\lambda^{-1/2}\psi_\xi \tag{6b}$$

is made. The quantity ϵ is a measure of the strength of the signal. The quantity K, to be identified as a similarity parameter, is defined

$$K=\Gamma\epsilon\lambda^{-5/2} \tag{7}$$

The basic equation (5) then becomes

$$\psi_{\eta\eta}-(\eta+b\lambda\xi+2K\psi_\xi)\psi_{\xi\xi}-2c\lambda\psi_{\xi\tau}=0 \tag{8}$$

with relative errors that are of the order of λ^2. If b and c are of the order of λ, or if they are of the order of one and λ is negligibly small, the two terms in $b\lambda$ and $c\lambda$ may be dropped. We assume that this is the case, and obtain the nonlinear Tricomi equation

$$\psi_{\eta\eta}-(\eta+2K\psi_\xi)\psi_{\xi\xi}=0 \tag{9}$$

The quantity R has in essence been defined in terms of its appearance in equation (2). At a given instant, the characteristics of equation (2) are approximately

$$\frac{4}{9}(y+bx_0)^3=R(x-x_0)^2 \tag{10}$$

The quantity R thus characterizes the cusps in the wave fronts. In general, then, the wave fronts in the linear problem should be found; their shape then determines the parameter R. Such a definition is preferable to one in terms of curvatures of rays and caustics, because the wave fronts are definite geometric entities and are Galilean invariant. Rays and caustics are kinematic entities, and their geometric projections are not Galilean invariant.

The boundary conditions must be chosen to correspond to the physical situation. The main boundary condition is one describing an incoming signal on the hyperbolic side of the caustic. On the elliptic side of the caustic we have simply the condition that the solution must approach zero. In a detailed analysis, the incoming signal should be described in terms of the theory of quasi-linear geometric acoustics, because this theory is consistent with equation (9) for large y or η. Here we take the simpler course of describing the incoming signal in terms of linear geometric acoustics, consistently with the Tricomi equation.

315-766 O—68——12

The ray-tube area may be readily shown to be proportional to $y^{1/2}$, so that the pressure according to linear geometric theory is proportional to $y^{-1/4}$. Thus we describe the incoming signal by

$$\frac{1}{2}C_p=\frac{p'}{\rho a_0^2}=-\Phi_x=\epsilon\left(\frac{y}{R}\right)^{-1/4}f\left(\frac{x+\frac{2}{3}R^{-1/2}y^{3/2}}{L}\right) \tag{11}$$

for x negative and y sufficiently large, with f known (dependent also upon z and t or ζ and τ). The transformation equation (6) was chosen to be consistent with equation (11), and gives

$$-\psi_\xi=\eta^{1/4}f\left(\xi+\frac{2}{3}\eta^{3/2}\right) \tag{12}$$

as the boundary condition to be used with equation (9). Equations (9) and (12) give us a problem for which the solution is of the form

$$\psi=\psi(\xi,\eta,K;f) \tag{13}$$

The function ψ is a functional of f. The parameter K is a basic similarity parameter.

With nonlinear effects taken into account there are more details in the boundary condition specification and the matching of inner to outer solution. There is little difference in principle, however, and the similitude result equation (13) will still hold with a slightly altered definition of f.

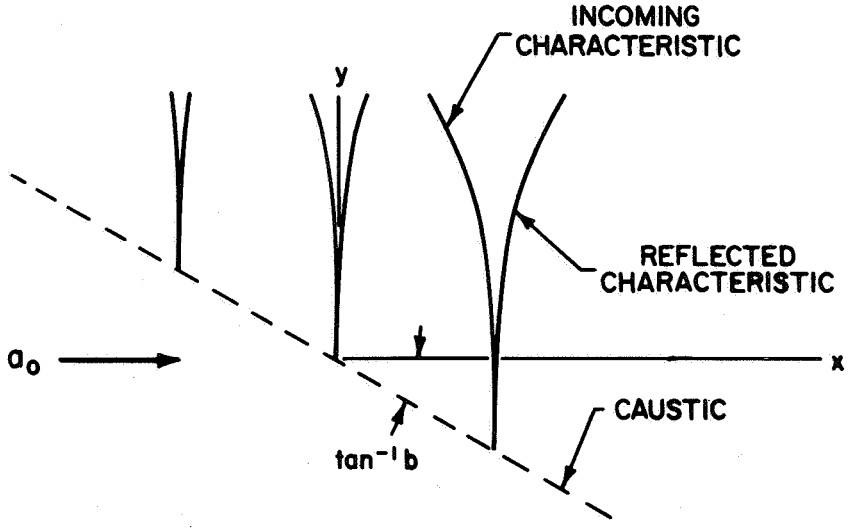

FIGURE 1.—Coordinate system for equation (2).

Figure 1 helps us interpret the constant b. If b is nonzero, there is a normal relative motion of the caustic with respect to the medium. This is characterized by a normal velocity Ma_0, where M is a Mach number for this normal velocity given by

$$M=b(1+b^2)^{-1/2} \tag{14}$$

LINEAR SOLUTIONS

In studying a nonlinear problem which reduces to a linear one in some limit, it is essential to understand the linear problem. In this case the linear problem is that for the Tricomi equation

$$\psi_{\eta\eta}-\eta\psi_{\xi\xi}=0 \tag{15}$$

Note that this equation is invariant with respect to ξ differentiation. The most familiar special solutions are those in terms of Airy functions, sinusoidal in ξ. Solutions must be chosen that are exponentially decreasing rather than increasing for large $-\eta$. With this condition, solutions for large η have the form

$$\psi\sim\eta^{-1/4}\left[\exp i\left(k\xi+\frac{2}{3}k\eta^{3/2}-\frac{1}{4}\pi\right)+\exp i\left(k\xi-\frac{2}{3}k\eta^{3/2}+\frac{1}{4}\pi\right)\right] \tag{16}$$

The terms in $\frac{1}{4}\pi$ give the interpretation that the reflected wave (second term) is the same as the incoming wave (first term) but with a phase advance of $\frac{1}{2}\pi$. By decomposing a general incoming signal in terms of a Fourier integral we see that the reflected signal may have a much different shape. This phase shift leaves the power spectrum unchanged, but not the shape of the signal. A jump (linearized shock) reflects as a positive logarithmic singularity (ref. 2), for example.

For our purposes we are interested in details of the solution in the caustic region, not just the outer asymptotic expansions. Though one attack would be through Fourier integral representations, a more direct and (in the author's opinion) easier method is through self-similar solutions (ref. 3). It is possible to find a solution which gives a jump in the incoming signal and a logarithmic singularity in the reflected signal. This solution is a suitable linear combination of

$$\psi_1=\eta^{-1/4}F\left(\frac{1}{12},\frac{5}{12};\frac{1}{2};\frac{9\xi^2}{4\eta^3}\right) \tag{17}$$

and

$$\psi_2=\xi\eta^{-7/4}F\left(\frac{7}{12},\frac{11}{12};\frac{3}{2};\frac{9\xi^2}{4\eta^3}\right) \tag{18}$$

with particular choices of the possible analytic continuations across the characteristics. The solution has a $-\frac{1}{6}$ power singularity in ξ on the caustic. It may be interpreted as a solution for ψ_ξ, or as a solution for ψ with a delta function in the incoming signal in terms of ψ_ξ.

The solution corresponding to an arbitrary incoming signal may directly be represented as a superposition of solutions of the type discussed. If the incoming signal has a singularity of power n, there will arise on the caustic a singularity in ξ of the power $n-\frac{1}{6}$. If the incoming signal in terms of f has no singularity of power $\frac{1}{6}$ or worse, the solution on the caustic will be bounded. In this case, with K defined in equation (7) negligibly small, the similitude of equation (13) holds with K set equal to zero. Pressures, obtained from equation (6b), are proportional to $\epsilon\lambda^{-1/2}$.

GUIRAUD'S SIMILITUDE

We consider finally the case in which K is very small but the function f has jumps representing incoming shock waves. The nonlinear similarity result does not give more than peripheral information, and the linear theory gives infinite pressures both on the caustic and in the reflected wave. No matter how small K is, nonlinearity is important within a narrow region near the caustic including each shock and its reflection. The scale of this region in the ξ direction we term L'.

We repeat the analysis above with L replaced by L', and determine L' by equation (7) with the condition that $K'=1$. We obtain thereby

$$\lambda'=\epsilon^{2/5}\Gamma^{2/5} \tag{19a}$$

$$L'=\epsilon^{6/5}\Gamma^{6/5}R \tag{19b}$$

The parameter ϵ is defined here so that the jump in f as defined in equation (11) is one. The new reduced variables (for a shock whose linear trace passes through the origin) are related to the old ones by

$$\xi'=K^{-6/5}\xi \tag{20a}$$

$$\eta'=K^{-4/5}\eta \tag{20b}$$

$$\psi'_{\xi'}=K^{1/5}\psi_\xi \tag{20c}$$

The pressure in the narrow region may be expressed

$$\frac{1}{2}C_p=-\Phi_x=\epsilon^{4/5}\Gamma^{-1/5}\psi'_{\xi'}(\xi',\eta') \tag{21}$$

This similitude result is in accord with that found by Guiraud (ref. 4). Because the pressure predicted by the linear similitude is of the order of $\epsilon\lambda^{-1/2}$, the pressure of equation (21) can predominate only if $K^{1/5}$ is very small. This rather severe condition may possibly be circumvented through additional analysis, treating the pressure field of equation (21) as a pressure difference relative to one given by some linear analysis.

REFERENCES

1. Buchall, R. N.; and Keller, J. B.: Boundary Layer Problems in Diffraction Theory. Commun. Pure Appl. Math., vol. 13, 1960, pp. 85–114.
2. Lighthill, M. J.: Reflection at a Laminar Boundary Layer of a Weak Steady Disturbance to a Supersonic Stream, Neglecting Viscosity and Heat Conduction. Quart. J. Mech. Appl. Math., vol. 3, 1950, pp. 303–325.
3. Guderley, K. G.: The Theory of Transonic Flow. Pergamon, 1962.
4. Guiraud, J. P.: Acoustique géométrique, bruit ballistique des avions supersoniques et focalisation. J. Mécanique, vol. 4, 1965, pp. 215–267.

CONTRIBUTED REMARKS

General Remarks on Sonic Boom

A. R. Seebass
Cornell University

I would like to begin these remarks by reiterating a comment that I made previously. We must not overlook the fact that advances in technology that result in an improved overall efficiency for SST aircraft, such as improvements in lift-to-drag and engine thrust-to-weight ratios, as well as in structural weight and specific fuel consumption, will provide direct reductions in the sonic boom intensities. Furthermore, attempts at sonic boom reduction cannot afford any penalties that result from a compromise in the overall efficiency of the aircraft if the reduction is to be a realizable one. Sonic boom reduction need not be at the expense of overall efficiency; indeed, the most direct route to sonic boom reduction is through the aircraft's overall efficiency.

During this meeting we have heard a number of papers that discussed the utilization of aerodynamic techniques to reduce the "impact" of the sonic boom. We are all aware, thanks to Professor Busemann, that the volume contribution to the sonic boom can be eliminated in all azimuthal planes by utilizing interference effects; it can also be eliminated in a single azimuthal plane by a configuration that exactly balances the lift and volume contributions to the equivalent body shape in that plane. Such a configuration has no net lift. While the lift contribution can be reduced by the addition of suitable volume elements, there is no way of escaping the boom attributed to lift alone, if the Bernoulli constant of the flow is unchanged. For a given lift and volume there is a lower bound to the far-field overpressure within the framework of the above proviso. Professor Ferri has attempted to approach this lower bound with realistic aircraft configurations. Personally, I feel his results are encouraging in that they point the way for modest improvements in far-field overpressure levels. Professor George has indicated how quadrupole effects can also be used to approach this theoretical lower bound.

Several of the configurations we have seen in the past 2 days have achieved a reduction in the overpressure by lengthening the equivalent body in the azimuthal plane under the aircraft, without lengthening the actual aircraft. It is important to keep in mind that the theoretical lower bound is for a given length of the equivalent body, and is proportional to the inverse fourth power of this length, not the actual length. Consequently, such reductions may accrue because the effective length of the aircraft is increased, not because the actual shape is near the optimum one. Indeed, reductions are sometimes obtained even though the new equivalent body shape is further from that prescribed by the lower bound than the original shape.

As I mentioned earlier, we cannot escape the boom attributed to lift without modifying the Bernoulli constant of the flow. The equivalent slender body of revolution attributed to lift never closes in the azimuthal plane under the aircraft; it has a finite base area far downstream that is proportional to the lift. Aircraft engines, however, modify the Bernoulli constant of the flow that passes through them, and it is not entirely unreasonable to think of aircraft in which a reduction in engine stream-tube area is used to compensate for the growth of the equivalent body of revolution attributed to lift. Hypothetically, it is possible to totally eliminate the boom attributed to lift in this way. Actually the second law of thermodynamics requires that infinitely far downstream the exit stream-tube area be larger than the entering one. This pluming of the engine exhaust, which takes many aircraft lengths to occur, will give rise to a weak pressure disturbance at the ground. A portion of this disturbance accounts for the support of the aircraft by the pressure field there. Because the disturbance is spread out over such a large longitudinal distance, it is reasonable to assume that no significant steepening of the disturbance into shock waves occurs. Professor Resler's careful analysis of the gains we may achieve by this route shows how very difficult it is to obtain a reduction in the overpressure with realistic restrictions on the turbine inlet temperature. Total elimination of the exhaust stream-tube area in the present configurations would only reduce the boom attributed to lift by about 5 percent (assuming this elimination is accomplished with no additional wave drag—which it cannot be). Nevertheless, this is an important area for further research because it gives us one more adjustable parameter with which to attempt to achieve overpressure reductions.

I would like to discuss in more detail another aerodynamic means of reducing the impact of the sonic boom: the possibility of designing aircraft with their overpressure signatures modified to reduce human annoyance. Here I tread dangerous ground. Our understanding of which features of the overpressure signature are the most undesir-

able ones is far from complete. If shock waves are absent from the signature and the compression rise times are on the order of hundredths of a second, then there is little acoustical energy present in the audible range. The most annoying feature of the sonic boom, as experienced outdoors, lies in the shock waves themselves. On the other hand, the low frequencies, which are inaudible outdoors, contain the majority of the acoustical energy and cause structures to vibrate and windows to rattle. As a consequence, an overpressure signature without shock waves may not be much less annoying indoors than its fully steepened counterpart. Let me leave these unanswered questions with the ad hoc assumption that one of the most annoying features of the sonic boom, at least as it is experienced outdoors, is attributable to the presence of shock waves in the overpressure signature, and turn to the technical and answerable question of whether or not it is possible to design aircraft with overpressure signatures that do not contain shock waves.

Several years ago, Ed McLean of the NASA Langley Research Center noted from his calculations that it takes several hundred aircraft lengths for the overpressure signature to reach its asymptotic form. This led McLean to examine the requirements on aircraft length and weight, for a fixed altitude and Mach number, to achieve finite rise time overpressure signatures. The results of his most recent study were given during this meeting. These results may seem to be fairly pessimistic ones. We note that to achieve rise times on the order of 10^{-2} seconds, instead of front and rear shock waves, requires that a 600 000-pound aircraft be nearly 1000 feet long.

In his study McLean has assumed the only effect of the atmosphere is that it alters the overpressure level and not the signature shape. But Professor Hayes pointed out previously that this was not the case, and he reminded us at this meeting that the signature shape that exists $\pi/2$ real atmospheric heights from the aircraft in a homogeneous atmosphere is, roughly speaking, the shape that persists to infinity in a real atmosphere. Because I disputed this point, and incorrectly so, I have taken it upon myself to correct McLean's results for atmospheric effects by calculating the advance, α, that would occur in isothermal atmosphere relative to that which would occur in a homogeneous atmosphere, α_h, for two scale heights: one characteristic of the stratosphere (H=20 000 feet) and the other characteristic of the troposphere (H=30 000 feet). These advance ratios have then been used to calculate the aircraft length, l, required for a finite rise time signature in an isothermal atmosphere, relative to the length, l_h, computed by McLean for a homogeneous atmosphere; the results are shown in figure 1.

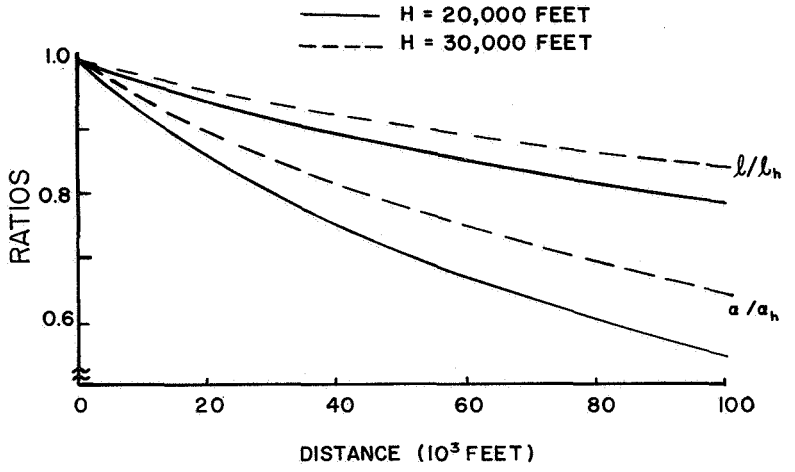

FIGURE 1.—Advance and length ratios.

McLean's analysis is also overly pessimistic from another point of view, in that it does not take advantage of the isentropic tail pressure wave that exists naturally in the signature to help eliminate the rear shock wave and reduce the aircraft length requirement. I have made a rough correction for this effect by employing the signature shown in figure 2, where I have taken the length of the aircraft to be 1.7λ and completed the signature using the asymptotic form of the tail wave for the given lift. Figure 3 shows the aircraft length required as a function of altitude, for two Mach numbers and two weights. As you can see, at 61 000 feet there is about a 30 percent reduction in the length required for a given weight when we include atmospheric and tail wave effects. Each contributes

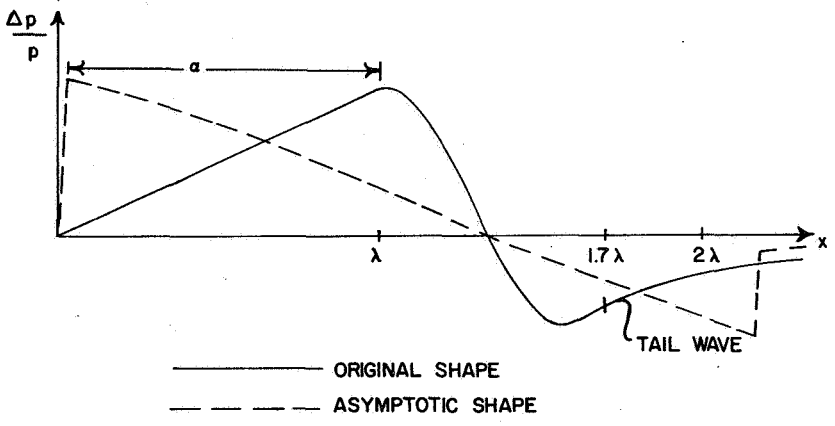

FIGURE 2.—Finite rise-time signature.

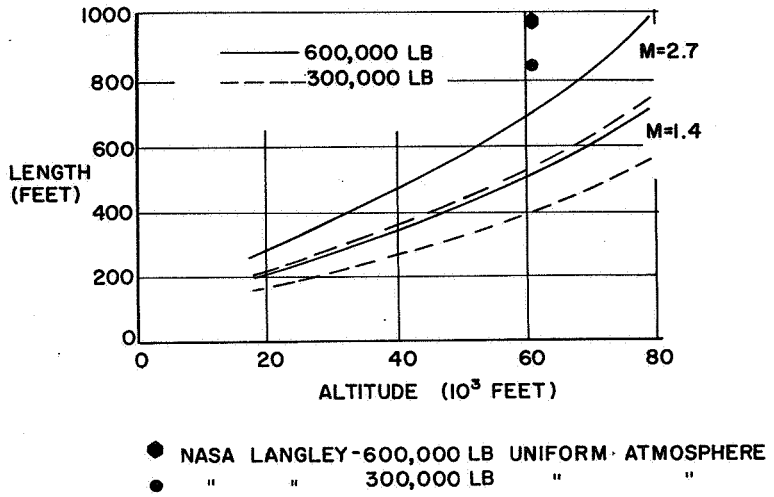

FIGURE 3.—Aircraft length for finite rise times.

about half of the total decrease in length. For typical SST altitudes and weights, the lengths that are required for a Mach number of 2.7 are about twice the length of the Boeing 2707. However, if we are willing to fly slower, and if we anticipate the usual improvements in specific fuel consumption, lift-to-drag ratio, structural weight and structural designs, then so far as I can judge, such aircraft are only one, or perhaps two, aircraft generations beyond the present SST design.

In conclusion, it seems to me that we can safely prognosticate a continual evolution of SST designs with improved sonic boom characteristics. Major gains may be expected from improvements in the overall efficiency of such aircraft, as well as through novel design features such as those just discussed. Whether or not these evolutionary gains will be sufficient to make a domestic SST an economically viable concept is unknown. We cannot hope to provide a definitive answer until we know what features of the overpressure signature are the most annoying ones, and what integrated overpressure loadings are likely to prove to be acceptable. My prognosis, based on our tentative answers to these questions, is that such gains will indeed be sufficient to allow commercial supersonic flight over populated areas.

State of the Art of Sonic Boom Theory

WALLACE D. HAYES
Princeton University

This paper could be divided roughly into two main questions. The first is, How far have we proceeded in developing methods of analysis and the requisite understanding of sonic boom phenomena? The second is, How far have we proceeded in devising methods of reducing sonic boom for feasible aircraft designs?

ANALYSIS OF SONIC BOOM

With respect to the straightforward analysis of the propagation of sonic boom from a slender aircraft, there appears to be no problem now. Linearized theory for the flow about the aircraft has been understood for a long time. Geometric acoustics with winds and variable sound speed is now quite well understood. With the assumption that nonlinearity does not affect the rays, the nonlinear modifications of the signature can be calculated directly. Developed second-order theory serves to justify the theory.

One problem of practical importance, though better understood, remains unsolved. This is the problem of predicting sonic boom signatures near a caustic (ray envelope). This problem, together with other theoretical problems as yet unsolved, is at least in focus. We know how they are to be attacked, and there is no reason to believe that practicable solutions will not emerge with time and labor. The other problems include that of nonlinear effects on ray tubes, diffraction into shadow zones, and nonlinear effects near the aircraft.

The effects of turbulence, in particular the creation of spikes in sonic boom signatures, are beginning to be understood (see the remark entitled "Atmospheric Turbulence" by Garrick in this volume). More work is clearly needed in this field.

REDUCTION OF SONIC BOOM

It is now generally recognized that the one inescapable parameter is the lift of the aircraft plus $\rho U^2\beta^{-1}$ times the increase of engine jet

area over capture area (discussed in NASA SP–147, p. 6). It is also recognized that general overall excellence in aircraft design is most important in reducing sonic boom. The first fact is important in that it gives the designer criteria for evaluating his design with respect to sonic boom production, and permits formulating an ideal toward which to aim. The second fact is important in establishing that sonic boom is but another element that must fit into the procedure of compromise that is aircraft design, that a preoccupation in design with sonic boom at the cost of other design factors is self-defeating.

To illustrate these points, with the lift plus engine area increase given, we can clearly reduce the sonic boom intensities from the volume distribution by suitable redesign. This procedure may, and generally does, entail some increase in wave or frictional drag. This drag increase would affect the overall design and require a larger gross weight and lift for a given mission.

How should we proceed in design studies to reduce sonic boom? Here we are faced with two completely different paths. The first path is somewhat better charted. We accept a signature with shock waves and assume that the signature is close to an N-wave. With the lift given and the drag estimated, we can design engines with small area increase. With the parameter lift plus engine area increase specified, we can minimize the boom beneath the aircraft. We are led to a family of problems in the calculus of variations, some of which have been solved. We then seek aircraft configurations that will come close to realizing our optimum solutions.

The second path is quite different. We adopt the psychoacoustic principle that it is the shocks in sonic boom signatures which are objectionable and are to be avoided. We do not assume an N-wave shape, and aim toward a finite rise time signature near the aircraft that will still have no shock waves in it at the ground. Here we take advantage of the "freezing" effect of atmospheric stratification on downward-propagating signals. The calculus of variations has not yet been applied in an attack along this path. The main effort, of course, is again in detail design, with very low wing loadings required.

Which of these two paths toward sonic boom reduction will be best is not known now. They must both be explored.

Reduction of Peak Overpressure by Configuration Design

ANTONIO FERRI
New York University

In connection with the comments and suggestions for future work, I believe the following points can be made: It appears that by some redesign of present configurations substantial changes in the peak overpressure can be obtained. In addition, it appears that near-field signature can be obtained if the total length of the airplane is utilized even if we fly at 60 000 feet. On this basis, a substantial effort must be made to investigate these two possibilities.

In connection with improvement of the existing theory related to sonic boom, my feeling is that the improvement must be obtained in two directions. First, we must obtain more realistic information of the initial distribution for a practical vehicle at Mach numbers on the order of 3 or higher. It is my impression from the presentations given that many of the higher order theories are based on expansion in terms of Mach number and similar to the expansion used by Busemann for the two-dimensional wing. Such expansions are not valid at high Mach numbers. If this is correct, the higher order theories are not very useful. In addition, the present theory does not permit analyzing wings of two-dimensional type or close to two-dimensional type. Such wings permit producing a lot of lift in a short length and therefore are useful for sonic boom considerations because it permits obtaining distribution close to optimum.

If you neglect tip effects by cutting the tips along the Mach wave, then the L/D of two-dimensional wing is proportional to the inverse of the angle of attack because the lift is proportional to α and C_D is proportional to α^2. Therefore, if we increase the span and decrease the cord leaving the area the same, and angle of attack the same, the L/D does not change.

In connection with propagation theories, the effect of the density variations as a function of the altitude z has been considered already by several people. Therefore, I do not see much necessity of increasing activities in this field. The part that has not been considered is the variation of density in a given plane as a function of x, y, and

315-766 O—68——13

not z. This we are planning to do for the next year; I believe that such effects will justify some of the variations obtained for similar flight conditions attributed to atmospheric conditions.

In addition, the work that Professor Hayes recommended in connection with maneuvering vehicles is also important. In my opinion the work that we have initiated connected with the effects of terrain configurations is very important. I feel that the linear theory is more than satisfactory if we are interested in pressure variations on surfaces from the stress analysis point of view. In any case, the higher order theory will not improve the situation because it can be done only for a far field and the reflections at the surface of the body depend only on the near field. Again, we plan to continue this work next year.

Notes on the Sonic Boom Minimization Problem

HARRY W. CARLSON
Langley Research Center, NASA

In view of the widespread current interest in sonic boom suppression, it is believed to be appropriate to review some observations on the prospects for sonic boom reductions based on analytic studies and the supporting experimental research program conducted at the Langley Research Center. An extensive wind-tunnel test program beginning about 10 years ago has treated a great variety of models including rather basic research shapes, airplane components, and complete airplanes. In addition, the tunnel has provided data for evaluation of a number of exotic or nonconventional airplane concepts and for evaluation of certain minimum boom and minimum drag shapes as well. Recurrent conclusions in all of these studies have emphasized the remarkable ability of the simple linearized theory (with the Whitham corrections) to provide accurate predictions of sonic boom signatures. It has been noted that the prediction ability increases with increasing model slenderness and with increasing distance from the model. Thus the theory is recognized to be all the more valuable as a minimization tool because the conditions of slenderness and extreme altitude are precisely those which encourage minimization.

An examination of the minimization problem by the author in 1962 led to the determination of an approximate far-field lower bound and to suggestions for achievement of this goal through airplane design (NASA TN D–1494). The equivalent body principle formulated by Hayes and the work of Whitham formed the theoretical basis for the study. Because the sonic boom had been shown to depend on the shape and magnitude of an airplane effective area distribution formed by both volume and lift components (fig. 1), and, because the magnitude of the effective area at the base of the airplane is fixed in large part by the airplane weight, Mach number, and altitude, a study was made of the effect of the shape of the curve or the bow shock pressure rise in the far field.

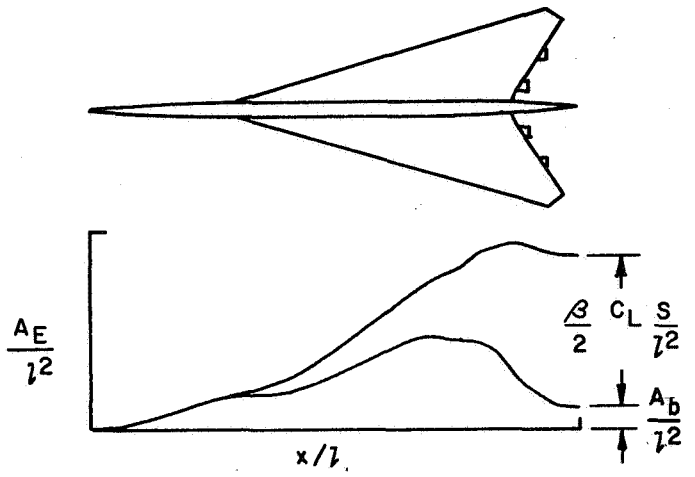

FIGURE 1.—Typical effective area distribution.

It was found that the overpressure could be expressed as

$$\Delta p=\bar{p}\left(\frac{l}{h}\right)^{3/4}\beta^{1/4}K_r\cdot K_s\sqrt{\frac{\beta}{2}C_L\frac{S}{l^2}+\frac{A_b}{l^2}} \tag{1}$$

where k_s is a shape factor that may be evaluated by employment of the machine computing program described in NASA Report R–213 or by analytic methods for curves that can be expressed as simple mathematical functions. The results of the aforementioned NASA study of many effective area distribution shapes indicated an approximate lower bound value of $K_s=0.60$. It was then discovered that L. B. Jones had earlier made a more rigorous mathematical study of the problem (for volume alone or lift alone, but not the combination) and had arrived at factors 10 percent lower. Jones's lower bound shape, however, requires an area development proportional to the square root of the distance from the airplane nose and, as a consequence, has a prohibitively high wave drag for practical consideration. The high drag is the result of the relatively intense shock strength near the blunt nose of the body. Only at extreme distances does the blunt shape have lower bow shock pressures than more conventional shapes. The k_s value of 0.60 thus may be accepted as a more practical lower bound. The corresponding effective area distribution shown in figure 2 is in fact the area development for a Von Kármán minimum drag body.

Equation (1) may be plotted as shown in figure 3. The ordinate represents an overpressure parameter which contains altitude, Mach number, and reflection factors. The abscissa is dependent primarily on the airplane lift. The relationship between the two parameters

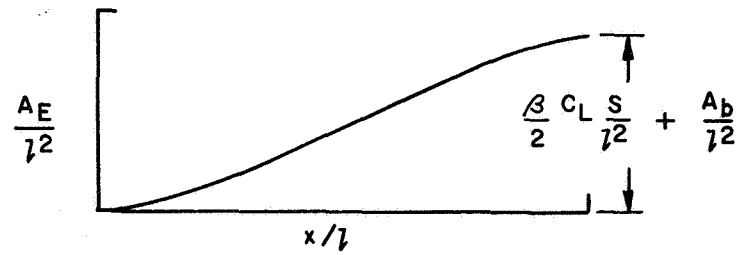

FIGURE 2.—Effective area distribution corresponding to far-field practical lower bound overpressure.

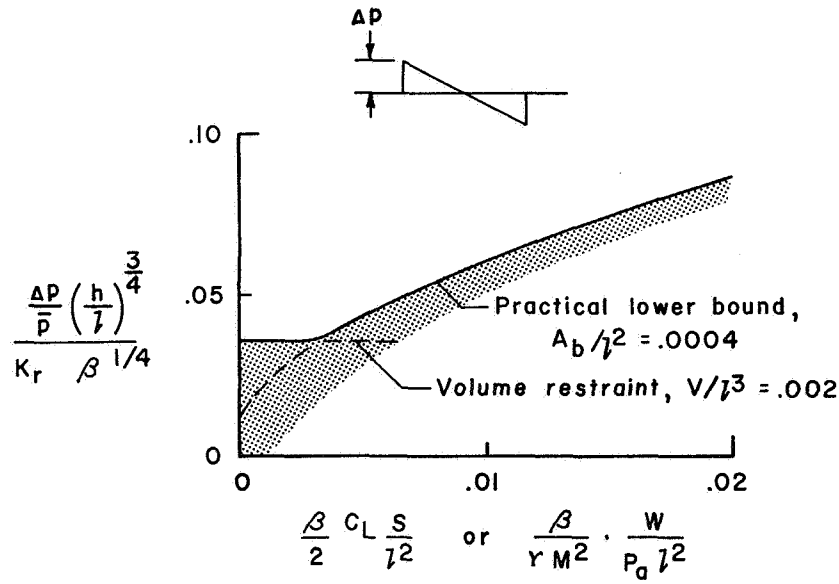

FIGURE 3.—Far-field practical lower bound overpressure in parametric form.

is an indication of the sonic boom efficiency of the design. When a shape factor of 0.60 is chosen, the curve as shown in figure 3 defines the practical lower bound of attainable overpressure levels. In other words, the area under the curve represents overpressure levels that are unattainable in the practical sense. In this case, the base area A_b was chosen to represent the engine exhaust effect for an SST at $M=2.7$ cruise altitude. There is one further restraint that must be applied. The area under the lower bound effective area development may not contain enough volume for a practical airplane at lower values of the lift parameter $\frac{\beta}{2} C_L \frac{S}{l^2}$ and thus the lower bound curve must be modified in that region as was done in TN–1494.

Figure 3 and equation (1) form a basis for a study of the means which may be utilized in attempts at minimization. Airplane shaping

considerations which allow an approach to lower bound overpressures and which lead to sonic boom minimization will be discussed subsequently; first, the dependence of the boom on the operational factors of altitude and Mach number and on the gross design features of airplane length and weight will be treated.

Figure 4 illustrates the lower bound pressure dependence on the primary factors of altitude, Mach number, airplane length, and airplane weight. The circular symbol indicates conditions for SST with a length of 300 feet and a weight of 600 000 pounds cruising at a Mach number of 2.7 and an altitude of 60 000 feet. The corresponding Δ_p is 1.83 psf.

As is well known, altitude is a powerful factor in the determination of overpressure not only because of the three-fourths power of the nondimensionalized distance h/l in the overpressure parameter, but also because the reference pressure $\bar{p}$ which must represent a mean pressure between the airplane and the ground, decreases rapidly with increasing altitude. As altitude increases, however, the lift parameter also increases, and the benefits of increased altitude become less. There is, in fact, little benefit to be derived from operation of the airplane at altitudes much above the altitude which gives maximum lift-drag ratio or maximum range. For the same range, an airplane flying at the higher altitude requires a larger fuel load which compensates for the increased altitude.

Increased Mach number is seen to have a beneficial effect beyond about $M=2$. Furthermore, increased speed will provide benefits beyond the pure Mach number effect because the optimum altitude

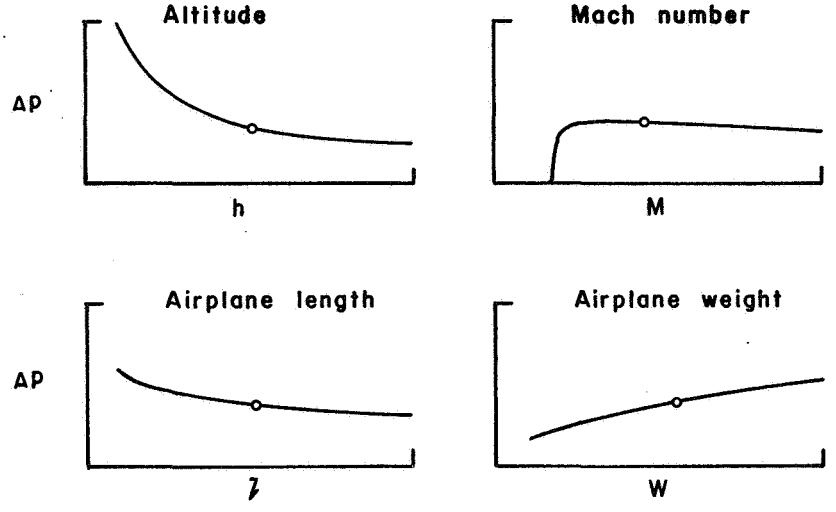

FIGURE 4.—Variation of lower bound overpressure with the various factors.

for airplane range is increased as speed is increased. The effects of the first two curves of figure 4 may thus be combined. However, current designs for hypersonic speeds tend to have large volumes for fuel storage, and good shape factors approaching 0.60 may be difficult to achieve.

An increase in airplane effective length is also seen to have a beneficial effect. Because the effective length is determined by supersonic area rule concepts, the effective length can be increased by employment of wing dihedral or other vertical displacement of airplane components from a flat surface. However, attempts to elongate the airplane effective length for sonic boom benefits will be limited by consideration of the effects on the aerodynamic efficiency and on the airplane weight.

It is clear that airplane weight reductions will be of utmost importance in sonic boom minimization. Weight reductions have a direct effect on sonic boom reduction and do not necessitate consideration of opposing factors as is the case for other minimization approaches. Actually the benefits of a given weight saving will tend to be amplified as the airplane design cycle is retraced. Unfortunately, the converse is also true, and history has shown far more weight increases than weight reductions in the path from concept to production airplane.

It can be concluded that maximization of the product of altitude and Mach number consistent with the maintenance of aerodynamic and propulsive efficiency will be instrumental in sonic boom reduction. It is also apparent that minimization of the ratio of weight to length (or lift loading per unit length) consistent with aerodynamic efficiency considerations will lead to sonic boom reductions.

Airplane shaping considerations will be discussed with the aid of figure 5. Superimposed on the lower bound plot taken from figure 3 are configurations which permit a good approach to the lower bound effective area distribution for two values of the lift parameter. Note that for lower values of the lift parameter, near the volume restraint curve, a relatively short chord wing, well aft on the airplane, can be combined with the volume to give a near optimum effective area distribution. In fact, if the lift is not concentrated near the rear of the configuration, it will be all the more difficult to provide the necessary airplane volume within the constraints of the lower bound shape. At higher values of the lift parameter, however, it is necessary that the lift be distributed over most of the airplane length in order to avoid a rather bulbous drag-producing fuselage. A highly swept arrow wing with considerable cutout helps in meeting the requirements. Present SST designs at cruise conditions would fall somewhere between the lift parameters for the two examples.

Another consideration worthy of note is that although the volume

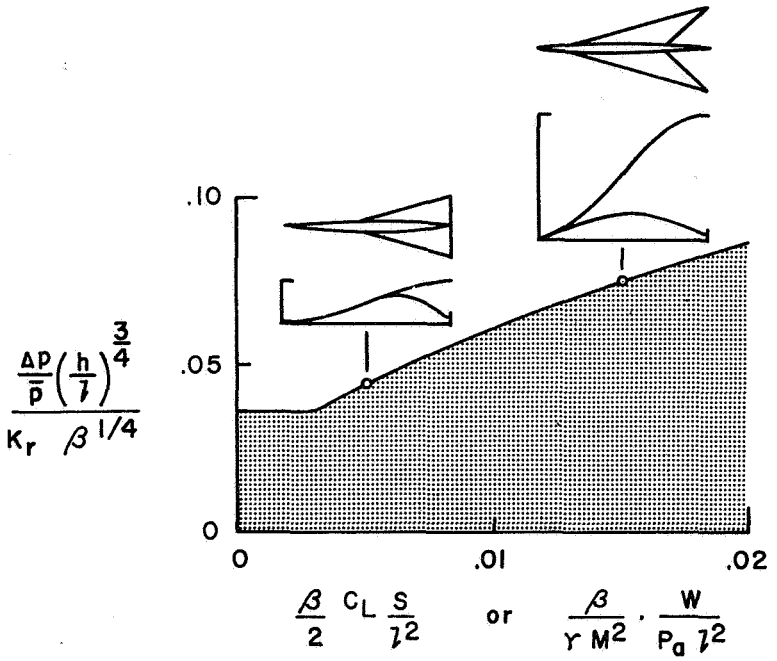

FIGURE 5.—An illustration of configuration requirements for lower bound overpressure.

contribution to the pressure field could be eliminated by employment of concepts related to the Busemann biplane, there is not necessarily an advantage in so doing. Volume effects can be combined with lift effects in a favorable fashion to produce lower overpressures than would be the case for the lift alone. In both of the examples shown in figure 5, the wing lift is generated in an expansion field created by the fuselage to bring about a favorable lift-volume interaction.

In this discussion, no account has been taken of the potential for near-field signature benefits such as the flat-top or finite rise time signatures discussed by McLean in another part of this document. The minimization concepts discussed herein do, however, apply to the impulse of the signature for all flight conditions, and from present indications apply to Δp for SST cruising conditions.

It is the author's contention that practical minimization concepts are well understood and are supported by a large body of experimental data. Furthermore, it is believed that the surviving SST designs in the national program have utilized this technology to nearly the full practical extent. Cruise overpressure levels are only 10 to 15 percent higher than the approximate lower bound used herein and 20 to 30 percent higher than the unattainable Jones lower bound for airplanes of that size and weight.

Atmospheric Turbulence

I. Edward Garrick
Langley Research Center, NASA

Professor Hayes raised the discussion question on likely further work on the interaction of atmospheric turbulence and the sonic boom. In response, Mr. I. E. Garrick stated that the question was obviously very broad and the problem areas offered much room for research, for example, in both topological and weather effects. Although the present sonic boom theories seem to predict very well the mean values of the statistics of sonic boom pressures, it should be feasible also to predict the variances of these statistics by including meteorological-turbulence parameters. Moreover, because it is the highest values, which occur least often, that may be of special concern, the prediction of the extreme value statistics deserves additional attention and effort.

Brief Comments on Sonic Boom Reduction

A. R. George
Cornell University

At the risk of stating the obvious, it appears that several boom reduction methods were reported that could reduce boom significantly, particularly cumulatively. Unfortunately the likely performance and/or structural weight penalties that would be associated with application of these methods would probably be intolerable for the present designs. However, in design studies for any future domestic SST, these various methods should certainly be considered and evaluated.

General Remarks on Sonic Boom

ADOLF BUSEMANN
Colorado University

If the psychological aspect of the sonic boom indicates that a reasonable finite rise time of the positive pressure steps (rather than a step function) is crucial for the acceptability of booms by man and animals, then increasing the flying altitude beyond 25 000 feet does not help alleviate the sonic boom effects. At ground level the absolute pressure jump attributed to lift is not decreased by changing the altitude from 25 000 feet to 70 000 feet, but the width of the audible path is doubled. The self-propagation of a pressure equal to 1/1000 of the atmospheric pressure on the ground (1/2000 prior to the doubling by reflection) corresponds to about 140 feet at 25 000 feet altitude and 400 feet at 70 000 feet altitude (for $M=3$). This is in addition to the original distance of the positive and negative pressure peaks. Spreading the near-field pressure rise created by the nose and the lifting portions of the aircraft over such a length to avoid forming the steep pressure rises of the common N-wave in the far field severely increases the minimum length of the airplane with increasing altitudes.

Therefore, because these arguments recommend a lower altitude than the planned flight altitude, I would like to learn more about the engineering reasons for going toward the higher altitudes. One crucial aspect could be the encounter of water droplets and ice crystals at these speeds. Another problem may be the larger heat input as compared with the radiation output from the skin. Of course there are other reasons. Whatever they may be, such engineering reasons are physical and open to cures according to the laws of science, while the disturbances to humans by sonic booms are emotional and psychological and, therefore, not so open to tradeoffs. Thus, with the limitations placed on sonic booms, the feasibility of lowering the flight altitude even by unconventional methods and the finding of a permanent or state-of-the-art limit for economical and safe flying seems to be a necessary study. The minimum length requirements mentioned above for the higher altitudes are much beyond the planned or state-of-the-art lengths as governed by engineering constraints.

The prerequisite for such considerations is, of course, the proof that the finite rise time is a great relief. I would prefer to have it demonstrated to my own ears rather than rely on statistical reports as to its effect.

U.S. GOVERNMENT PRINTING OFFICE: 1968—O-315-766

NATIONAL AERONAUTICS AND SPACE ADMINISTRATION
WASHINGTON, D. C. 20546

OFFICIAL BUSINESS

FIRST CLASS MAIL

POSTAGE AND FEES PAID
NATIONAL AERONAUTICS A
SPACE ADMINISTRATION

POSTMASTER: If Undeliverable (Section 15
Postal Manual) Do Not Ret

"The aeronautical and space activities of the United States shall be conducted so as to contribute . . . to the expansion of human knowledge of phenomena in the atmosphere and space. The Administration shall provide for the widest practicable and appropriate dissemination of information concerning its activities and the results thereof."

— NATIONAL AERONAUTICS AND SPACE ACT OF 1958

NASA SCIENTIFIC AND TECHNICAL PUBLICATIONS

TECHNICAL REPORTS: Scientific and technical information considered important, complete, and a lasting contribution to existing knowledge.

TECHNICAL NOTES: Information less broad in scope but nevertheless of importance as a contribution to existing knowledge.

TECHNICAL MEMORANDUMS: Information receiving limited distribution because of preliminary data, security classification, or other reasons.

CONTRACTOR REPORTS: Scientific and technical information generated under a NASA contract or grant and considered an important contribution to existing knowledge.

TECHNICAL TRANSLATIONS: Information published in a foreign language considered to merit NASA distribution in English.

SPECIAL PUBLICATIONS: Information derived from or of value to NASA activities. Publications include conference proceedings, monographs, data compilations, handbooks, sourcebooks, and special bibliographies.

TECHNOLOGY UTILIZATION PUBLICATIONS: Information on technology used by NASA that may be of particular interest in commercial and other non-aerospace applications. Publications include Tech Briefs, Technology Utilization Reports and Notes, and Technology Surveys.

Details on the availability of these publications may be obtained from:

SCIENTIFIC AND TECHNICAL INFORMATION DIVISION

NATIONAL AERONAUTICS AND SPACE ADMINISTRATION

Washington, D.C. 20546